Photoactive Materials Based on Cyclodextrin-Functionalized Gold Nanoparticles

Marc Padilla Barriento

2017

Director/s:

Dr Jordi Hernando Campos

Dr José Luis Bourdelande

Programa de Doctorat en Química

Departament de Química

Universitat Autònoma de Barcelona

Chapter 5:

Controlled Assembly of Gold Nanoparticles Using Cyclodextrin-Based Supramolecular Chemistry

5.1-INTRODUCTION

As already commented in previous sections, during the last ten to fifteen years there has been an increasing interest towards the nanoscale-related research. In particular, nano-scientists have paid important attention to gold nanoparticles and their potential applications, some of which have already been discussed in chapter 1 of this thesis. In this field, special interest is being given to the preparation, characterization and application of assemblies of Au NPs, because of their special optical properties. The prepartion of Au NP assemblies has served to develop new detection methods where Au NPs act as sensors in optical detection (see Figure 1.3 in section 1.1) or Raman spectroscopy (see Figure 1.4 in section 1.1). Moreover, Au NP assembly is of great interest to exploit the hot spots formed between nearby Au NPs (see figure 1.5 in section 1.1) since this phenomena are highly distance dependent. Au NP assembly also opens the possibility for catalyst recycling owing to the high tendency of bigger NP aggregates to precipitate, making easier their separation by filtration/centrifugation procedures. Therefore, the capacity to control the formation of Au NP assemblies with an external estimulus is highly desirable. In this chapter, the formation of Au NP heteroassemblies mediated by supramolecular host-guest chemtry is pursued as will be introduced in the following sections.

There are a number of reviews describing the assembly of Au (and other noble metal) NPs in colloids using molecular and, specially, supramolecular approaches.[1-8] Different supramolecular strategies are reported for achieving NP aggregates, such as oligonucleotide hybridization, ionic interactions, hydrogen bonding, van der Waals interactions and host-guest chemistry involving cyclodextrins (CDs), calixarenes, cucurbiturils or pillararenes as supramolecular hosts. This section will only focus on the previous work dealing with the assembly of Au (or other noble metal) NPs via CD-based supramolecular chemistry, which is the final objective of this chapter.

5.1.1- Cyclodextrin-based methodologies for the assembly of plasmonic nanoparticles

Different approaches involving the use of CDs have led to the obtention of Au NP assemblies. The simplest approach is based on the variation (decrease) of the amount of stabilizing agent around the nanoparticles. With this strategy, CD-coated nanoparticles aggregate without requiring guest addition, but simply by using less CD ligand than required for efficient stabilization. For instance, Huang *et al* reported the

obtention of gold nanowires when decreasing the β-CD / $HAuCl_4$ ratio in a direct synthesis of Au NPs.[9] Actually, instead of NP assemblies, what they eventually obtained was just the result of an uncontrolled growth of Au^0 nanostructures where defined NPs could not to be formed due to a lack of stabilization (Fig. 5.1). In another example of a direct synthesis of Au NPs with α-CD as a stabilizer, Huang *et al* studied the effect of NaOH addition.[10] As the amount of NaOH increased, more hydroxyl groups of α-CD were deprotonated, which resulted in electrostatic repulsion between close-by CD molecules and less efficient coating of the NP surface. As a result, colloidal stability decreased and the NPs aggregated.

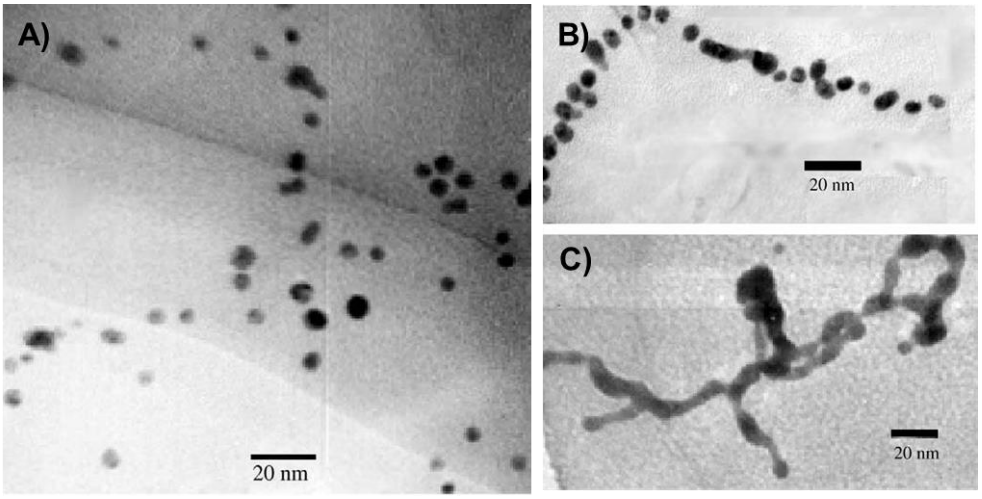

Figure 5.1. TEM images of the gold structures obtained after the direct synthesis of β-CD-coated Au NPs when the molar ratio of β-CD to $HAuCl_4$ was A) 10, B) 1.25 and C) 0.02. Adapted from reference 9.

Alternatively, direct hydrogen bonding between surface-tethered CDs was also proposed as a mechanism for the obtention of NP assemblies without the need of using host-guest supramolecular interactions. For instance, Ng *et al* found the formation of what they called “pearl necklace” arrays of Ag NPs when α-CD was present at dilute concentrations (Fig. 5.2).[11] Devi and Mandal reported the same behaviour when using α- and β-CD and their 2-hydroxypropyl derivatives for the preparation of Ag NPs.[12] Actually, in this work we have also observed hydrogen bonding-driven aggregation of CD-coated Au NPs, as previously discussed in chapters 3 and 4.

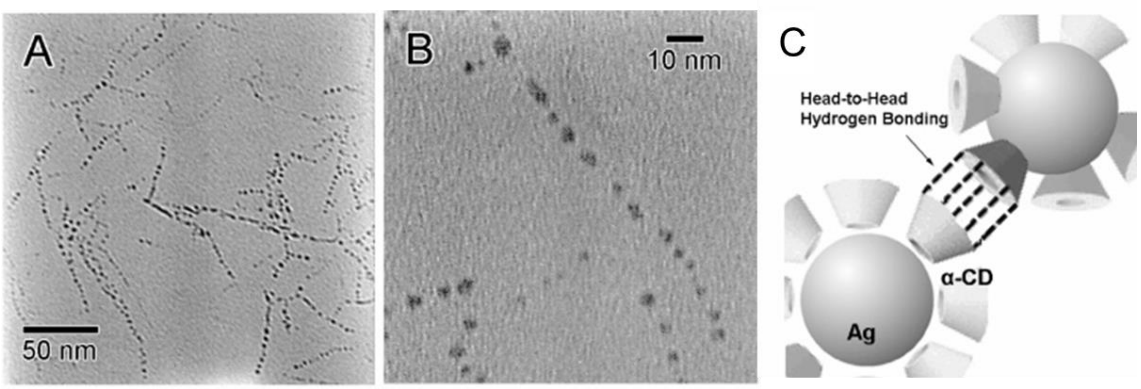

Figure 5.2. (A and B) TEM images illustrating the self-assembly of α-CD-coated Ag NPs into 1-D pearl necklace arrays via hydrogen bonding. (C) Schematic of the hydrogen bond interactions between the secondary -OH groups of the suface-attached CDs (not drawn on scale). Adapted from reference 11.

In another group of assembly strategies, native CDs are also used as stabilizers of the isolated NPs, but instead of diluting the amount of ligand in solution or exploiting CD-CD hydrogen bonding, aggregation occurs after addition of a suitable supramolecular guest to the medium. Huang *et al* reported the formation of 1D assemblies of α-CD-capped 20 nm Au NPs in the presence of toluene.[10] This approach was also used by Wen *et al* to aggregate β-CD-capped Au NPs into "peanut-shaped", short nanochains and interfused 3D nanowire network architechtures upon addition of different amounts of dopamine (Fig. 5.3).[13] With the same strategy, Wen *et al* also prepared Au aerogels due to 3D aggregation of Au NPs induced by dopamine.[14] It must be noted that all these examples use native non-thiolated CDs as stabilizers, which implies that only weak interactions are formed between the Au core and the capping layer. As such, manipulation of the colloidal suspensions of these nanoparticles (e.g. dilution, addition of supramolecular guests) results in a decrease of the number of stabilizing molecules onto their surface, which may favor the formation of low-stability 1D assemblies that aggregate into more complex structures at the expense of a complete loss of NP integrity Consequently, this assembly process is definitely not reversible and other approaches have to be explored in order to find a suitable way to obtain reversible Au NP aggregates.

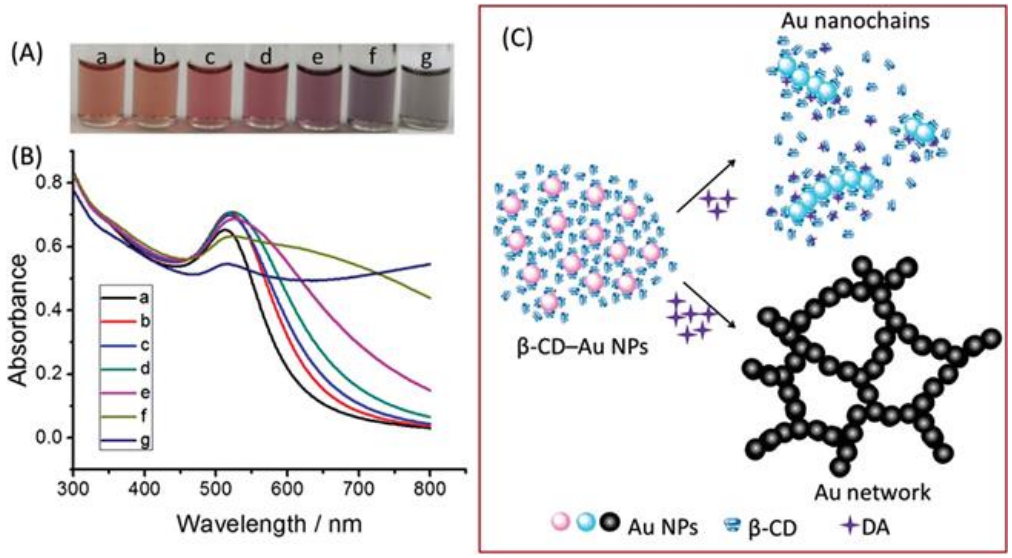

Figure 5.3. (A) Photographs of β-CD-Au NP aqueous colloids (A) before and (b-g) after the addition of dopamine (DA) and (B) their corresponding UV-Vis spectra. The concentrations of dopamine were 2.0, 2.1, 2.25, 2.75, 3.6 and $7.5 \cdot 10^{-6}$ M respectively. (C) Schematic diagram of the dopamine-induced Au NP assembly. Reproduced from reference 13.

To solve this problem thiolated CD derivatives can be employed as NP stabilizers, since the larger strength of the Au-S bond formed increases the stability of the capping layer of the nanoparticles. With this approach and the use of free ligands that bear two or more supramolecular guest units, reversible noble metal NP assemblies can be prepared. This is by far the most common methodology followed and, indeed, there are plenty of examples in the literature that ilustrate this strategy. Different guest molecules have been used to exploit this approach depending on which CD is employed. For instance, ferrocene and adamantyl derivatives are preferred when using β-CD, since they display very high association constant values with this host.[15] Thus, Liu *et al* were able to obtain Au NP assemblies with β-CD-capped nanoparticles and a bis-ferrocene ligand, and the observed flocculation could be prevented and partially reverted by the addition of a free ferrocene derivative.[16] Not only ditopic guest molecules, but also multitopic molecules can be used in this case. For example, dendrimers bearing multiple terminal adamantyl moieties were exploited by Crespo-Biel *et al* to form Au NP layer-by-layer assemblies,[17,18] which could even be patterned over surfaces (Fig. 5.4).[19]

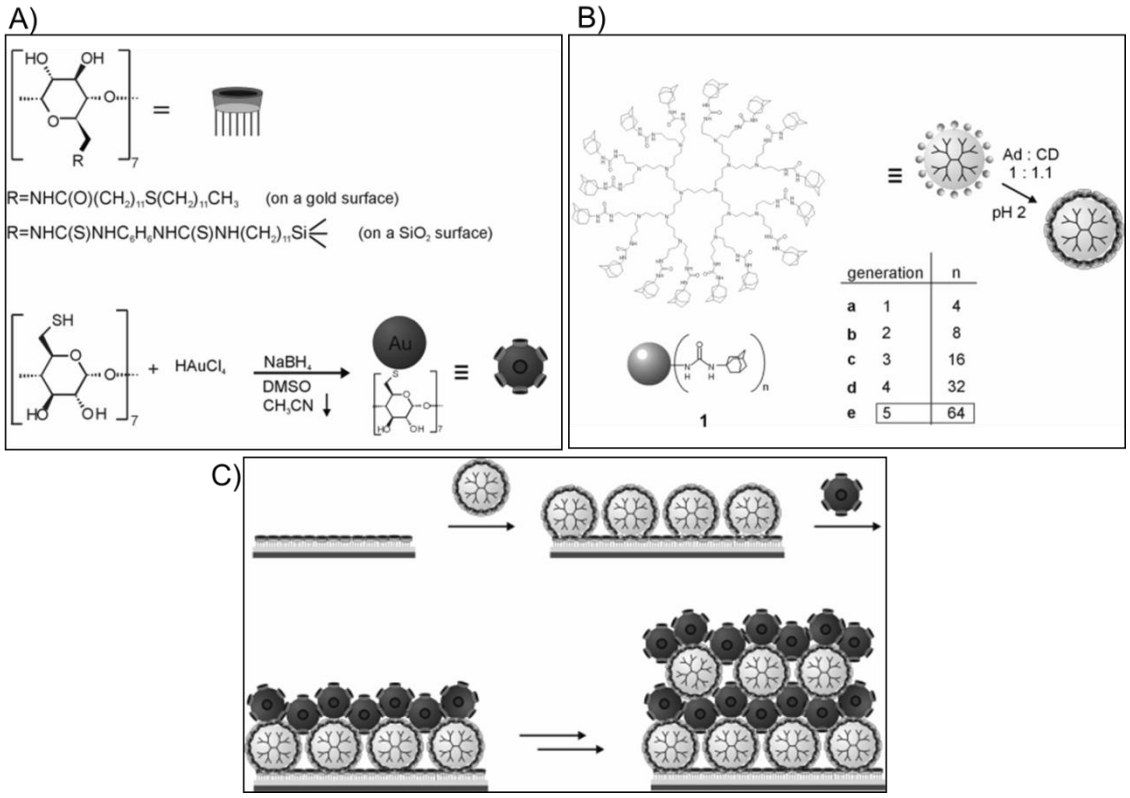

Figure 5.4. A) Chemical structure of the surface adsorbates and the CD-functionalized Au NPs. B) Adamantyl-terminated polypropylenimine (PPI) dendrimers (**1**). C) Layer-by-layer assembly scheme for the alternating adsorption of adamantyl-terminated PPI dendrimer **1e** and CD-capped Au NPs onto CD SAMs. Adapted from ref. 19.

In a similar way, some guests capable of forming 1:2 (guest:CD) complexes with cyclodextrins have also been used, such as 1,10-phenanthroline[20] and C_{60}. The latter was employed by Yu *et al* to aggregate β-CD-capped Au NPs, a process that could be reverted back by the addition of 2-adamantanol (Fig. 5.5).[21] Even higher stoichiometry host-guest complexes can be used for this purpose, which is the case of the 1:4 complexes of some porphyrin dyes and β-CD.[22] In a more elaborated form of this approach, Xi-Le *et al* prepared an adamantyl-dye-monosaccharide ligand where the adamantyl moiety forms an inclusion complex with the β-CD hosts on the surface of the NPs, whereas the pending monosaccharide group attaches to a tetrameric receptor added to the medium, thus finally resulting in NP assembly.[23]

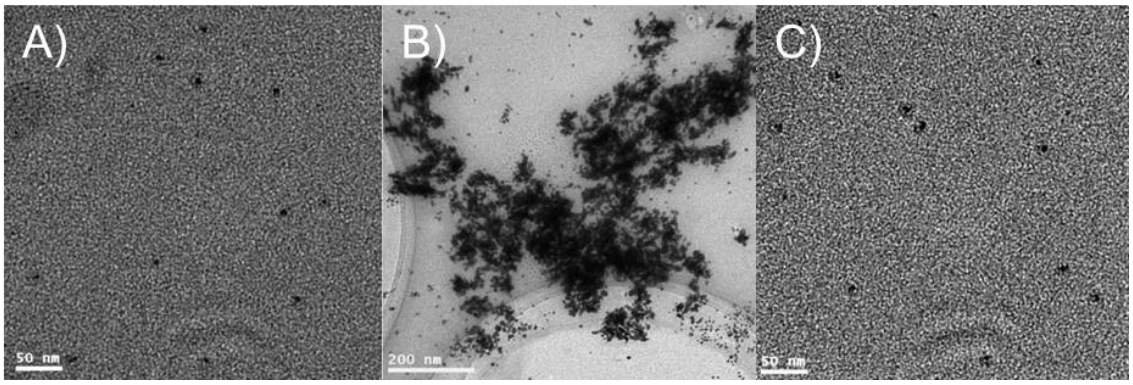

Figure 5.5. TEM images of A) initial β-CD-modified Au NPs, B) C60-induced assembly of these nanoparticles, and C) NP disaggregation achieved after addition of 2-adamantanol. Adapted from reference 21.

Another approximation consists in the use of rotaxane-like ligands as NP stabilizers composed of oligomers/polimers threaded through CD macrocycles. The supramolecular interactions established between the rotaxane-like ligands of different NPs lead to their assembly. Contrary to what has been explained so far, in this strategy the guest molecules are attached to the NP surface instead of the macrocyclic host. For instance, Liu *et al* obtained assemblies from Au NPs functionalized with amino-terminated polypropylene glycol chains and both free native and derivatized β-CD.[24] In recent studies the use of this approach has led to the formation of Au NP hydrogels that can sometimes be redissolved. Thus, thiolated PEG chains and α-CD were used by Jing *et al* to form hybrid hydrogels containing Au NPs and Au nanorods (Au NRs) that could serve as drug delivery carriers, since gel-sol transition was observed when rising the temperature up to 60 ºC (Fig. 5.6).[25] With the same strategy, Coelho *et al* reported the formation of reversible crystals of Au NPs mediated by polyrotaxane supramolecular interactions. A thiolated surfactant was used in this case together with α-CD to induce the assembly process. Removal of water caused the formation of nanocrystals that could be fully redissolved in the same solvent.[26]

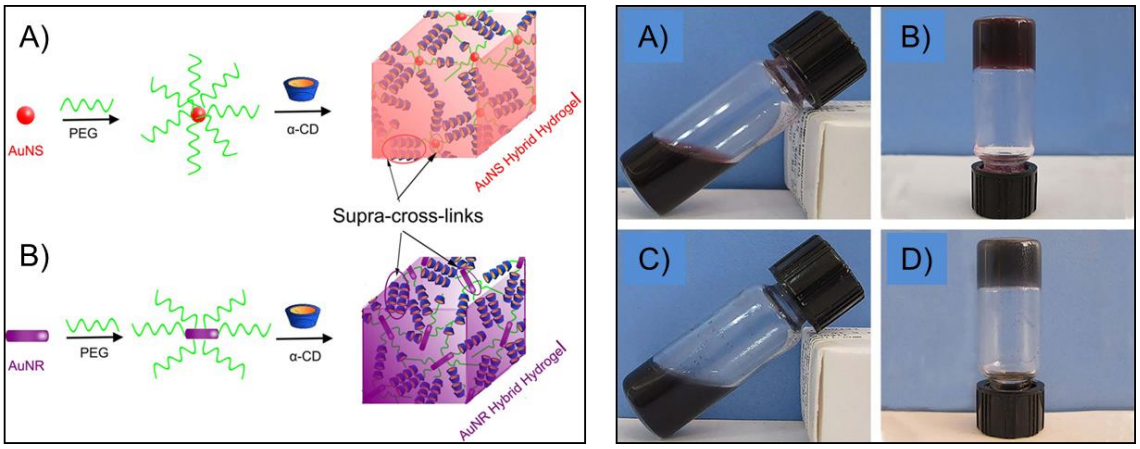

Figure 5.6. Left: Schematic representation of hybrid hydrogels made of AuNS-PEG/α-CD A) and AuNR-PEG/α-CD B). Right: A) Optical photo of AuNS-PEG/α-CD sols before converted to gels, B) AuNS-PEG/a-CD supramolecular hydrogels, C) AuNR-PEG/α-CD sols before converted to gels, D) AuNR-PEG/α-CD supramolecular hydrogels. For all samples [α-CD] = 200 mg / mL. Adapted from reference 25

It must be noted that all the previous strategies and examples described lead to the formation of homoaggregates of Au (or other noble metal) NPs. However, the controlled preparation of heteroaggregates has been much less investigated, though it is potentially more interesting since it may allow linking different types of particles on a selective way. Wang *et al* were among the first to explore this idea.[27] In their work, Fe_3O_4 or other inorganic NPs coated with a mixture of oleic acid/oleylamine/hexadecylamine and an adamantyl derivative were dissolved in an organic medium. Upon addition of an aqueous solution of thiolated or amino-functionalized β-CD, adamantyl-CD complexes were formed, bringing the NPs to the interphase. When metallic Ag/Au NPs were then added, interaction with the functional groups at the rim of the CDs favoured their assembly in the interphase between the organic and the water phases, resulting in the formation of a trilayer of different types of NPs (Fig. 5.7).

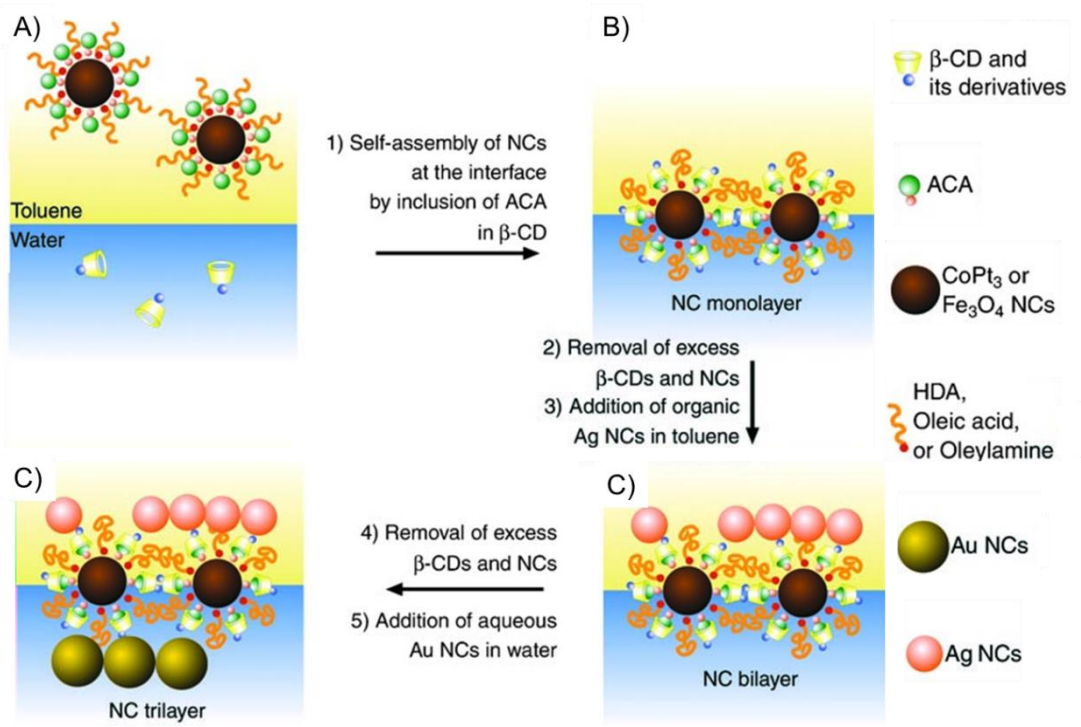

Figure 5.7. Schematic ilustration of nanocrystals (NCs) capped with 1-adamantylcarboxylic acid (ACA) and other organic ligands, which aggregate with Au/Ag NPs at the water/oil interface by addition of thiolated or amino-functionalized β-CD derivatives and the formation of supramolecular complexes with ACA. Adapted from reference 27.

A more rational approach to prepare heteroaggregates of noble metal nanoparticles consists in the use of both CD-coated NPs and guest-coated NPs. With this strategy in mind, Chen *et al* prepared Au NPs stabilized with thiolated α-CDs and other type of NPs (Fe_3O_4 or up-converting NPs) stabilized with oleic acid. When mixing a hexane suspension of the latter together with an aqueous solution of Au NPs, they observed assembly at the interphase or even complete phase transfer from the organic to the aqueous phase, as a result of the supramolecular interactions between α-CD and oleic acid (Fig. 5.8).[28]

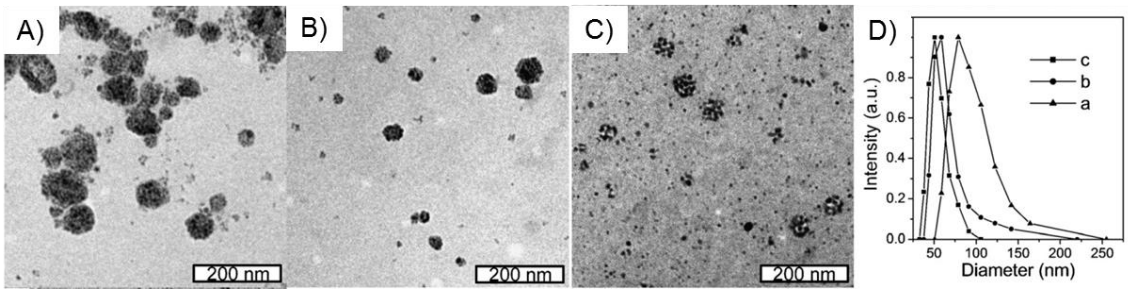

Figure 5.8. TEM image of Au/Fe_3O_4 NP superstructures constructed from Fe_3O_4 NPs functionalized with oleic acid and α-CD-capped Au NPs with concentrations of A) 2 mg/mL and B) 0.5 mg/mL. C) Partial disassembly of the Au/Fe_3O_4 NP superstructures in A) upon addition of 0.5 mM of free α-CD. D) DLS size distribution of the corresponding samples in A), B) and C). Adapted from reference 28.

5.1.2- Objectives: stimulus-responsive heteroassemblies of gold nanoparticles via cyclodextrin-based supramolecular chemistry

Our aim in this part of the thesis is the preparation of Au NP heteroassemblies) that are capable to respond to an external stimulus leading to a controlled and reversible aggregation process. As an external stimulus, we have chosen the use of light, since it can be applied remotely, non-invasively and with spatial and temporal control. For this purpose, the strategy discussed in the last example of the previous section has been used, which requires two different sets of Au NPs to be prepared. One of them has been coated with an azobenzene derivative, the guest molecule of choice, due to its ability to interconvert between its *E* and *Z* state by means of UV and visible light. The other set of NPs has been coated with the hexathiolated form of α-CD due to its capability to discriminate between the *E* and the *Z* configurations of azobenzenes. Thus, K_a(α-CD:*E*-azobenzene) is about 2000 M^{-1}, while the value for the association constant with the more voluminous *Z* isomer is much lower (K_a(α-CD:*E*-azobenzene) ~ 35 M^{-1})[29] because it does not properly fit into the small cavity of α-CD. As illustrated in Figure 5.9, this should allow light-controlled assembly and disassembly of the Au NPs of interest.

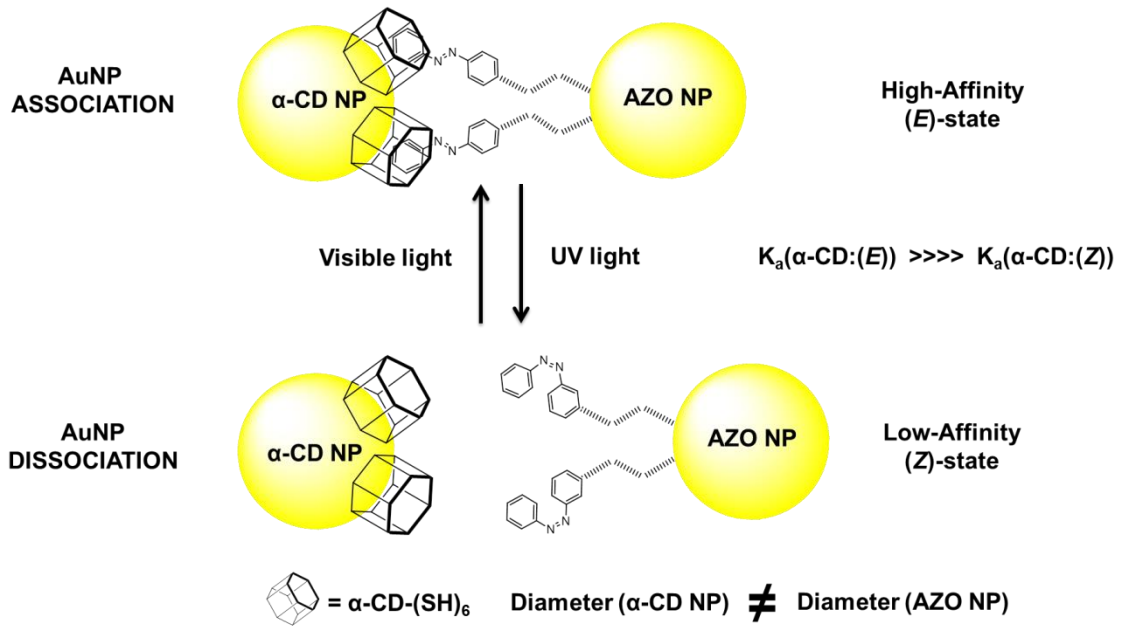

Figure 5.9. Schematic representation of reversible AuNP heteroaggregation mediated by supramolecular host-guest chemistry. The high-affinity *E*-state of azobenzene is converted to the low-affinity *Z*-state upon UV light irradiation leading to nanoparticle disassembly. The *E*-state can be recovered by irradiation with visible light allowing the system to reassociate.

To explore this strategy to fabricate reversible Au NP heteroaggregates, the following steps have been followed, which are described in the next sections: (i) synthesis and characterization of the thiolated ligands; (ii) synthesis of Au NPs and subsequent functionalization with previously prepared thiolated lligands; (c) preparation of Au NP heteroaggregates between CD- and azobenzene-modified Au NPs.

5.2- SYNTHESIS AND PHOTOCHEMICAL CHARACTERIZATION OF LIGANDS

The first step towards the preparation of light-controllable Au NP heteroaggregates was the synthesis and characterization of the functional thiolated ligands with which the nanoparticles had to be coated. Since the preparation of the hexathiolated form of α-CD (**αCD(SH)$_6$**) was already discussed in chapter 3 this section focuses on the development of the other ligands of interest. The most important of them is the azobenzene photoresponsive ligand, which should contain 3 different functional blocks (Fig. 5.10A): (i) a terminal thiol group at one end to attach the ligand to the NP surface; (ii) a central oligoethylene glycol (OEG) block to afford water solubility of the final colloid, which is crucial since CD-azobenzene supramolecular complexes are formed in aqueous media; and (iii) a terminal azobenzene moiety at the other end to act as a photoresponsive molecular guest.

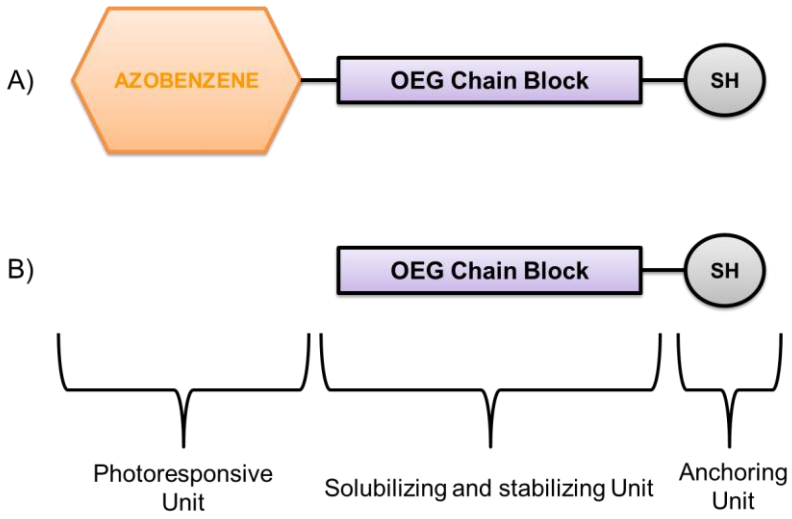

Figure 5.10. Schematic representation of the different functional blocks of (A) the photoresponsive azobenzene ligand, and (B) the stabilizing oligoethylene glycol ligand.

In addition to this compound, a simpler ligand with the same structure but lacking the photoresponsive unit was synthesized as shown in Figure 3.10B. This was necessary to form a mixed monolayer together with the azobenzene ligand around the NP in order to assure (i) high colloidal stability, and (ii) high suspensibility in water. These are two key factors since the azobenzene moiety is poorly soluble in water and it could lead to undesired aggregation processes of the resulting NPs that would interfere with their supramolecular association via host-guest interactions. Moreover, the length

of this auxiliary ligand was chosen such that the azobenzene group of the photoresponsive ligand should stick out of the mixed capping layer surrounding the particles, therefore preventing the host-guest supramolecular interaction with **α-CD(SH)$_6$**-coated NPs to be disrupted because of steric hindrance effects.

It must be noted that in contrast to stilbene photoswitches discussed in chapter 4, azobenzenes are T-type photochromes. This means that their *Z* state is normally not thermally stable and it isomerizes back to the *E* isomer directly in the dark in the microsecond-to-hour timescale depending on the substitution pattern and the solvent.[30] Therefore, the photoresponsive azobenzene moiety should be choosen so that it has a long-lived *Z* isomer in order to maximize the thermal stability of the disassembled state of the heteroaggregates. This, however, restricts the type of substituents at its 4- (and 2-) position. For instance, it must not be a strong electro-donating group, such as an amino or an ether group, neither should the azobenzene of choice present a push-pull substitution pattern. Bearing in mind these considerations, a photoresponsive α-CD guest molecule (**Azo-OEG-1**) consisting in a thiol-terminated tetraethylene glycol chain attached to a non-substituted azobenzene unit by means of a methylene linker was designed. Figure 5.11 shows the chemical structure of **Azo-OEG-1** and its chromophore-less version **OEG-SH**.

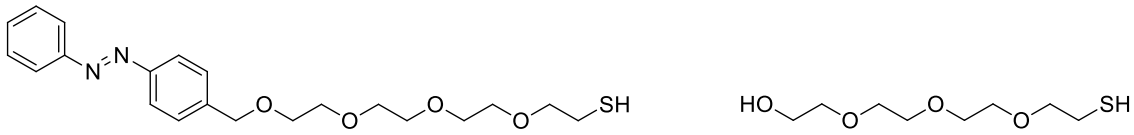

Azo-OEG-1 **OEG-SH**

Figure 5.11. Chemical structures of the thiolated ligands **Azo-OEG-1** and **OEG-SH**.

5.2.1-Synthesis of OEG-SH

The simpler thiolated OEG-SH ligand was first synthesized. There are several synthetic routes available in the literature for the preparation of this product. Scheme 5.1 shows the synthetic strategy chosen in this work in which procedures from several of those routes have been combined. In this strategy commercially available tetraoligoethylene glycol **7** must be first selectively monotosylated. In the following steps, a suitable substitution-hydrolysis strategy is used to obtain the target compound **OEG-SH**.

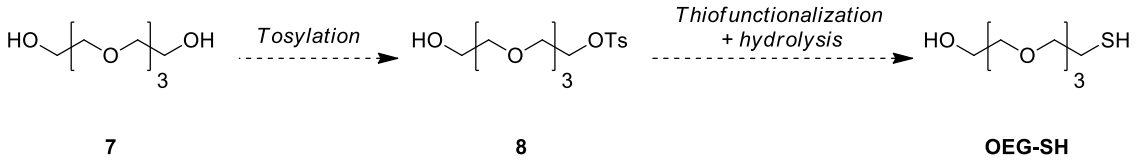

Scheme 5.1. Synthetic strategy for the synthesis of **OEG-SH**.

The preparation of the monotosylated derivative **8** was carried out according to Bouzide and Sauvé using tosyl chloride, potassium iodide and silver oxide.[31] As proposed by these authors, silver and/or potassium ions are coordinated by the OEG chain, favouring the approximation of the terminal hydroxyls one to each other and allowing the formation of an intramolecular hydrogen bond. This activates one of the –OH groups, which is first deprotonated by Ag_2O and where the reaction selectively takes places. Scheme 5.2 shows the results obtained when applying this methodology. Although the reported yield for this reaction is about 85 %, in our hands it slightly exceeded 50% yield, which was explained on the basis of: (i) lower reactivity, since 25 % of the initial diol was recovered after purification of the reaction mixture, and (ii) lack of selectivity, because the amount of ditosylate **9** formed (22 % yield) was 3 times higher than the reported value. We ascribed these results to two main factors. First, we did not use freshly prepared Ag_2O, the quality of which may strongly affect the reaction. Second, although anhydrous conditions were applied, remaining traces of water could interact both with the substrate and the catalyst, influencing reactivity and selectivity. The structure and the purity of the product obtained were confirmed by ^{1}H and ^{13}C NMR spectroscopy, in agreement with reported data.[REF]

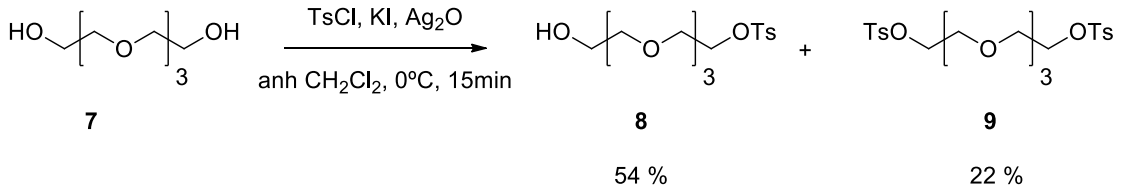

Scheme 5.2. Monotosylation reaction of tetraethylene glycol **7** to prepare **8**.

The following step for the obtention of **OEG-SH** was the introduction of a protected-thiol functionality, which had to be further hydrolized to provide the final thiol. The strategy that was found to be more suitable in this case was the preparation of **OEG-SH** via a thioacetate derivative. This step was performed according to Frisch *et*

al.[32] The results obtained for this reaction are showed in Scheme 5.3. It proceeds through a typical S_N^2 reaction mechanism, where the sulfur atom of potassium thioacetate acts as a nucleophile displacing the tosylate leaving group. The 73 % yield found after purification by flash column chromatography exceeded the value reported in the literature (51 %). The structure and purity of **10** was confirmed by ^{1}H and ^{13}C NMR spectroscopy, in agreement with reported data.[32]

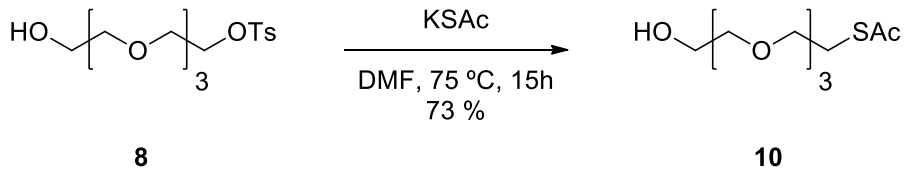

8 **10**

Scheme 5.3. Thiofunctionalization of **8** to synthesize **10**.

The last step towards the preparation of **OEG-SH** was the basic hydrolysis of thioacetate **10**. The results obtained for this reaction are depicted in Scheme 5.4. Even though the reaction was carried out under inert conditions, the thiolated OEG derivative **OEG-SH** is very sensitive to air and oxidizes very fast to form disulfide **11**. ^{1}H-NMR analysis of the crude reaction mixture indeed revealed the formation of a 60:40 thiol:disulfide mixture (Fig. 5.12). Both compounds were characterized by ^{1}H and^{13}C NMR spectroscopy.

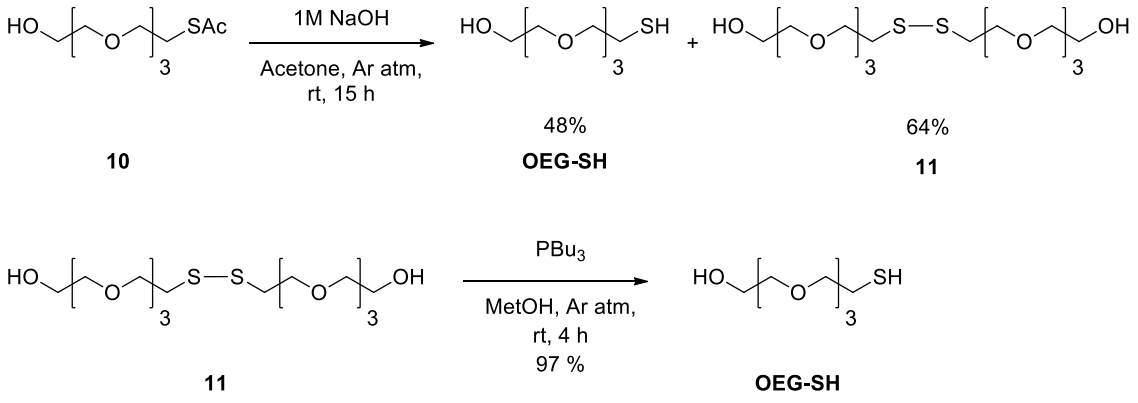

Scheme 5.4. Hydrolysis of **10** to yield target ligand **OEG-SH**, which provided a mixture of the desired product and disulfide **11**. Reduction of the latter quantitatively provided **OEG-SH**.

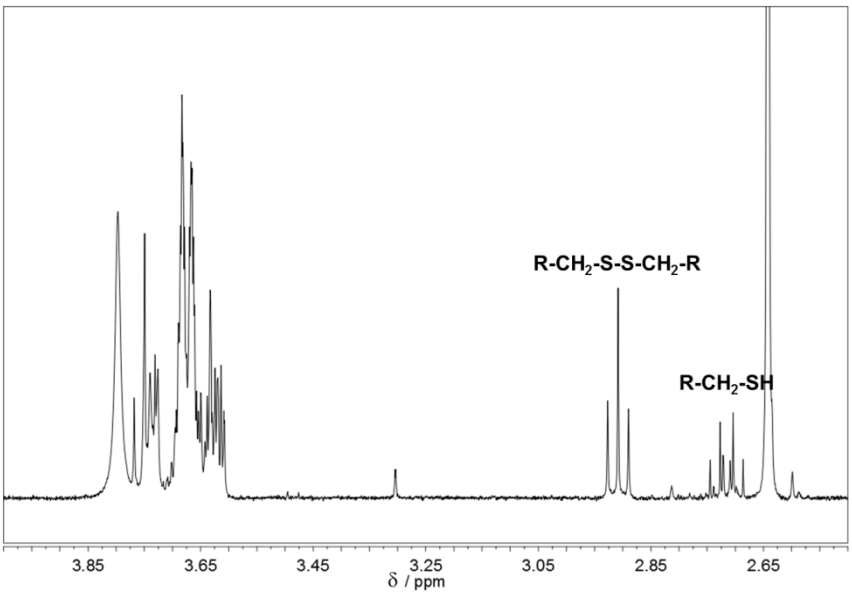

Figure 5.12. ^{1}H NMR of the crude reaction mixture of the synthesis of **OEG-SH** before purification. The triplet signal of the R-CH_2-S-S-R' group of the disulfide is shifted down-field with respect to the doublet of triplets of the same methylene group in the free thiol.

After separation of both products, disulfide **11** was reduced back to the corresponding thiol with PBu_3 (Scheme 5.4). This allowed increasing the yield of this last step of the synthetic procedure up to 80 % and, overall, target ligand **OEG-SH** was synthesized in four steps and an overall 30 % yield. It must be noticed that after prolonged storage of **OEG-SH**, significant amounts of disulfide **11** were formed owing to partial oxidation of the product. This could be almost prevented by storing **OEG-SH** in the freezer.

5.2.2- Synthesis of Azo-OEG-1

Scheme 5.5 shows the synthetic strategy that was devised for the preparation of target ligand **Azo-OEG-1** starting from commercially available 4-(phenylazo)benzoic acid (**12**) and already synthesized compound **10** (vide supra). Reduction of **12** should provide 4-(phenylazo)benzyl alcohol **13**, which can be tosylated to furnish **14**. In the next step tosylate derivative **14** has to be reacted with thioacetate-protected OEG derivative **10** to furnish **15**. This is the key step towards the obtention of **Azo-OEG-1** because further hydrolisis of the thioacetate protection of **15** would lead to the product of interest.

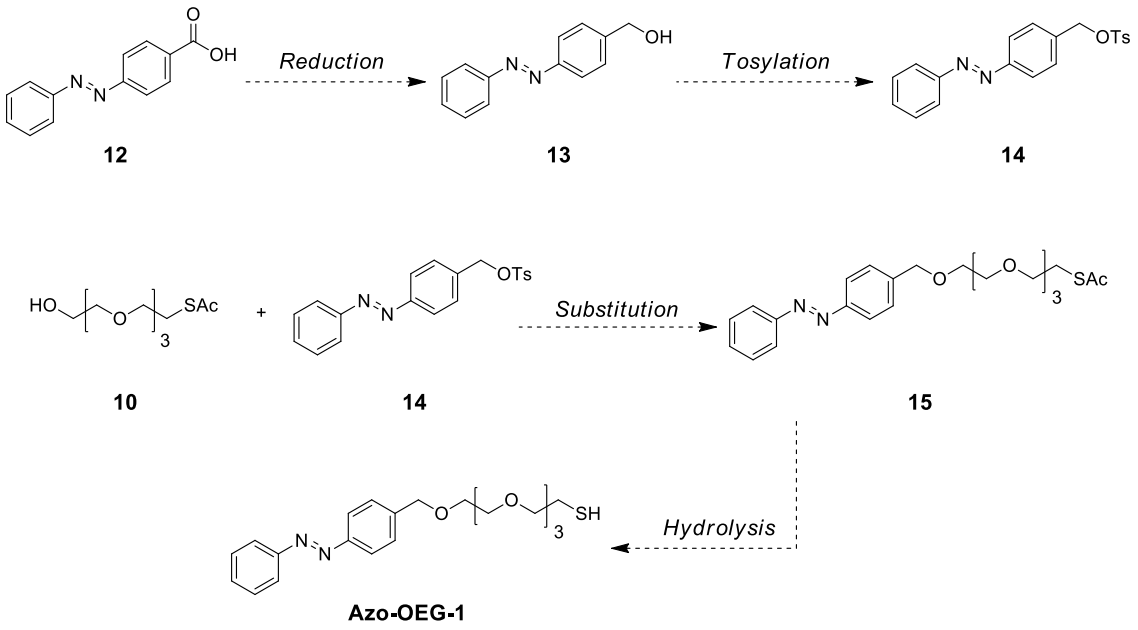

Scheme 5.5. Synthetic strategy for the preparation of ligand **Azo-OEG-1**.

The first step in the preparation of **Azo-OEG-1** was the reduction of 4-(phenylazo)benzoic acid **12** to 4-(phenylazo)benzyl alcohol **13**. This reaction was carried out using $LiAlH_4$ as the reducing agent according to Fatás *et al*, as shown in Scheme 5.6.[33] It proceeded in anhydrous THF under Ar atmosphere and cooling at 0ºC during the addition of the hydride. In this way, alcohol **7** was obtained in 73 % yield after purification. This product was characterized by ^{1}H and ^{13}C NMR spectroscopy, in agreement with reported data.[33]

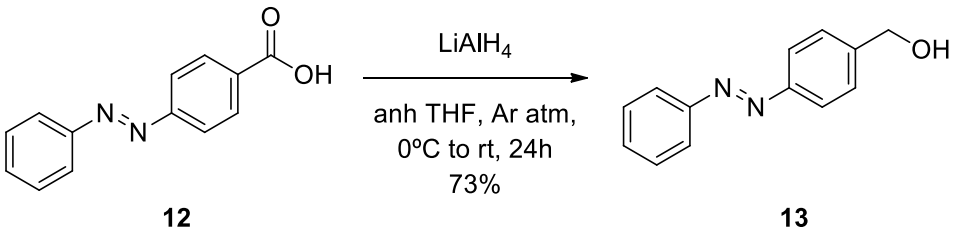

Scheme 5.6. Reduction of 4-(phenylazo)benzoic acid with $LiAlH_4$ to obtain alcohol **13**.

Next, the tosylation of alcohol **13** was performed for the obtention of tosylate **14**. Scheme 5.7 shows the optimized conditions employed and the results obtained for this reaction. Even though this transformation was expected to be rather simple, it presented some drawbacks. First of all, incubation of the starting material with NaH for

serveral hours was required to observe the formation of the desired product, which indicated that deprotonation of benzyl alcohol **13** surprisingly took place at a very slow rate. Second, addition of stoichiometric amounts of tosyl chloride provided low-to-moderate conversions (~40-60 %), as demonstrated by ^{1}H NMR. As a consequence, an excess of TsCl was needed to reach nearly quantitative conversions (~95 %). Finally, purification of the reaction mixture by flash column chromatography resulted in a dramatic loss of the desired product, while a significant amount of alcohol **13** was recovered and the stationary phase used irreversibly got impregnated with azobenzene chromophore. This suggested that **14** was being hydrolyzed and anchored to the silica, probably due to the high lability of its tosylate group. The use of other stationary phases (alumina) did not prevent this degradation processes and, actually, once isolated and stored under ambient atmosphere, product **14** was observed to slowly undergo hydrolysis towards starting material **13**. As a consequence, tosylate **14** could only be obtained in 30 % yield, and it was characterized by ^{1}H NMR, ^{13}C NMR and HR-MS.

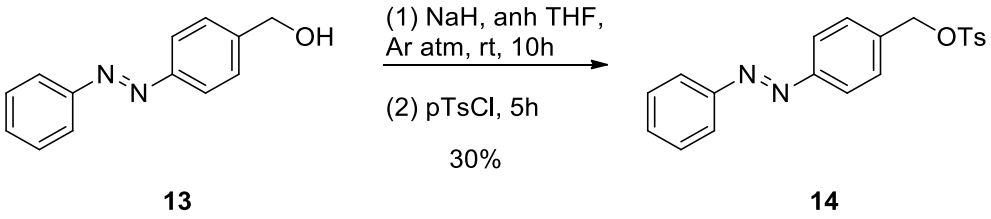

13 **14**

Scheme 3.7. Tosylation reaction of 4-(phenylazo)benzyl alcohol **14**.

As already mentioned, the key step in the preparation of the thiolated azobenzene derivative was the coupling between alcohol **10** and tosylate **14** by simple nucleophilic substitution. Further basic hydrolisis of the product **15** formed in this reaction would afford target compound **Azo-OEG-1**. Unfortunately, it was not possible to obtain product **15** by any means. Scheme 5.8 and table 5.1 show the conditions assayed when attempting the obtention of product **15**. First, typical conditions for this type of reaction were attempted (Table 5.1, entry 1) where NaH was employed as base in anhydrous THF/DMF mixture at room temperature under Ar atmosphere. ^{1}H NMR inspection of the crude reaction mixture revealed a rather complicated sample with almost 100 % conversion of tosylate **14**, according to the signal corresponding to the benzilic position. However, no trace of the desired product could be detected. Since tosylate **14** was being converted almost quantitatively without providing thioacetate **15** it was decided to force the reaction conditions (Table 5.1, entry 2) and synthesis of **15**

was attempted in anhydrous DMF at 85 ºC with no base. According to ^{1}H NMR analysis, quantitative conversion of tosylate **14** was again observed with no formation of thioacetate **15**.

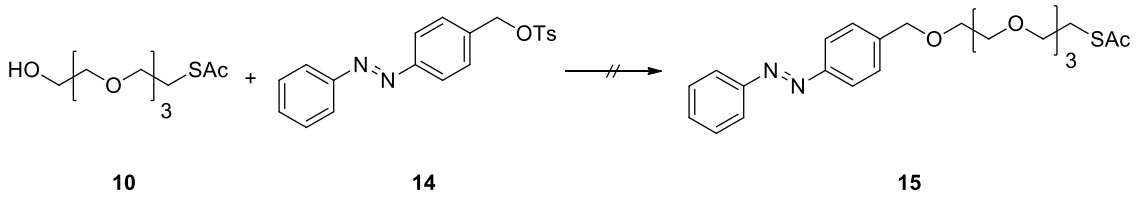

10 **14** **15**

Scheme 5.8. Attempted coupling between thioacetate **10** and tosylate **14**.

Table 5.1. Conditions assayed for the preparation of thioacetate **15**.

Condition	Base	Solvent [a]	T / ºC	Time / h	Conversion / %	Yield / %
1	NaH	THF:DMF 3:1	rt	36	95[b]	0
2	-	DMF	85	8	99[b]	0

[a] anhydrous conditions were always applied. [b] as determined by ^{1}H NMR of the crude reaction mixture.

Against all odds, after purification and characterization by ^{1}H and ^{13}C NMR spectroscopy as well as HR-MS it was realized that the major product obtained in our different assays was acetate **XV**, a consitutional isomer of the desired product. (Scheme 5.9). This transformation can be explained in the following manner: first, intermolecular (or even intramolecular) trans esterification of **10** should have taken place, which would have provided the acetate group of the final product and a free thiol/thiolate functionality that would have subseqüently attacked the benzylic position of **14** to yield **XV**.

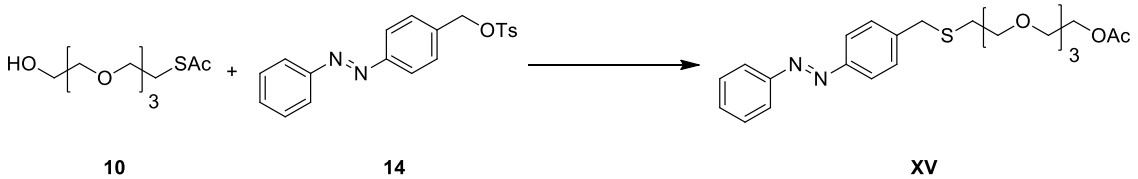

10 **14** **XV**

Scheme 5.9. Coupling reaction between thioacetate **10** and tosylate **14** to provide **IX**.

In view of these results, the synthesis of **Azo-OEG-1** was abandoned and it was necessary to find an alternative route for the preparation of a useful thiolated azobenzene guest.

5.2.3 Synthesis of Azo-OEG-2

As an alternative to **Azo-OEG-1**, a new azobenzene derivative was devised, to which the pending thiolated oligoethylene glycol chain was to be tethered via an ester group (**Azo-OEG-2**, Scheme 5.10). The election of this compound was based on three main factors: (i) the ester functionality should not induce a large decrease of the thermal lifetime of the *Z* isomer of the product; (ii) as the azobenzene starting material, commercially available 4-(phenylazo)benzoic acid **12** could also be used; (iii) the target product could be achieved in two steps taking profit of thiol-protected alcohol **11** obtained as a by-product during the synthesis of **OEG-SH**. As shown in Scheme 5.10, the coupling between the starting carboxylic acid **12** and disulfide **11** would provide ester **16**, which would be further reduced in mild conditions to obtain **Azo-OEG-2**.

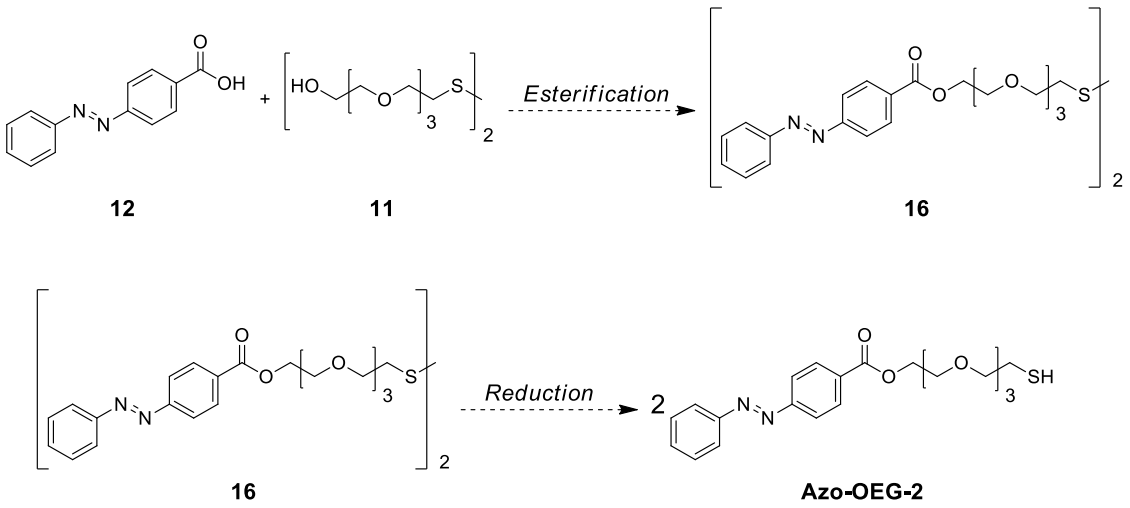

Scheme 5.10. Synthetic strategy for the preparation of ligand **Azo-OEG-2**.

The first reaction of this pathway was attempted using Steglich esterification condictions (Scheme 5.11). In particular, it was carried out in dichloromethane at room temerature and in the presence of dicyclohexilcarbodiimide (DCC) and 4-dimethylaminopyridine (DMAP) as activating agent and catalyst, respectively. The reaction proceeds via the deprotonation of the carboxylic acid by DMAP. Then, the carboxylate formed attacks the diimide carbon atom of DCC forming an activated *O*-

acyl intermediate that can react with the alcohol to yield the final product. However, this intermediate can also undergo a 1,3 rearrangement to form the corresponding *N*-acyl intermediate that does not further react and prevents the formation of the desired ester. The use of DMAP intends to prevent this process, since it reacts faster with the *O*-acyl intermediate to generate an alcohol-reactive *N*-acyl-4-DMAP species that can finally evolve to the target ester product.

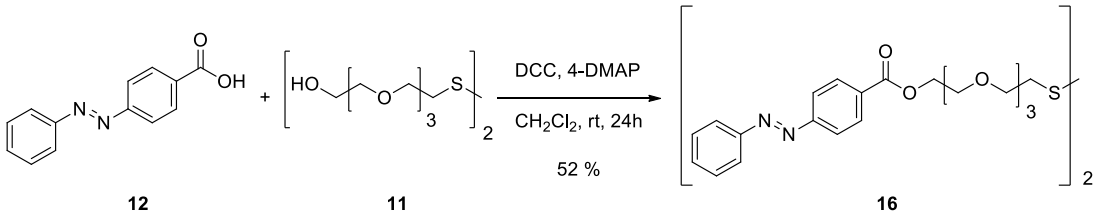

Scheme 5.11. Esterification reaction between acid **12** and alcohol **10** to provide ester **16**.

Direct purification of ester **16** by flash column chromatography was not easy ecause it eluted together with dicyclohexylurea (DCU), a by-product of the reaction, in all the conditions that were assayed. For this reason, we first minimized the amount of DCU in the crude by fractional precipitation, since it is poorly soluble in acetone. Thus, after three precipitation-filtration cycles in this solvent, we could eliminate about 80 % of the initial quantity of DCU. Finally, the resulting mixture was purified by flash column chromatography to obtain ester **16** in 52 % yield. This product was characterized by ^{1}H, ^{13}C NMR spectroscopies and HR-MS.

The last step in the preparation of **Azo-OEG-2** ligand was the reduction of disulfide **16** to obtain the final thiolated azobenzene derivative. This reaction proceeded nearly quantitatively in the presence of tributyl phosphine in degassed methanol at room temperature and under inert atmosphere (Scheme 5.12). After purification by flash column chromatography, **Azo-OEG-2** was obtained in 95 % yield (overall 49 % yield for the two-step procedure from acid **12**). This product was characterized by ^{1}H and ^{13}C NMR spectroscopy, and HR-MS. As previously observed for **OEG-SH**, slow oxidation to the corresponding disulfide was observed in **Azo-OEG-2** stock solutions, and therefore, the same precautions were taken to minimize such process by storing **Azo-OEG-2** in the freezer.

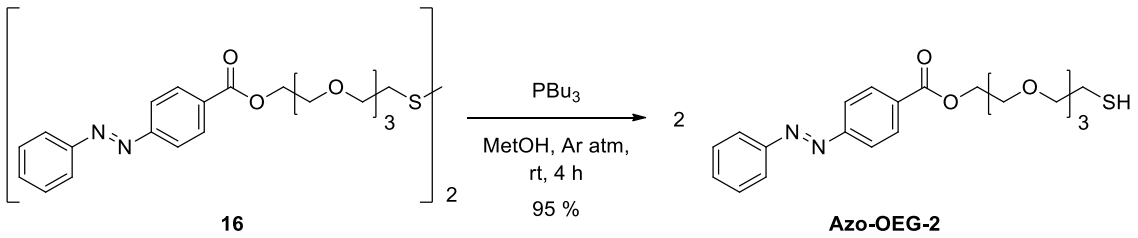

Scheme 5.12. Reduction of disulfide **16** to afford target compound **Azo-OEG-2**.

5.2.4- Photochemical characterization of Azo-OEG-2

As already mentioned in the introduction of this chapter, azobenzenes can interconvert between its *E* and *Z* states by irradiation with UV or visible light (Scheme 5.13). The *E*→*Z* photoisomerization is mediated by the excitation of the π→π* absorption band of the *E* isomer, while the *Z*→*E* photoisomerization process is normally promoted by the excitation of the n→π* absorption band of the *Z* isomer. In addition, the *Z* state is not thermally stable and spontaneous back isomerization to the more stable *E* state is observed, a thermally induced process the kinetics of which depends on the substitution pattern of the azobenzene core. All this processes were investigated in detail for the azobenzene derivative **Azo-OEG-2**.

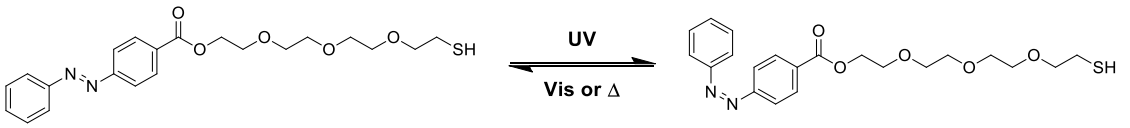

Scheme 5.13. Photoinduced *E*→*Z* photoisomerization of **Azo-OEG-2** upon excitation with UV light. *Cis*→*trans* back isomerization takes place either by irradiation with visible light or it can also take place thermally.

(a) Absorption spectra

First of all, the absorption spectrum of **Azo-OEG-2** was inspectioned. *E* azobenzene derivatives with neither strong electron-donor substituents nor push-pull substitution patterns usually present a very intense π→π* absorption band in the UV region of the electromagnetic spectrum, and a weaker n→π* band in the violet-blue region of the visible spectrum.[30] As seen in Figure 5.13, the absorption spectrum of ***(E)*-Azo-OEG-2** displays both features. It presents three maxima, from which the one

centered at 325 nm corresponds to the π→π* electronic transition and the one in the visible region at 443 nm to the corresponding n→π* transition.

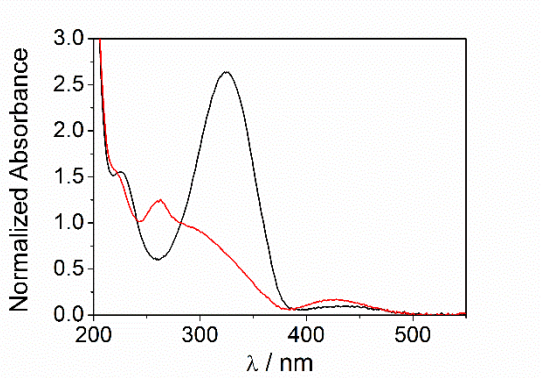

Figure 5.13. Normalized absorption spectra of ***(E)*-Azo-OEG-2** (black line) ***(Z)*-Azo-OEG-2** (red line) in water. Measurements were carried out at concentrations *ca* $2 \cdot 10^{-5}$ M.

Because of the limited lifetime of the *Z* isomer of **Azo-OEG-2**, its absorption spectrum could not be directly measured. However, it could be estimated from the ^{1}H NMR and spectrophotometric characterization of the photostationary state created upon irradiation of ***(E)*-Azo-OEG-2**, a set of experiments that will be described in detail below. The estimated absorption spectrum of ***(Z)*-Azo-OEG-2** is also shown in Figure 3.13, and it displays two noticeable differences with respect to that of the *E* isomer. First of all, it shows a significant hypsochromical shift (from 325 to 262 nm) together with a clear intensity decrease for the π→π* electronic transition band, which are ascribed to the loss of planarity of the azobenzene moiety. Second, a hypsochromical shift is also observed for the n→π* transition (from 443 to 427 nm) and, more importantly, a slight intensity increase is found for the corresponding absorption band. In view of these spectral differences, the *E*-*Z* isomerization of **Azo-OEG-2** can be monitored in a straightforward manner by means of UV-vis absorption measurements.

(b) Photochemical *E*-*Z* interconversion of Azo-OEG-2

According to the absorption spectra determined for the two isomers of **Azo-OEG-2**, *E*→*Z* photoisomerization should be favoured upon irradiation of the π→π* transition of the *E* state at λ~ 300-375 nm, while *Z*→*E* photoisomerization should be promoted by photoexcitation of the the n→π* transition of the *Z* state at λ~ 400-450 nm, in

agreement with the reported data for similar azobenzenes. However, since both isomers are able to absorb at any of these two spectral regions, quantitative light-induced transformations between them are not expected and photostationary mixtures should be instead obtained, as already discussed for the case of stilbenes in chapter 4.

First, *E*→*Z* photoisomerization of ***(E)*-Azo-OEG-2** upon irradiation at 365 nm in water was attempted, which was monitored by means of absorption measurements. Typical spectral changes accounting for azobenzene photoisomerization were observed (Figure 5.14A). As long as the sample was irradiated, a significant decrease of the π→π* transition band was observed, whereas the intensity of the n→π* band increased. It is important to notice that clear isosbestic points at 222, 240, 282 and 388 nm were found in our measurements, which indicated that *E*→*Z* photoisomerization of ***(E)*-Azo-OEG-2** took place without apparent degradation. Similar results were obtained in organic solvents, such as acetonitrile, in which the thermal lifetime of ***(Z)*-Azo-OEG-2** and the solubility of both isomers of the compound were large enough as to allow additional characterization of the *E*→*Z* photoisomerization by ^{1}H NMR. From the NMR data obtained in this case and the spectrophotometric results determined in water, the obtained *E*→*Z* conversion at the $PSS_{E\rightarrow Z}$ state was estimated to be around 90 % in water.

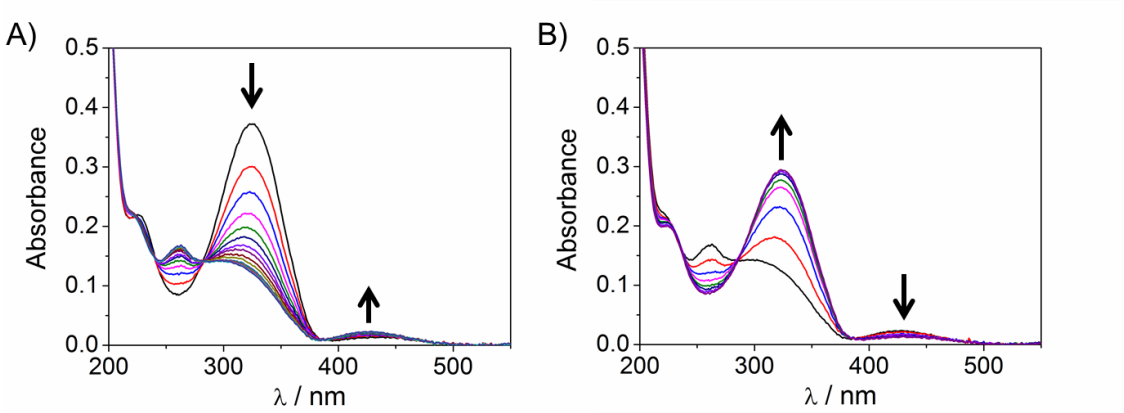

Figure 5.14. A) Variation of the UV-Vis absoprtion spectrum of **(*E*)-Azo-OEG-2** in water upon irradiation with UV light at 365 nm (concentration *ca* $2 \cdot 10^{-5}$ M). Every spectrum was recorded after 10 seconds of irradiation. The arrows indicate the direction of the changes observed in time. B) Variation of the UV-Vis spectra of a mixture of **(*E*)** and ***(Z)*-Azo-OEG-2** corresponding to the $PSS_{E\rightarrow Z}$ upon irradiation with visible light at 406 nm. Every spectrum was recorded after 2 seconds of irradiation. The arrows indicate the direction of the changes observed in time.

Starting from the $PSS_{E\rightarrow Z}$ mixture generated in water, *Z*→*E* photoisomerization of ***(E)*-Azo-OEG-2** was then attempted by excitation at 406 nm. As previously observed for the forward process, the expected spectral changes accounting for azobenzene back-isomerization could also be found (Figure 5.14B). Thus, when irradiating the sample with visible light, a significant recovery of the π→π* spectral band toghether with a slight decrease of the intensity of the n→π* transition band was observed. Analysis of the final $PSS_{Z\rightarrow E}$ obtained allowed us estimating that it was composed of a 72:28 *E:Z* mixture. Again, clear isosbestic points were observed during the light-induced transformation, which further supported the photochemical stability of the system.

These results revealed the ability of **Azo-OEG-2** to photochemically interconvert between its *E* and *Z* states upon irradiation with UV and visible light, thus opening the possibility for further controlling the capacity of this ligand to stablish stronger or weaker supramolecular interactions with α-CD-based hosts once incorporated onto the surface of Au NPs.

(c) Thermal isomerization of *(Z)*-Azo-OEG-2

Regarding the thermal *Z*→*E* isomerization process of **Azo-OEG-2**, it was investigated by monitoring the absorption spectral changes of a $PSS_{E\rightarrow Z}$ mixture in the dark over time at room temperature. As shown in Figure 5.15A, the intensity of the absorption band of ***(E)*-Azo-OEG-2** clearly increased in time even in the absence of visible light irradiation, which unambiguously indicated that thermal *Z*→*E* isomerization took place. Figure 5.15B plots the absorption recovery time trace at 325 nm, the wavelength of the absorption maximum of the π→π* transition band for ***(E)*-Azo-OEG-2**. This trace could be fitted with a monoexponential growth function, which demonstrates that the thermal *Z*→*E* isomerization of **Azo-OEG-2** follows a first order kinetics, as expected. From this fit, the rate constant of this process was determined to be $k_{Z\rightarrow E}$ = 0.022 min^{-1}, which corresponds to a half-life of the ***(Z)*-Azo-OEG-2** in water at room temperature of $t_{1/2}$ = 31.5 min. This means that the thermal *Z*→*E* isomerization of **Azo-OEG-2** occurs in the time scale of hours at room temperature, as expected for analogous azobenzene-type molecules in water.[30] This should provide us with a sufficiently broad time window as to be capable of monitorizing the reversible assembly/disassembly of heteroaggregates of Au NPs targeted in this chapter according to the strategy depicted in Figure 5.9.

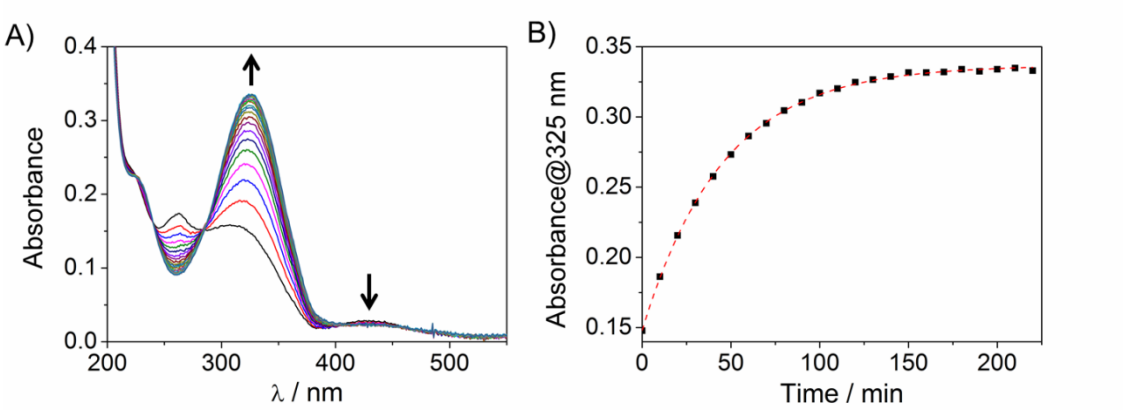

Figure 5.15. (A) Variation of the absorption of the $PSS_{E\rightarrow Z}$ mixture of **Azo-OEG-2** in the dark at 25 ºC in water. The arrows indicate the direction of the observed changes in time. (B) Time dependence of the absorption at λ = 325 nm under these conditions, which reports on the recovery of the concentration of ***(E)*-Azo-OEG-2** upon thermal *Z*→*E* isomerization. Points correspond to the experimental data, while the dashed line was obtained from a monoexponential growth function fit.

5.2.5- Host-Guest complexation of Azo-OEG-2 with α-CD

After preparation of **Azo-OEG-2,** the photoresponsive guest for the assembly experiments, we characterized its supramolecular interaction with α-CD, the corresponding host of choice. Since α-CD-azobenzene complexes are mainly driven by hydrophobic effects, this study was performed in aqueous media. However, because of the insolubility of **α-CD-(SH)$_6$** at the range of concentrations needed, such characterization was carried out with pristine α-CD. As commented in chapter 4, there are different methods available in the literature for the determination of the K_a values of a given host-guest pair. In this part of the thesis we decided to evaluate the association constant of (*E*)-**Azo-OEG-2** using Benesi-Hildebrand plots according to reference 29. This method is based in the variation of the NMR signal of the guest molecule upon complexation with the corresponding host. Figure 5.16 shows the ^{1}H NMR spectra correponding to different samples in D_2O containing equal amounts of **Azo-OEG-2** and increasing amounts of α-CD. As can be seen a clear down-field shift is observed for two of the signals of (*E*)-**Azo-OEG-2** when increasing host concentration.

With this methodology, a K_a value for the α-CD:(*E*)-**Azo-OEG-2** complex of 584 ± 83 was determined, a value which is below what was expected according to reference data.[29] Nevertheless, this should not prevent the eventual modulation of the

Azo-OEG-2 affinity towards α-CD given that the K_a values for (*Z*)-**Azo-OEG-2** are expected to be much lower than for the (*E*)-**Azo-OEG-2**.

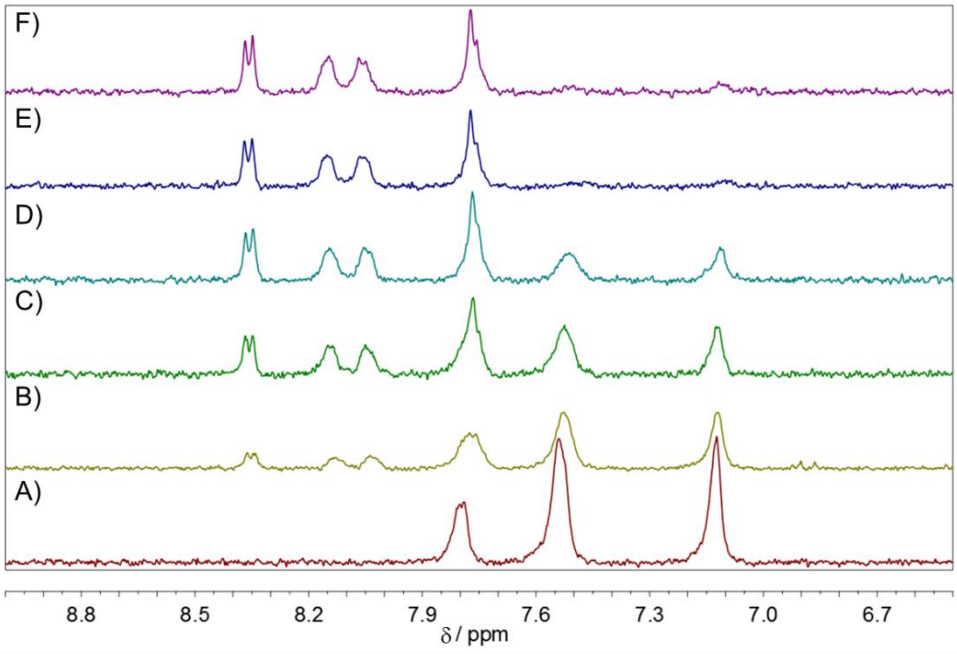

Figure 5.16. ^{1}H NMR spectral changes of A) **Azo-OEG-2** (0.5 mM) in D_2O upon addition of B) 2 mM, C) 4 mM, D) 6 mM, E) 8 mM and F) 10 mM α-CD.

5.3- PREPARATION OF GOLD NANOPARTICLES FUNCTIONALIZED WITH α-CYCLODEXTRIN AND AZOBENZENE LIGANDS

Once the thiolated ligands had been prepared and characterized, attention was focused on the preparation of the corresponding functionalized Au NPs. As commented in the introduction of this chapter, two different sets of Au NPs had to be synthesized in order to study the formation of Au NP heteroaggregates promoted by host-guest interactions. One set of NPs had to be functionalized with the desired host, in this case the thiolated derivative of α-CD **αCD(SH)$_6$**, and the other with the corresponding guest, in this case **Azo-OEG-2**, the synthesis and characterization of which has been already described in section 5.2. In order to be able to distinguish the eventual formation and dissociation of heteroaggregates, both sets of NPs had to have unambiguously different radii. In addition, NPs with a big difference in size should exhibit a larger area where their coating layers can interact when they are close to each other, thus enabling the formation of a higher number of supramolecular host-guest interactions with respect to NPs of the same diameter. Both sets of functionalized Au NPs were prepared via the the two-step process described in chapter 3 for the preparation of CD-coated Au NPs. Consequently, citrate-stabilized Au NPs had to be previously synthesized and, later on, subjected to ligand exchange processes. However, regarding the synthesis of Au NPs with large diameters, the preparation of such colloidal dispersions having good monodispersities is usually difficult. Fortunately, this problem could be solved with the use of the seed-growth method described in chapter 3.

5.3.1- Preparation of citrate-stabilized Au NPs using the seed-growth method

Although the seed-growth method choosen for the preparation of Au NPs can provide nanoparticles with diameters up to 180 nm, for the purpose of this study it was not necessary to reach such large sizes and, as such, to perform a large number of growth steps. In particular, we decided to realize seed-growing of Au NPs up to the 5th generation, which should have an expected diameter of about 45 nm.[34] This would provide a 35-nm-difference with respect to the Au NP seeds of the process, which were to be selected as the group of small particles in our studies. As already commented,

such difference in diameter would permit to easily distinguish between both populations of Au NPs by electron microscopy, thus ensuring unambiguous monitorization of the selective formation of heteroaggregates.

Table 5.2 summarizes the results obtained for the synthesis of Au NPs using the seed-growth method described in chapter 3 up to the 5th generation. These nanoparticles were characterized by means of TEM and UV-vis spectroscopy.

Table 5.2. Sizes and optical properties of the Au NPs obtained after different growth steps compared with reference data.

Growth step	$\lambda_{SPR,max}$ [a] / nm	Expected diameter [b] / nm	Mean diameter [c] / nm
Seeds	519	3.2	8.2 ± 1.1
G1	522	19.7	11.6 ± 1.6
G2	525	31.9	17.7 ± 2.6
G3	525	31.9	18.8 ± 2.5
G4	527	38.5	23.0 ± 2.8
G5	530	46.9	32.1 ± 4.9

[a] Wavelength of the maximum of the surface plasmon resonance band. [b] According to equation 3.1. [c] As determined from TEM.

As shown in Figure 5.17, TEM analysis of the obtained gold collids revealed that, indeed, succesive synthetic steps led towards bigger NPs, all of which displaying rather spherical shapes. Monodispersity was essentially preserved during the growth cycles, the standard deviation of the mean size oscillating between 12 and 15 % of the average diameter. However, the measured diameter differed in all cases from the expected value. Thus, larger NPs were expected to be formed from G0 to G5 and the measured diameters presented discrepancies from 5 to 15 nm. Even though we aimed at the preparation of NPs with ~ 45 nm in diameter, the obtained G0 and G5 NPs presented a ~ 25 nm diference in diameter that still allowed the visualization of an eventual formation of Au NP heteraggregates upon host-guest complexation.

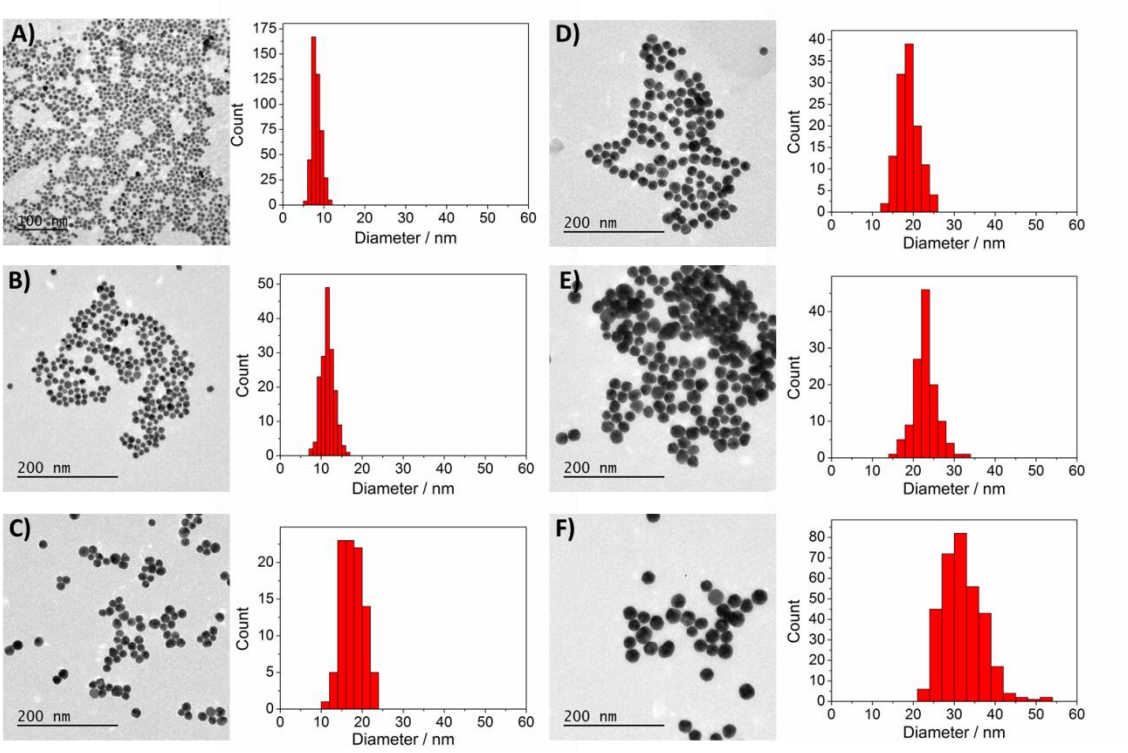

Figure 5.17. TEM images of citrate-stabilized Au NPs synthesized by the seed-growth method. (A) seeds (**G0**) and (B-F) successive **G1**-**G5** generations. In each case, the corresponding size distribution histogram is shown, which was obtained after analysis of a population of more than 100 nanoparticles.

Figure 5.18 shows the UV-Vis spectra recorded for the different generations of Au NPs synthesized. As expected, the size increase of the gold colloids correlated with an increase of their molar absorptivities in the visible region together with a bathochromic shift of the λ_{max} corresponding to the SPR band. Actually, a total 11-nm red shift was observed from Au seeds to G5, thus further proving the growth of Au NPs.

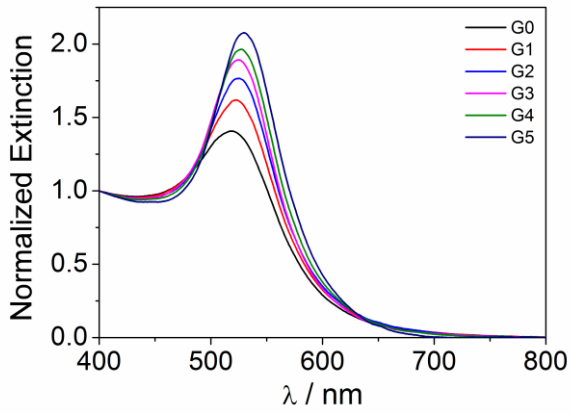

Figure 5.18. UV-Vis extinction spectra of the Au NP colloids in water obtained by the seed-growth method up to the 5th generation. All spectra are normalized at 400 nm for better comparison. The initial seeds are depicted as **G0**.

Even though the results obtained for citrate-stabilized Au NPs prepared by the seed-growth method were not those expected in terms of size, they were still good enough to proceed with the preparation of functionalized Au NPs. Au NP seeds and G5 with diameters of 8 and 32 nm, respectively, served perfectly well as the small and the big sets of nanoparticles that we wanted to use in the preparation of heteroaggregates. Threfore, these two sets of citrate-stabilized Au NPs were separately functionalized with both host and guest ligands, in order to study how their capacity to form Au NP heteroassemblies was influenced by the presence of the host or guest molecules in the small or the big NPs.

5.3.2- Preparation of α-CD(SH)$_6$-functionalized gold nanoparticles: AuNP-G0@αCD and AuNP-G5@αCD

The preparation of Au NPs functionalized with the supramolecular host **αCD(SH)$_6$** was carried out as described in chapter 3 for the preparation of β-CD-functionalized Au NPs. Addition of the thiolated ligand partially disolved in a basic ethanol solution to a freshly prepared citrate-stabilized Au NPs colloid provided the host-capped NPs desired. Two sets of Au NPs functionalized with **αCD(SH)$_6$** of different diameters were prepared:

(a) AuNP-G0@αCD

These NPs were prepared from the seeds colloid of the seed-growth method employed for the preparation of larger Au particles, which had ~8 nm in diameter. After ligand exchange, the sample was purified to remove the excess of free macrocyclic hosts and the citrate molecules replaced. For this, the same procedure already discussed in chapter 3 was employed, which involved precipitation of the nanoparticles, dialysis against DMF and final resuspension in the minimum amount of water.

(b) AuNP-G5@αCD

The other set of NPs functionalized with **αCD(SH)$_6$** corresponded to the 5th generation (~30 nm in diameter) of the seed-growth procedure described earlier in this chapter. The obtention and purification of **AuNP-G5@αCD** was completely analogous to that of **AuNP-G0@αCD**. The final redispersion of **AuNP-G5@αCD** in deionized water also served as a stock solution for further experiments.

After ligand exchange, **AuNP-G0@αCD** and **AuNP-G5@αCD** were characterized by TEM. As can be seen in Figure 5.19, the resulting Au NPs preserved their size and shape, revealing that ligand exchange occured without NP aggregation.

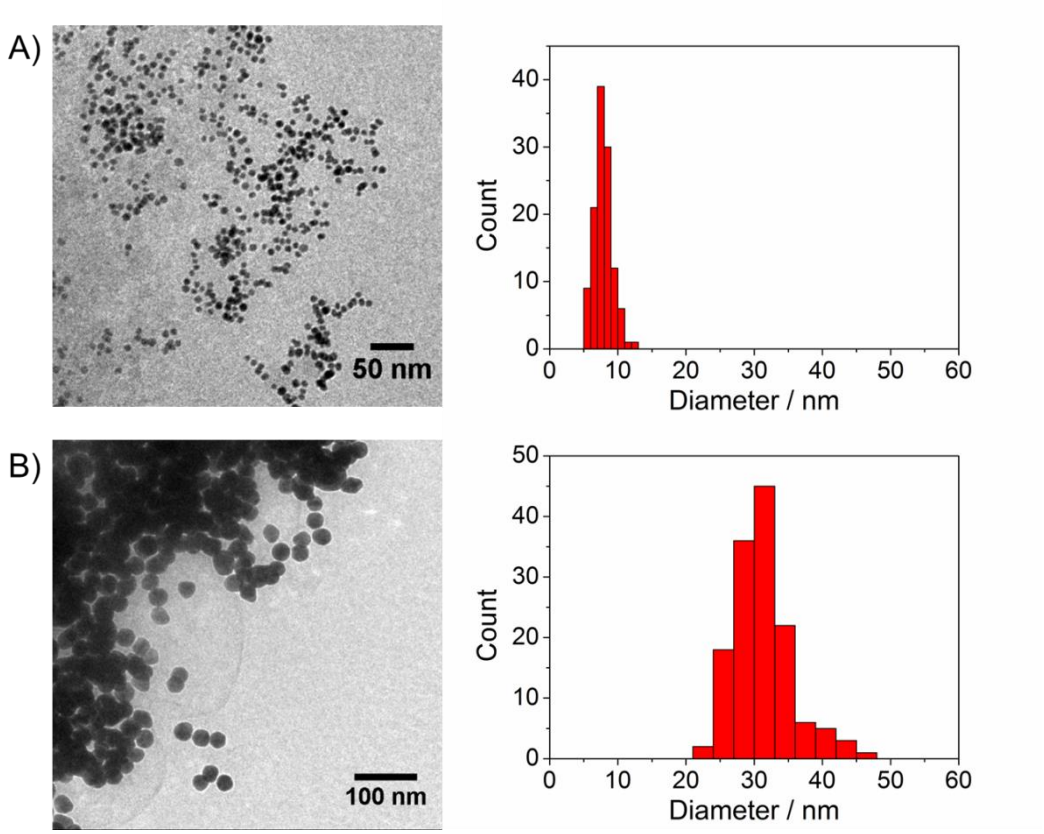

Figure 5.19. TEM images of aCD-functionallized Au NPs prepared by the ligand exchange procedure A) **AuNP-G0@αCD**, mean diameter 7.9 ± 1.3 nm and B) **AuNP-G5@αCD**, mean diameter 30.6 ± 4.2 nm. In both cases the corresponding size distribution histogram is shown, which was obtained after analysis of a population of more than 100 anoparticles.

5.3.3. Preparation of azobenzene/olygoethyleneglycol-functionalized gold nanoparticles: AuNP-Gn@ AzoOEG/OEG

Au NPs bearing a mixture of the photoresponsive azobenzene derivative **Azo-OEG-2** and the chromophoreless oligoethylene glycol ligand **OEG-SH** were prepared with the already described ligand exchange method (**AuNP-Gn@AzoOEG/OEG**). Thus, the proper amounts of ligands were dissolved in basic ethanol and subsequently added to the citrate-stabilized Au NPs colloidal dispersion of interest. Importantly, different sets of AuNPs bearing variable amounts of the thiolated ligands **Azo-OEG-2** and **OEG-SH** were prepared, since we wanted to tune the molar ratio of these two

compounds in the mixed monolayer around the nanoparticles to maximize: (i) resuspensibility of **AuNP-Gn@AzoOEG/OEG** in aqueous media; and (ii) supramolecular host-guest interaction with **AuNP-Gn@αCD** as to ensure heteroassembly formation. Typical **Azo-OEG-2:OEG-SH** molar ratios used in such ligand exchange processes were 1:5, 1:10 and 1:20.

Although the ligand exchange conditions were equal to those used for the preparation of CD-modified Au NPs, the purification procedure of **AuNP-Gn@AzoOEG/OEG** had to be modified. The **G3** and **G2** generations of the previously synthesized citrate-stabilized Au NPs were used as benchmark samples to alter such purification process, which was finally implemented in the preparation of **AuNP-G1@AzoOEG/OEG** and **AuNP-G5@AzoOEG/OEG**. The reasons for this modification were two-fold. First, in contrast to most of the cyclodextrin derivatives used, **Azo-OEG-2** and **OEG-SH** are monothiolated ligands that can only anchor to the surface of Au NPs by means of a single sulfide bond. As a consequence, they should be more weakly bound to the nanoparticles and, therefore, should be more prone to undergo desorption during manipulation (e.g. centrifugation, dialysis). Second, **Azo-OEG-2** has a limited solubility in water, which means that it might be difficult to remove by centrifugation-resuspension cycles in aqueous media.

In a first set of experiments, we focused our attention on making purification conditions milder as to prevent the thiolated monolayer to suffer from any ligand loss. For this reason, separation of the nanoparticles from the medium were ligand exchange had taken place was done by centrifugation at much lower velocities (~ 4000 rpm or lower). However, instead of providing a well-pelleted Au NP sample with an almost colourless supernatant, centrifugation of a **AuNP-G3@AzoOEG/OEG** ligand exchange mixture at around 4000 rpm gave rise to a sample with a concentrated and loose pellet of AuNPs, from which the supernatant that still displayed a pinkish colour had to be removed with extreme caution; otherwise, redispersion of the colloid often occurred. In addition, the excess of free ligands was next removed by repetitive redispersion-centrifugation cycles in water instead of dialysing the sample in the proper solvent. Unfortunately, this procedure presented two main drawbacks. First, because of the aforementioned limitations of the centrifugation process applied, a non-negligible amount of Au NPs were lost in each of these cycles, as demonstrated by the UV-vis spectra measured for the supernatants collected (Figure 5.20A). Thus, the typical surface plasmon resonance band of Au NPs was observed in those spectra, together with a larger band at around 320 nm arising from the azobenzene chromophore of free

Azo-OEG-2 molecules. Second, the efficiency of the removal of the excess of ligands was found to be poor, since the azobenzene absorption band could still be visible when measuring the UV-vis spectrum of the resulting purified sample (Figure 5.20B). It is important to note that the absorptivity coefficient of the azobenzene moiety in **Azo-OEG-2** ($\varepsilon \sim 2 \cdot 10^4$) is about 5 decades lower than that of Au NPs ($\varepsilon \sim 10^9$). This means that, even in the most favourable scenario where particles were fully coated with a monolayer of **Azo-OEG-2** instead of a mixture of **Azo-OEG-2** and **OEG-SH**, the azobenzene absorption band should have been mainly hidden below the SPR signal, since a maximum amount of ~ 600 azobenzene molecules per particle was expected according to typical packing values of self-assembled monolayers of alkylthiols onto Au NPs.[35]

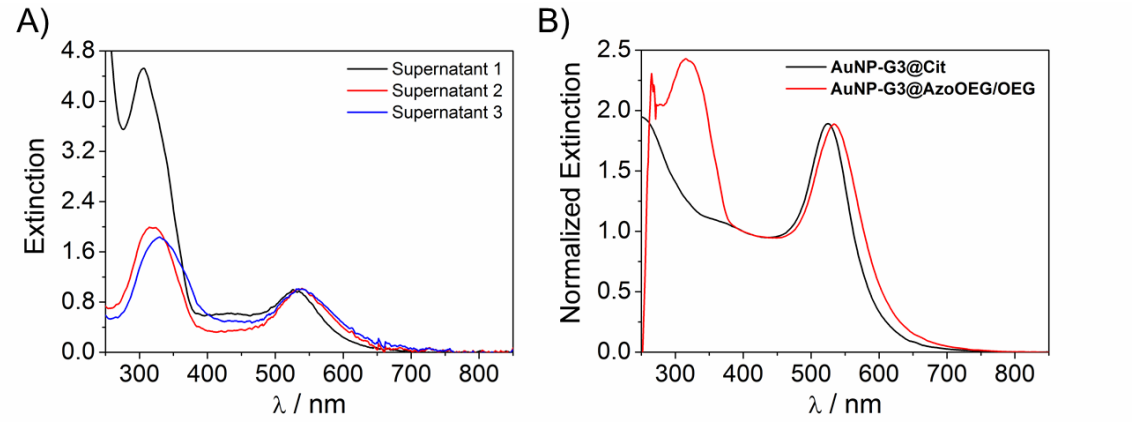

Figure 5.20. (A) UV-Vis spectra of the supernatants obtained after 3 redispersion-centrifugation cycles during the purification of **AuNP-G3@Azo-OEG/OEG** as described in the text. (B) UV-Vis spectrum of the finally separated **AuNP-G3@AzoOEG/OEG** sample compared to that of the initial citrate-stabillized Au NPs.

In view of this result, a second set of purification experiments were run, where it was decided to introduce the use of ACN for the removal of the excess of ligands. With this aim, at the end of the ligand exchange period for a **AuNP-G2@AzoOEG/OEG** sample, the reaction mixture was diluted by the addition of an equal amount of ACN. Centrifugation at 3000 rpm during 40 min then provided a black-metal pellet along the glass tube, from which the supernatant could be easily discarded. Next, further purification of the Au NPs obtained was carried out by a resuspension-centrifugation cycle in a 1:1 ACN:water mixture. The final pelleted AuNPs were resuspended in deionized water and sonicated in an ultrasonic bath, and finally characterized by UV-Vis spectrophotometry (Figure 5.21A). Two main features were revealed by these

measurements. First, no azobenzene absorption band was observed, which indicated efficient removal of the excess of **Azo-OEG-2**. Second, the colloidal dispersion obtained displayed blue colour and a broad SPR band peaking around 650 nm, evidencing agglomeration and/or aggregation of the NPs. No spectral changes were observed upon redispersion in polar protic solvents like MeOH or EtOH, while partial recovery of the narrow, blue-shifted SPR band expected for disaggregated nanoparticles was observed in DMF and DMSO. This suggested that the observed agglomeration was not due to insufficient surface coverage of Au NPs, but to supramolecular interactions between the azobenzene moieties sticking out form the surface of one nanoparticle and the oligoethylene glycol inner coating layer of nearby nanoparticles. Such interactions should be mainly ascibed to solvophobic effects and van der Waals forces, which would explain why Au NPs disassembled upon redispersion in better solvents of the azobenzene group (e.g. DMF and DMSO).

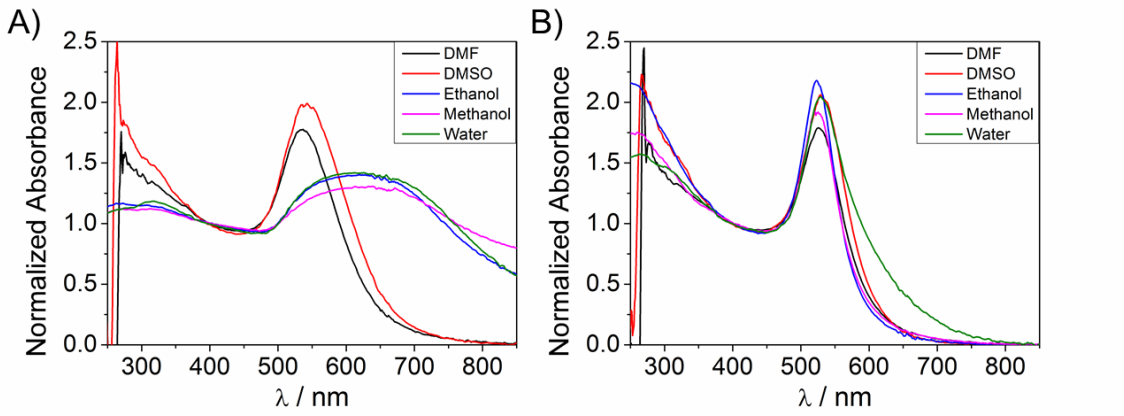

Figure 5.21 UV-Vis spectra of a purified **AuNP-G2@AzoOEG/OEG** sample upon redispersion in different solvents (A) before and (B) after ns-pulsed irradiation at 532 nm during variable times. All spectra were normalized at 400 nm for better comparison.

Based on these observations and the results obtained in previous chapters, disaggregation of the purified **G2@AzoOEG/OEG** sample was attempted through photothermal effects upon irradiation at 532 nm with a ns-pulsed laser source (output power ~ 70 mW). For most solvents considered, this allowed the narrow SPR band centered around 525 nm to be recovered (Figure 5.21B), although variable illumination times were required in each case: as expected, the shortest times were needed for DMF and DMSO, whereas irradiation in water for several min did not enable complete disaggregation of the nanoparticles, as proven by the long absorption tail measured for this sample at $\lambda > 550$ nm.

With all these considerations in mind and applying the last purification process described, different sets of Au NPs bearing the photoresponsive **Azo-OEG-2** ligand were prepared. Table 5.3 shows the **Azo-OEG-2**/**OEG-SH** molar ratios used in this case and the sizes of the initial and final Au NPs after TEM analysis. An **Azo-OEG-2**-free set of nanoparticles was prepared from citrate-stabilized **G4**, which would serve as a reference in the posterior supramolecular association experiments. As in the case of **AuNP-Gn@αCD**, both small (**G1**) and large (**G5**) nanoparticles were functionalized to obtain **AuNP-G1@AzoOEG/OEG** and **AuNP-G5@AzoOEG/OEG** and, for the latter, two different mixing ligand ratios were considered: 1:20 **Azo-OEG-2**/**OEG-SH** (**AuNP-G5@AzoOEG/OEG_1**) and 1:5 **Azo-OEG-2**/**OEG-SH** (**AuNP-G5@AzoOEG/OEG_2**). It must be noticed that, **G1** NPs were finally employed to serve as the small NP set bearing **Azo-OEG-2** instead of seeds, due to an experimental misfortune with the latter. Moreover, only the **Azo-OEG-2/OEG-SH** 1/5 ratio was prepared for this set of NPs since homoaggregation studies of **AuNP-G5@AzoOEG/OEG** (see below) suggested that it was the proper ligand ratio to maximize eventual host-guest interactions between Au NPs. In addition, the **Azo-OEG-2/OEG-SH** 1/5 ratio with **OEG-SH** as the major component of the NP coating layer assured good resuspensibilty in water of the final colloids.

Table 5.3. Ligand ratio and diameter of NPs bearing the photoresponsive unit **Azo-OEG-2**

Au NP generation	AuNP-Gn size / nm	Azo-OEG-2	OEG-SH	Au NP size / nm
G4	23.0 ± 2.8	0	1.00	24.3 ± 2.2
G5 (1)	32.1 ± 4.9	1	20	34.3 ± 4.7
G5 (2)	32.1 ± 4.9	1	5	33.8 ± 5.5
G1	11.6 ± 1.6	1	5	11.4 ± 2.0

After purification of the obtained particles, it was decided to redisperse **AuNP-G4@OEG**, **AuNP-G5@AzoOEG/OEG_1**, **AuNP-G5@AzoOEG/OEG_2** and **AuNP-G1@AzoOEG/OEG** in the minimum amount of DMF to allow maximum disaggregation of Au NPs. Such disaggregation could also have been done by photothemal effects

upon ns-pulsed laser irradiation, but it was decided to avoid such procedure to prevent possible adsorbate desorption due to the monothiolated nature of stabilizing molecules. The aforementioned colloids were characterized by TEM, evidencing that their size and morphology were maintained after ligand exchange (Table 5.3).

5.4- SUPRAMOLECULAR HOST-GUEST SELF-ASSEMBLY OF GOLD NANOPARTICLES

As already discussed in the introduction of this chapter, many different strategies have been used in order to prepare Au NP assemblies, among which supramolecular host-guest association has been profusely exploited. However, it has mainly been used for the preparation of Au NP homoassemblies, while the preparation of Au NP heteroassemblies has only been scarcely attempted. The different Au NPs that have been prepared in the previous sections of this chapter intend to open new avenues for the preparation of such aggregates, eventually aiming at controlling the assembly-disassembly process with an external stimulus. Before entering the discussion on the experiments performed to achieve this goal and the results obtained, two important aspects must however be previously considered. First, it must be taken into account that, as already discussed along this thesis, Au NPs coated with organic ligands are susceptible to undergo non-selective homoaggregation, which would compete with the selective heteroaggregation process targeted in this work via host-guest chemistry. For this reason, a detailed study was conducted on this issue prior to exploring the formation of heteroassemblies upon mixing nanoparticles functionalized with complementary supramolecular host and guests.

Second, experimental techniques are needed that unambiguously report on the formation of Au NP aggregates in colloidal suspension, the medium in which nanoparticle homo- and heteroassembly are expected to take place. TEM analysis of the samples prepared by simply drop-casting or spin-coating an aliquot of the liquid suspension onto a proper support is not the best option, since artifacts may appear due to undesired Au NP aggregation occurring during solvent evaporation. Two main alternatives could in principle solve this problem. On the one hand, dinamic light scattering (DLS) techniques are able to give information on the size and shape of nm-sized species in solution, but unfortunately it is not accesible to us in a daily work basis. On the other hand, due to the optical properties of Au NPs, it could be possible to monitor Au NP assemblies by UV-Vis spectroscopy. However, it may give very contrasting results depending on the size and nature of the aggregates formed, since relatively big Au NP aggregates may lead to rather small spectral changes[36] that may be misattended depending on the effect of the aggregation over the initial sample.

As an alternative, Cryo-TEM analysis was found to be a good choice to evaluate the self-assembly processes of Au NPs in this work. In this technique, sample

preparation for TEM characterization is performed via ultrafast freezing of the small liquid volume of interest by quick immersion in liquid ethane. Although a specific apparatus is required for sample preparation as well as a special TEM sample holder is needed to prevent the sample to defreeze, data is then acquired using typical instruments and procedures in transmission electron microscopy. The main benefit of this technique compared to conventional TEM arises from the fact that a more representative image of the actual situation in the initial liquid sample can be obtained. Therefore, this should allow decreasing the amount of artifacts that may appear in conventional analysis due to unwanted aggregation induced by solvent evaporation.

5.4.1- Ligand-free AuNP homoassembly

As previously commented, before studying the association of different Au NPs driven by host-guest chemistry, we first investigated their tendency to form unspecific supramolecular interactions that could result in nanoparticle homoaggregation. Hydrogen bonding, hydrophobic effects, and other types of supramolecular interactions between surface ligands in different particles and with solvent molecules are very important to determine the actual aggregation state of Au NPs colloids, as it is the case for host-guest-mediated Au NP assembly. Therefore, the different sets of Au NP that were prepared in previous sections were separately submitted to Cryo-TEM analysis to check their tendency to self-assemble in the absence of the complementary host and guest molecules. Samples for this analysis were prepared by dilution of an aliquot of the corresponding stock solution, which were subjected to the fast freezing procedure described above.

(a) AuNP-G4@OEG

This set of NPs was prepared to serve as a reference when studying the supramolecular host-guest-based interaction between of host- and guest-functionalized nanoparticles. As commented in the previous section, **AuNP-G4@OEG** were only stabilized by means of **OEG-SH** and, therefore, had no capacity to form host-guest interactions. However, owing to their terminal hydroxyl groups, they could associate via hydrogen bonding between close-by NPs. Such behaviour was however not observed even for highly concentrated samples in water, as evidenced by Cryo-TEM analysis. Figure 5.22 shows representative Cryo-TEM images of these samples, where almost only separated NPs are observed. Actually, even when proximal to each other,

separation distances between the nanoparticles in these images are way beyond the length of two interacting **OEG-SH** molecules (~ 3 nm according to molecular mechanics calculations). A possible explanation for these results is that hydrogen bonds between nearby molecules in a single NP are preferred over hydrogen bonds between ligands in different NPs. In addition, hydrogen bond formation between solvent molecules and the surface hydroxyl groups may also compete with NP aggregation.

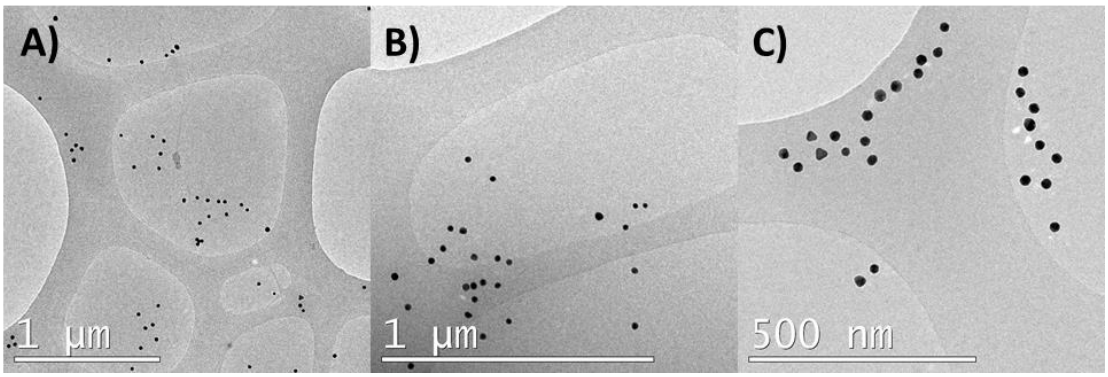

Figure 5.22. Representative Cryo-TEM images of **AuNP-G4@OEG** in water suspension.

As a further proof of this behaviour, the UV-Vis spectra of **AuNP-G4@OEG** samples in water and different concentrations were measured and compared to those of citrate-stabilized **G4**. Negligible spectral changes were observed, which was in agreement with the absence of aggregates in the Cryo-TEM images.

(b) Host-functionalized Au NPs

Two different sets of **AuNP-Gn@αCD** were prepared. One with a small diameter, corresponding to the seed solution of the seed-growth method employed for the synthesis of citrate-stabilized Au NPs, and the other one with a large diameter, corresponding to the 5th generation of the grown nanoparticles.

AuNP-G0@αCD: As previously observed for β-CD- and γ-CD-modified Au NPs, **AuNP-G0@αCD** aggregated in water in the absence of any supramolecular guest. Thus, Cryo-TEM images in Figure 5.23A-C reveal that, indeed, **AuNP-G0@αCD** in aqueous suspension could be found in the form of big and small clusters as well as free NPs. This phenomenon was mainly observed after the dialysis purification process, as it was

the case for the other cyclodextrin-functionalized nanoparticles. In all probability, the effect of precipitating the Au NPs during this process and the high concentration of the stock solution that was prepared afterwards favoured the formation of Au NP assemblies via rather stable hydrogen bonding networks, which likely benefited from the cooperative effects arising from the interaction of two cyclodextrin moieties via multiple hydrogen bonds. Becasue of the supramolecular nature of these interactions, they were supposed to be weakened upon an eventual temperature rise and, as previously observed for other host-modified NPs, such assemblies could be disaggregated almost completely under ns-pulsed laser irradiation at 532 nm (Figure 5.23D-F).

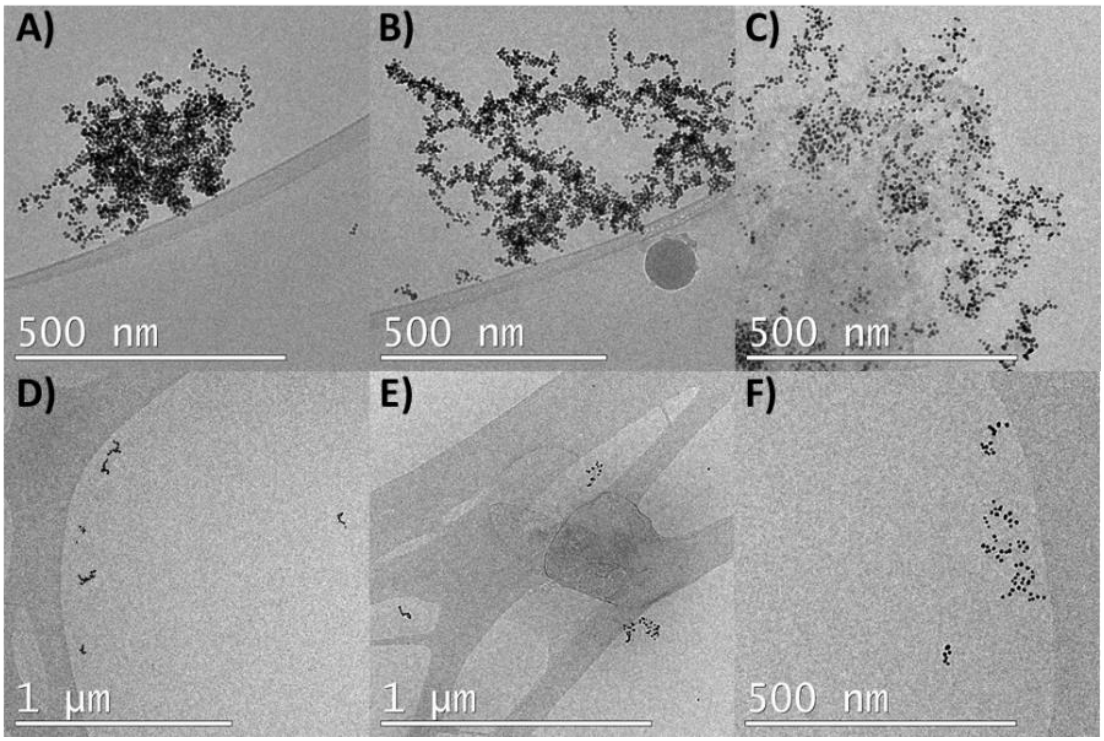

Figure 5.23. Representative Cryo-TEM images of **AuNP-G0@αCD** in aqueous colloids (A-C) before and (D-F) after ns-pulsed laser irradiation at 532 nm (10 mJ/pulse, 10 Hz).

AuNP-G5@αCD: **AuNP-G5@αCD** presented nearly the same behaviour as **AuNP-G0@αCD**. After the purification process, Cryo-TEM analysis of the final stock suspension reveled the formation of big and small clusters as well as isolated NPs (Figure 5.24). As in the case of **AuNP-G0@αCD**, ns-pulsed laser irradiation at 532 nm of **AuNP-G5@αCD** aqueous suspensions resulted in the dissociation of the assemblies observed, thus uncovering the supramolecular nature of the aggregates. In this case,

however, a very low irradiation power had to be used (~50 mW), since we had previous experience that large particles are more prone to undergo light-induced ablation than smaller particles.

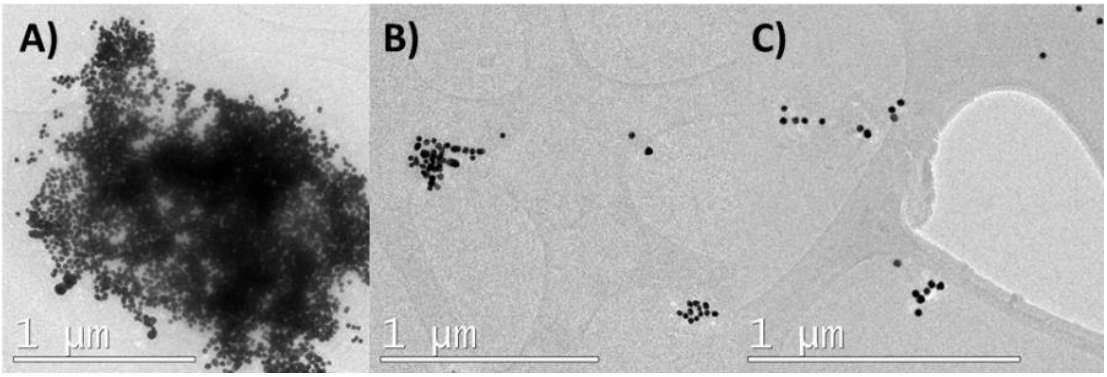

Figure 5.24. (A-C) Representative CRYO-TEM images of **AuNP-G5@αCD** in aqueous suspension.

(c) Guest-functionalized Au NPs

Three different sets of guest-functionalized Au NPs were studied: two distinct **AuNP-G5@AzoOEG/OEG** samples bearing a 1:20 (**AuNP-G5@AzoOEG/OEG_1**) and 1:5 (**AuNP-G5@AzoOEG/OEG_2**) molar ratio of **Azo-OEG-2** and **OEG-SH** respectively and **AuNP-G1@AzoOEG/OEG** with a 1:5 molar ratio of both thiolated ligands.

AuNP-G5@AzoOEG/OEG: Figure 5.25 shows different Cryo-TEM images of **AuNP-G5@AzoOEG/OEG_1** (A-C) and **AuNP-G5@AzoOEG/OEG_2** (D-F) in aqueous suspension, which illustrate their tendency to form aggregates of nanoparticles. Interestingly, both sets of NPs appeared to be very different in behaviour. On the one hand, the sample with a lower load of the azobenzene ligand (1:20 **Azo-OEG-2**/**OEG-SH** ratio) gave rise to the formation of chain-like aggregates of NPs. As explained before for the **AuNP-G1@AzoOEG/OEG** sample, this might be due to the supramolecular intractions established between azobenzene groups in different nanoparticles or azobenzene groups in one nanoparticle and OEG chains in another. Surprisingly, the sample with a higher load of azobenzene ligands (1:5 **Azo-OEG-2**/**OEG-SH** ratio) produced a much lower number of aggregates with smaller dimensions and many isolated NPs could be observed. A possible explanation to this behaviour would be that **Azo-OEG-2** and **OEG-SH** seggregated in such particles

because of the higher concentration of the azobenzene-containing ligands. As a result, patches of close-packed azobenzene groups would appear onto the nanoparticle surface, which would strongly interact via π-π interactions, thus disfavouring supramolecular aggregation with other nanoparticles.

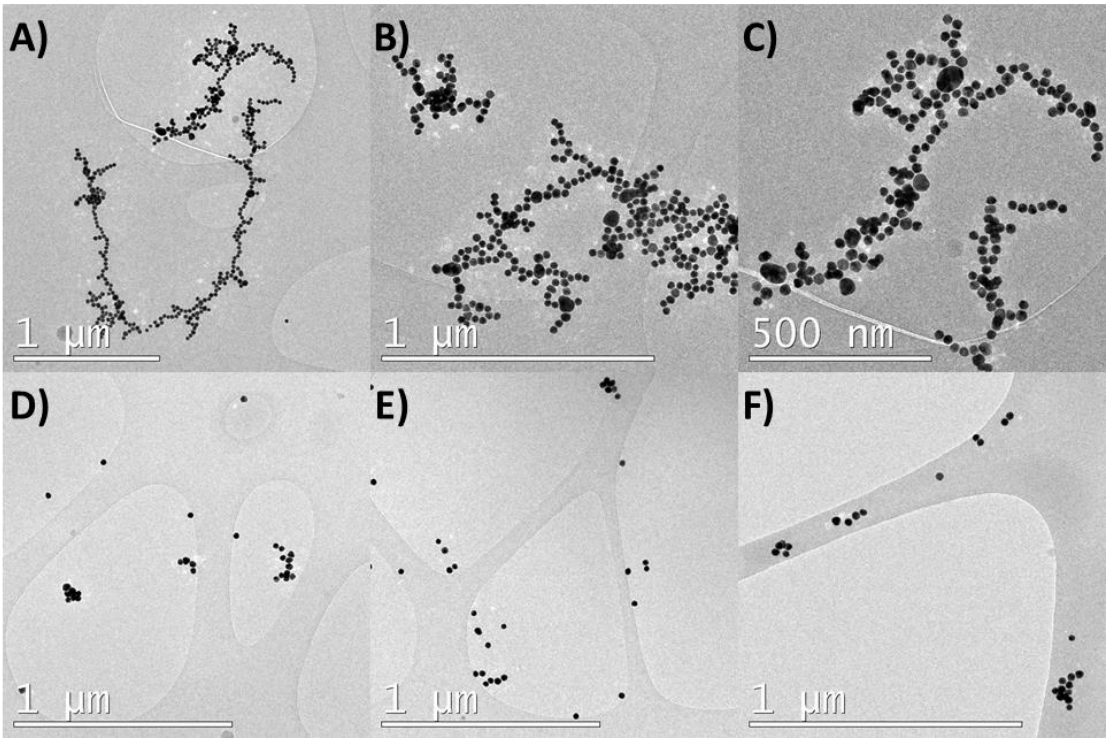

Figure 5.25. Representative Cryo-TEM images of **AuNP-G5@AzoOEG/OEG** with a molar ratio of **Azo-OEG-2**/**OEG-SH** of 1/20 (**AuNP-G5@AzoOEG/OEG_1**) (A)-(C) and 1/5 (**AuNP-G5@AzoOEG/OEG_2**) (D)-(F). At higher **Azo-OEG-2**/**OEG-SH** molar ratios, small clusters and isolated particles can be seen whereas at lower **Azo-OEG-2**/**OEG-SH** ratios, chain-like structures could be seen rather than isolated particles.

AuNP-G1@AzoOEG/OEG: As observed in the Cryo-TEM images in Figure 5.26, **AuNP-G1@Azo-OEG/OEG** in water suspension was found to give rise to two main distinct structures of aggregates: large nanoparticle agglomerations (Figure 5.26A-B) and small flower-like clusters formed by a reduced number of Au NPs (Figure 5.26D-F). Surprisingly, the latter type of structure was found all along the sample and, even though it was not formed by a regular number of NPs, it somehow had a regular size of about 40 nm in diameter. By contrast, almost no individual particles were found (Figure 5.26C). The reason for such unspecific aggregation process was attributed to the interdigitation of the azobenzene moieties on the surface of a NP into the OEG domains of another particle, which probably was driven by a combination of

hydrophobic effects and van der Waals forces. An alternative explanation would be the formation of π–π attractive interactions between nearby azobenzenes in close-by nanoparticles and, actually, a combination of all these supramolecular effects would probably account for the aggregation of Au NPs. In any case, we hypothesized that, in a first stage, this led to the formation of the smaller clusters observed by Cryo-TEM, which in time slowly merged into the larger aggregates.

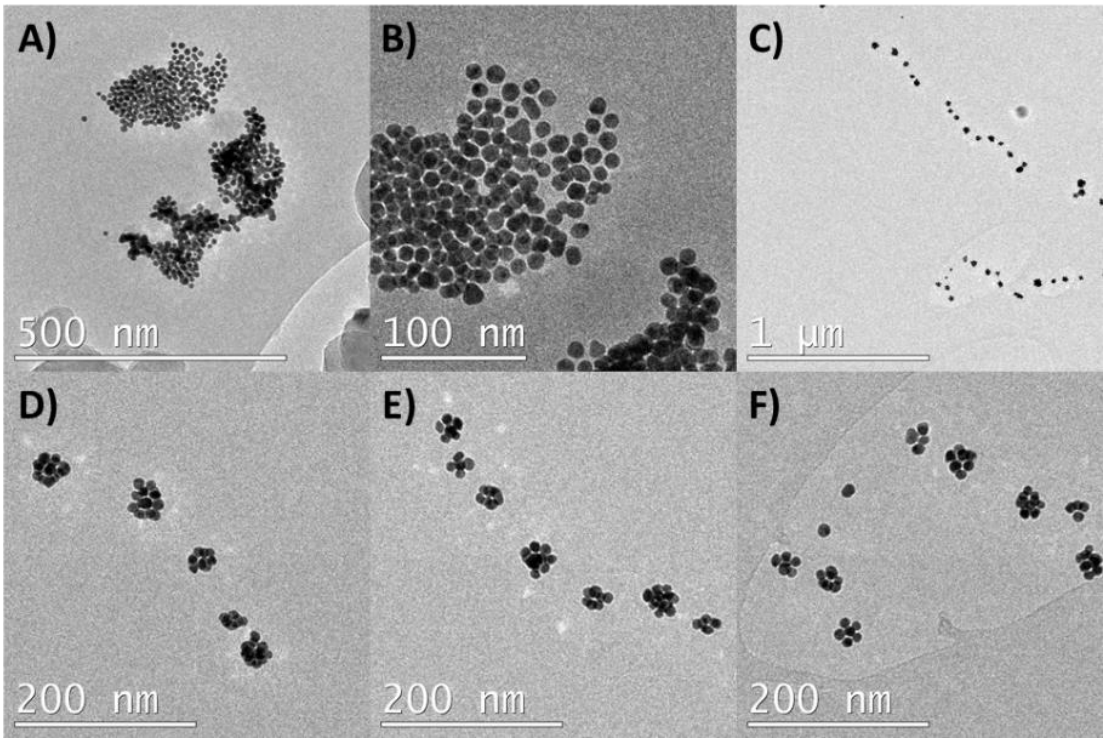

Figure 5.26. Representative Cryo-TEM images of **AuNP-G1@Azo-OEG/OEG** in water suspension where (A-B) large aggregates, (C) some individual particles and (D-F) small flower-like clusters are observed.

5.4.2- Ligand-induced Au NP homoaggregation

In view of the results observed when separately studying the self-assembly processes of the different Au NPs prepared, it was decided to perform some additional preliminary experiments where the aggregation of each type of nanoparticle was to be induced by addition of free host or guest molecules.

(a) AuNP-G4@OEG + 11

This experiment was found to be very interesting from the molecular interaction point of view. Contrary to what was observed for the NPs functionalized with azobenzene ligands, no homoaggregation was observed for **AuNP-G4@OEG**. On the other hand, one of the possible association mechanisms for the azobenzene-containing NPs was postulated to be the inclusion of the azobenzene groups on the surface of one nanoparticle inside the OEG domains of the coating layer of other particles. Based on these precedents, the addition of the free bis-azobenzene ditopic ligand **11** to a solution of **AuNP-G4@OEG** should cause the homoaggregation of the NPs.

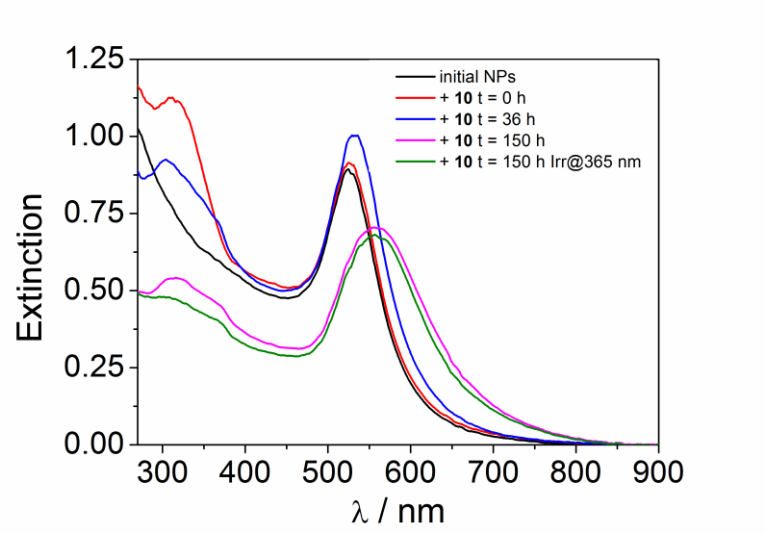

Figure 5.27. Variation of the UV-Vis spectra of **AuNP-G4@OEG** in water suspension over time after the addition of 30 μL of a 1.9 mM acetonitrile solution of bis-azobenzene **11**. After 150 h, the sample was irradited at 365 nm to induce *E*→*Z* photoisomerization of the free ligand.

This process was mainly investigated by UV-vis spectroscopy. As can be seen in Figure 5.27, the addition of disulfide **11** to a colloidal dispersion of **AuNP-G4@OEG** caused the SPR band of Au NPs to slightly red-shift almost instantaneously, thus proving the formation of Au NP assemblies. Moreover, additional changes were observed in time, the SPR band further red-shifted and broadened due to the formation of even larger aggregates, some of which precipitated and were observable by naked eye. Additionally, the π→π* absorption band of **11** also red-shifted and decreased in intensity, probably due to its distinct absorption inside the OEG environment and its co-precipitation with NP aggregates. As expected, all these observations can be explained on the basis of the supramolecular interactions between the azobenzene moieties of the free ligand and the OEG coating-layer of the nanoparticles, which must be mainly driven by hydrophobic effects and van der Waals forces because of the apolar nature

of azobenzene groups. Furthermore, they are an indirect proof that the homoaggregation previously observed for separated **AuNP-G1@AzoOEG/OEG** and **AuNP-G5@AzoOEG/OEG** colloids was mainly due to the interdigitation of the azobenzene chromophoric units in one nanoparticle and the OEG domains of another. Therefore, this demonstrates that the importance of unspecific supramolecular interactions such as hydrophobic effects must not be overlooked when considering NP aggregation by means of specially desgined supramolecular interactions that may be driving this process.

Once **AuNP-G4@OEG** were assembled by addition of **11**, we attempted the *E*→*Z* photoisomerization of the azobenzene groups of this ligand by irradiation with UV light, in order to influence on the aggregation state of the sample. Unfortunately, although changes in the $\pi \rightarrow \pi^*$ band of the azobenzene moiety were observed that suggested that photoisomerization indeed took place, no clear variation of the SPR band was found (Figure 5.27). This allowed us concluding that the unspecific interaction between azobenzenes and OEG layers was not significantly affected by the isomerization state of the chromophore.

(b) AuNP-G0@αCD + 11

An analogous experiment to that already described for **AuNP-G4@OEG** was also performed with **AuNP-G0@αCD**, for which addition of bis-azobenzene **11** might result in nanoparticle aggregation by means of supramolecular host-guest complex formation. In this case, the addition of increasing amounts of **11** to different samples of **AuNP-G0@αCD** was carried out and, afterwards, the evolution of the resulting mixtures was monitored in time (Figure 5.28). Immediately after the addition of **11**, no clear spectral changes were observed for the SPR band of the nanoparticles, specially due to the distorsion introduced by the intense absorption band at ~325 nm arising from the azobenzene groups of the free ligand. Surprisingly, after incubation of these mixtures for 245 h in the dark and at room temperature, major spectral changes were only observed for the azobenzene absorption band, which slightly red-shifted and dramatically decreased in intensity. This behaviour could only be attributed to precipitation of **11** owing to its poor solubility in water, since formation of inclusion complexes into the α-CD cavity should not have resulted in such large variations of the chromophore absorptivity.

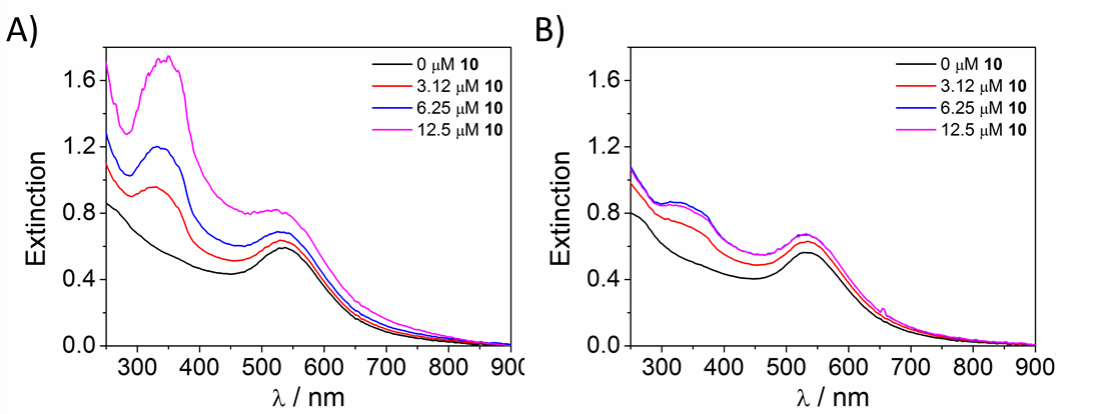

Figure 5.28. UV Vis spectra of 4 different samples of **AuNP-G0@αCD** in water suspension (A) right after the addition of variable amounts of a 1.9 mM acetonitrile solution of **10** and (B) after incubation for 245 h.

On the other hand, contrary to what was observed in the case of **AuNP-G4@OEG**, the SPR band of Au NPs remained almost unaffected in time regardless of the amount of **11** added. It must be noted that this observation did not exclude the possibility that supramolecular host-guest association indeed happened, but it was an indication that the aggregates that would have resulted from such interaction would not have been larger than those already formed by unspecific homoassembly. Therefore, this uncovered the difficulties that we might encountered when attempting ligand-induced Au NP heteroaggregation.

5.4.3- Ligand-induced Au NP heteroagreggation

Owing to severe time and material constraints, we could not explore in depth the heteroassembly of Au NPs driven by supramolecular host-guest interactions. For this reason only preliminary and qualitative results are being exposed in this last section of the chapter. The final heteroassembly experiments were reduced to three cases that tried to serve as a starting point towards the understanding of the formation of such aggregates. Those cases explored two possible situations: the functionalization of large NPs with the photoactive guest molecule and small NPs with the supramolecular host, and the opposite scenario. Additionally, the effect of the amount of guest ligand in the coating layer of Au NPs was also investigated for the former case. Since all the experiments were undergone at high NP concentration, UV-Vis

spectroscopy analysis culd not be performed and the resulting mixed samples were only analysed by Cryo-TEM.

(a) AuNP-G0@αCD mixed with G5@AzoOEG/OEG_1

In this first case, small NPs capped with thiolated α-CD (**AuNP-G0@αCD**) and large NPs bearing a small quantity of azobenzene groups (**G5@AzoOEG/OEG_1**, 1:20 **Azo-OEG-2**/**OEG-SH** ratio) were mixed together in water. Only the **AuNP-G0@αCD** sample was previously irradiated at 532 nm with pulsed laser light to minimize initial homoaggregation, since **AuNP-G5@AzoOEG/OEG_1** was stabilized by monothiolated ligands that could suffer desorption from the NP surface, as commented above. To assure that larger NPs could be fully covered by smaller ones in the heteroaggregates formed, the two components were mixed in a 10:1 **G0:G5** ratio and the resulting sample was incubated under stirring for 24 h in the dark and at room temperature. Then, Cryo-TEM analysis was performed (Figure 5.29).

As can be seen in the selected Cryo-TEM images, large and small NPs were randomly distributed throughout the sample, suggesting a lack of supramolecular host-guest association between them. In particular, **AuNP-G0@αCD** were present in the form of isolated particles, small clusters and chain-like structures, which had already been observed for this separate sample and attributed to unspecific homoaggregation due to hydrogen bonding. By contrast, **AuNP-G5@AzoOEG/OEG_1** mainly appeared as isolated particles and, only in very few cases, they were found to be surrounded by smaller nanoparticles at short enough distances as to expect the formation of supramolecular interactions between them (Figure 5.29E). It must be noted that when the **AuNP-G5@AzoOEG/OEG_1** suspension had been analyzed separately, chain-like aggregate structures had been mostly found. Therefore, it seemed that the presence of the host-coated smaller NPs somehow prevented the formation of such structures presumably by transient host-guest interactions between **AuNP-G5@AzoOEG/OEG** and **AuNP-G0@αCD**.

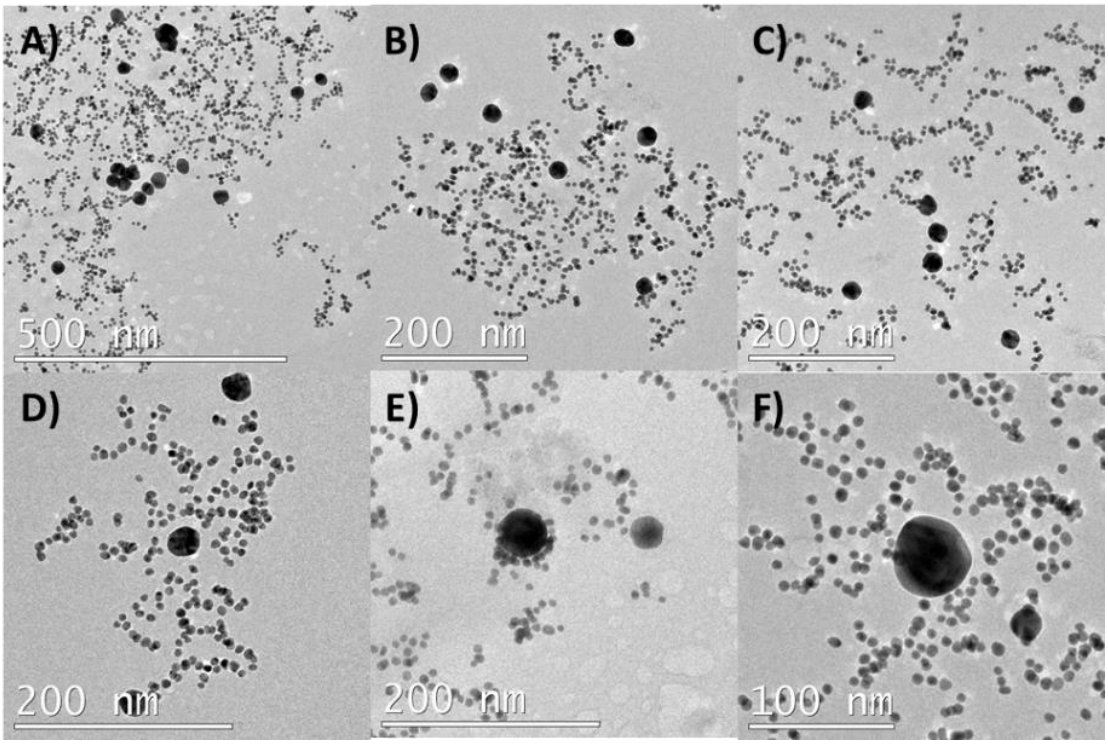

Figure 5.29. Representative Cryo-TEM images of **AuNP-G0@αCD** mixed with **AuNP-G5@AZO-OEG/OEG_1** in water.

(b) AuNP-G0@αCD mixed with AuNP-G5@AzoOEG/OEG_2

In this other case, the effect of increasing the amount of guest molecules around the large NPs was studied, for which **AuNP-G5@AzoOEG/OEG_2** (1:5 **Azo-OEG-2/OEG-SH** ratio) was mixed with **AuNP-G0@αCD** in water in a 10:1 **G0:G5** ratio and incubated for 24 h in the dark and at room temperature under stirring. Again, only the seed sample was previously irradiated at 532 nm with a ns-pulsed laser to try to disassemble the existing clusters and facilitate their eventual association. Unfortunately, as can be seen in Figure 5.30, similar results were obtained to those already presented for the mixture with **AuNP-G5@AzoOEG/OEG_1**. Unspecific and undesired homoclusters were found both for the small and large NPs, mainly in the form of small clusters and chain-like structures. In addition, large assemblies of Au NPs composed of a mixture of both sets of nanoparticles could also be observed (Figure 5.30A), probably indicating that supramolecular host-guest association was taking place. However, because of the higher amount of homoaggregates found, it was clear that selective heteroaggregation of small NPs coated with α-CD and large NPs functionalized with azobenzenes could not be obtained. For this reason, attempts to

induce nanoparticle disassembly by means of photoisomerization of the azobenzene guests were not carried out.

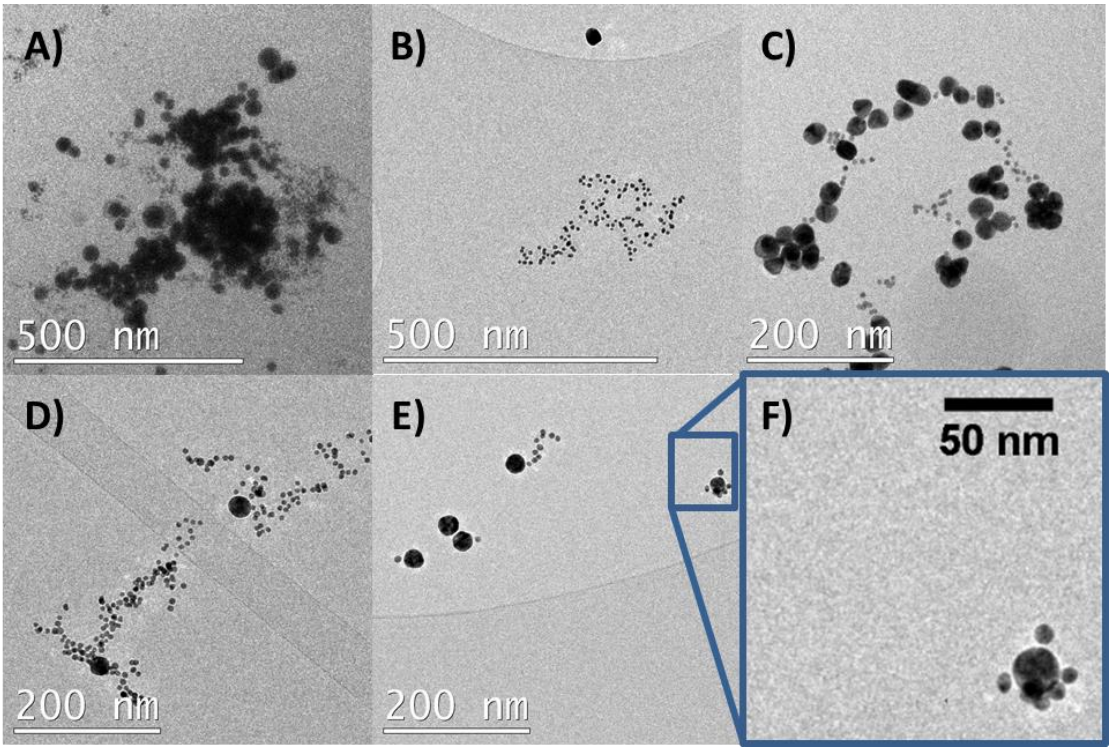

Figure 5.30. Representative Cryo-TEM images of **AuNP-G0@⟨CD** mixed with **AuNP-G5@AzoOEG/OEG_2** in water.

(c) AuNP-G1@AzoOEG/OEG mixed with AuNP-G5@αCD

In this last case we explored the use of small NPs covered with supramolecular guests (**AuNP-G1@Azo-OEG/OEG**) and large NPs functionalized with supramolecular hosts (**AuNP-G5@αCD**). The same conditions of previous experiments were applayed and **AuNP-G1@Azo-OEG/OEG** were mixed together with **AuNP-G5@αCD** in a 10:1 **G1:G5** ratio and were incubated under stirring in the dark and at room temperature. As in the previous cases the α-CD NP set was irradiated at 532 nm.

When analyzing the resulting mixture, Cryo-TEM measurements showed that both large and small NPs appeared to be distinctly distributed. **AuNP-G5@αCD** were found to be rather self-associated but still randomly situted throughout the sample where individual particles could be clearly identified (Figure 5.31A-B) as already observed for this NP set when investigated separately (Figure 5.24). On the other hand **AuNP-G1@AzoOEG/OEG** appeared in the form of big similar homoaggregate

structures to those previoulsy observed, which resembled the flower-like assemblies for this sample shown in Figure 5.26C-F, but in this case displaying bigger sizes (Figure 5.31C-F). The presence of these structures uncovered the big tendency of **AuNP-G1@Azo-OEG/OEG** to self-assemble. Regarding the formation of NP heteroaggregates **AuNP-G5@αCD** appeared in some cases partially surrounded by small particles (Figure 5.31E-F) probably indicating that supramolecular host-guest interactions where stablished. However, undesired homoaggregation of **G1@Azo-OEG/OEG** was the major observation of this experiment.

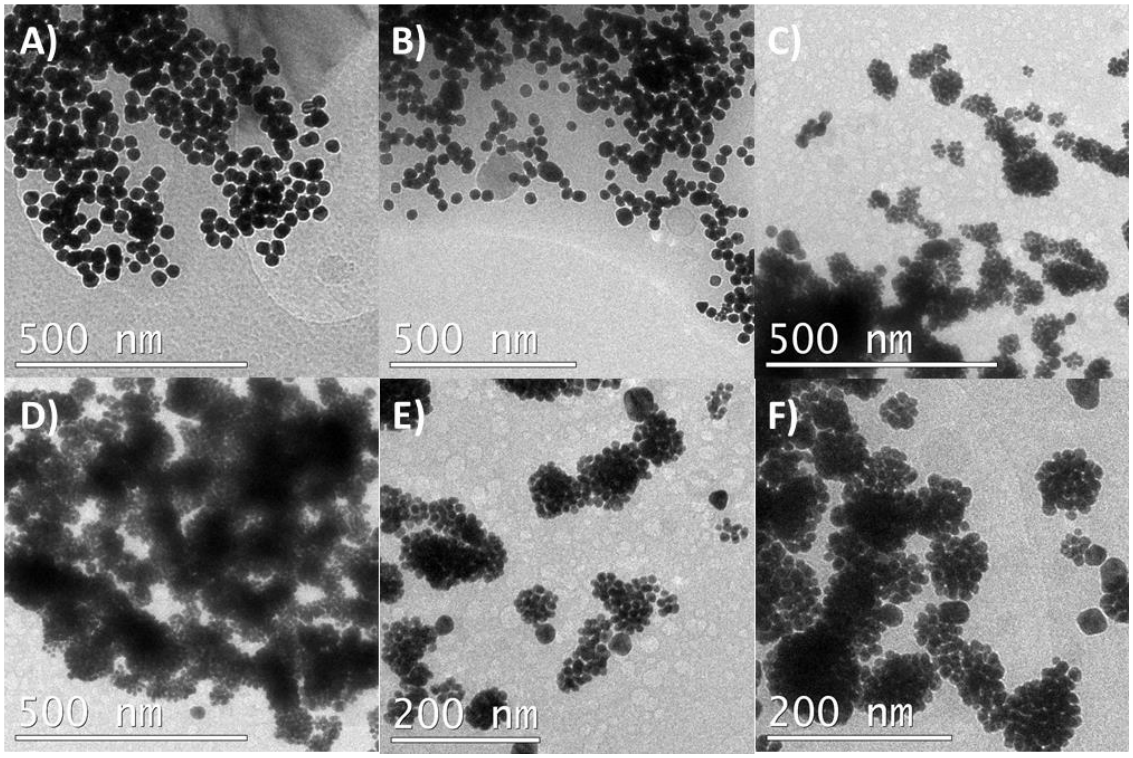

Figure 5.31. Representative CRYO-TEM images of **AuNP-G1@Azo-OEG/OEG** mixed with **AuNP-G5@αCD** in water.

The results obtained in these association experiments clearly evidence the difficulty to study supramolecular interactions at the nanoscale. Even though some behaviour can be predicted, the overall response of each system is unpredictable. With respect to the results exposed so far, the observed NP assemblies were the consequence of interactions that were expected to be less important than those which occupy the central topic of this chapter. Supramolecular host-guest interactions appear to be hindered by less-favoured interactions when the latter are present in such amount

that act cooperatively rising over an eventual threshold which makes them strongly determining of the final state.

Our experiments suggested that the competition between specific and non-specific interactions difficulted the formation of heteroaggregates but favored the formation of homoassemblies. Interestingly, this aspect has not been taken into account in the literature and based in our results in should be profusely revised. Moreover, the vast majority of this type of studies deal with NP homoaggregates which depending on the technique used for their characterization can be missatributed to specific interactions, and perhaps they could be ultimately due to unspecific NP aggregation.

Different factors may explain why unspecific interactions appeared to be more important than the specific supramolecular host-guest association: (i) the number of interactions formed, which should not be a determing factor, since both the specific and the unspecific interactions are based on the same azobenzene ligand; (ii) the strenght of the interactions formed which is a very challenging feature to be investigated and difficult to assess in these type of nano-sized systems; (iii) the kinetics of the association process which is probably faster for the homoaggregation than for the heteroaggregation process,which in turn is mainly due to the steric requirements of the latter. This factor probably explains our results on Au NP heteroassembly, and highlights the necessity to develop new techniques that permit to study the dynamics of these types of processes.

5.5 SUMMARY AND CONCLUSIONS

In this chapter, we explored the controlled formation of Au NP heteroaggregates using cyclodextrin-based host-guest chemistry. For that a system composed of NPs with distinct size bearing **α-CD-(SH)$_6$** or photoresponsive azobenzene-based ligands was devised. First the synthesis of the photoresponsive guest and a chromofore les derivative of it were carried out and aterwards, the methodolgy described in chapter 3 was applied to obtain different sets of host- and guest-functionalized Au NPs. Finally their supramolecular behavior was investigated by UV-vis spectroscopy and Cryo-TEM analysis.

(a) Target compound **OEG-SH** was obtained in four steps and 30% overall yield. The preparation of target compound **Azo-OEG-1** could not be achieved with any of the conditions assayed. Instead, the unexpected formation of thioether compound **XV** was found and an alternative synthesis was devised which provided thiolated target compound **Azo-OEG-2** in 2 steps from disulfide **11** and 49% overall yield.

(b) The homoassembly studies revealed that **α-CD-(SH)$_6$**-functionalized Au NPs had a great tendency to self assemble as previously observed for **β-CD-(SH)$_7$**- and **γ-CD-(SH)$_8$**-functionalized Au NPs with independence of the NP size. A behavior that has not been observed for **G4@OEG** which showed almost no tendency to homoaggregate in solution. Regarding guest-functionalized Au NPs, the low-azobenzene-loading NP set **AuNP-G5@AzoOEG/OEG_1** showed higher tendency for the homoaggregation than the high-azobenzene-loading NPs **AuNP-G5@AzoOEG/OEG_2**. **AuNP-G1@AzoOEG/OEG**, with high azobenzene loading self-assembled in the form of small flower-like clusters of about 5-10 NPs.

(c) Ligand-induced self-assembly of **AuNP-G0@CD(SH)$_6$** with ditopic guest **11** was not detected even after 10 days of incubation. In the case of **G4@OEG**, NP homoassembly was effectively induced by ditopic guest **11** presumably via unspecific supramolecular interactions with the oligoethylene environment around Au NPs.

(d) Au NP heteroassembly mediated by supramolecular host-guest interactions could not be achieved at our experimental conditions. Instead, important Au NP

homoassembly was observed for **AuNP-G1@Azo-OEG/OEG** which highlighted the importance of unspecific supramolecular interactions, the kinetics of which are problalbe faster than those of host-guest processes, due to the lack of preorganization needed in the former case.

5.6. BIBLIOGRAPHY

[1] Descalzo, A. B.; Martínez-Máñez, R.; Sancenón, F.; Hoffmann, K.; Rurak, K. *Angew. Chem. Int. Ed.* **2006**, 45, 5924.

[2] Grzelczak, M.; Vermant, J.; Furst, E. M.; Liz-Marzán, L. M. *ACS Nano* **2010**, 4, 3591.

[3] Wang, L.; Xu, L.; Kuang, H.; Xu, C.; Kotov, N. A. *Acc. Chem. Res*. **2012**, 45, 1916.

[4] Kim, H. J.; Lee, M. H.; Mutihac, L.; Vicens, J.; Kim, J. S. *Chem. Soc. Rev.* **2012**, 41, 1173.

[5] Ying-Wei, Y.; Yu-Long, S.; Nan, S. *Acc. Chem. Res.* **2014**, 47, 1950.

[6] Montes-García, V.; Pérez-Juste, J.; Pastoriza-Santos, I.; Liz-Marzán, L. M. *Chem. Eur. J.* **2014**, 20, 10874.

[7] Chen, Y.; Liu, Y. *Adv. Mater.* **2015**, 27, 5403.

[8] Boles, M.A.; Engel, M.; Talapin, D. V. *Chem. Rev.* **2016**, 116, 11220.

[9] Huang, Y.; Li, D.; Li, J. *Chem. Phys. Lett.* **2004**, 389, 14.

[10] Huang, T.;Meng, F.; Qi, L. *J. Phys. Chem. C* **2009**, 113, 13636.

[11] Ng, C. H. B., Yang, J.; Fan, W. Y. *J. Phys. Chem. C* **2008**, 112, 4141.

[12] Devi, L. B.; Mandal, A. B. *RSC Adv*. **2013**, 3, 5238.

[13] Wen, D.; Liu, W.; Herrmann, A.-K.; Haubold, D.; Holzchuh, M.; Simon, F.; Eychmüller, A. *Small* **2016**, 12, 2439.

[14] Wen, D.; Liu, W.; Haubold, D.; Zhu, C.; Oschatz, M.; Holzchuh, M.; Wolf, A.; Simon, F.; Kaskel, F.; Eychmüller, A. *ACS Nano* **2016**, 10, 2559.

[15] Aqui va una referencia amb valors de Ka per a beta-CD

[16] Liu, J.; Mendoza, S.; Román, E.; Lynn, M. J.; Xu, R.; Kaifer, A. E. *J. Am. Chem. Soc.* **1999**, 121, 4304.

[17] Crespo-Biel, O.; Jukovic, A.; Karlsson, M.; Reindhout, D. N.; Huskens, J. *Isr. J. Chem.* **2005**, 45, 353.

[18] Crespo-Biel, O.; Dordi, B.; Reindhout, D. N.; Huskens, J. *J. Am. Chem. Soc.* **2005**, 127, 7594-7600.

[19] Crespo-Biel, O.; Dordi, B.; Maury, P.; Péter, M.; Reindhout, D. N.; Huskens, J. *Chem. Mater.* **2006**, 18, 2545.

[20] Yu, L.; Shi-Hui, S.; Ying-Wei, Y.; Yong, C. *J. Chem. Res.* **2004**, 152.

[21] Yu, L.; Shi-Hui, S.; Ying-Wei, Y.; Yong, C. *Chem. Commun.* **2005**, 4208.

[22] Trapani, M.;Romeo, A.; Tiziana, P.; Sciortino, M. T.; Patanè, S.; Villari, V.; Mazzaglia, A. *RSC Adv.* **2013**, 3, 5607.

[23] Xi-Le, H.;Yi, Z.; Jia, L.; Guo-Rong, C.; James, T. D.; Xiao-Peng, H.; He, T.; *Chem. Sci.* **2016**, 7, 4004.

[24] Yu, L.; Hao, W.; Yong, C.; Chen-Feng, K.; Min, L. *J. Am. Chem. Soc.* **2005**, 127, 657.

[25] Jing, Y.; Wei, H.; Jian-nan, S.; Yan-ping, S. *ACS Appl. Mater. Interfaces* **2014**, 6, 19544.

[26] Coelho, J. P.; González-Rubio, G.; Delices, A.; Barcina J. O.; Salgado, C.; Ávila, D.; Peña-Rodríguez, O.; Tardajos, G.; Guerrero-Martínez, A. *Angew. Chem. Int. Ed.* **2014**, 53, 12751.

[27] Wang, J.; Wang, D.; Sobal, N. S.; Giersig, M.; Jiang, M.; Möhwald, H. *Angew. Chem. Int. Ed.* **2006**, 45, 7963.

[28] Chen, Z.; Li, J.; Zhang, X.; Wu, Z.; Zhang, H.; Sun, H.; Yang, B. *Phys. Chem. Chem. Phys.* **2012**, 14, 6119.

[29] Yamaguchi, H.; Kobayashi, Y.; Kobayashi, R.; Takashima, Y.; Hashidzume, A.; Harada, A. *Nat. Commun.* **2012**, 3:603.

[30] Halabieh, R. El; Mermut, O.; Barret, C. *Pure Appl. Chem.* **2004**, 76, 1445.

[31] Bouzide, A; Sauvé, G. *Org. Lett.* **2002**, 4, 2329.

[32] Frisch, H.; Fritz, E.-C.; Stricker, F.; Schmüser, L.; Spitzer, D.; Weidner, T.; Ravoo, B. J.; Besenius, P. *Angew. Chem. Int. Ed.* **2016**, 55, 7242.

[33] Fatás, P.; Longo, E.; Rastrelli, F.; Crisma, M.; Toniolo, C.; Jiménez, A. I.; Cativiela, C.; Moretto, A. *Chem. Eur. J.* **2011**, 17, 12606.

[34] Bastús, N. G.; Comenge, J.; Puntes, V *Langmuir*, **2011**, 11098.

[35] Hinterwirth, H.; Kappel, S.; Waitz, T.; Prohaska, T.; Lindner, W.; Lämmerhofer, M. *ACS Nano*, **2013**, 26, 1129-1136.

[36] Wang, Y.; Zeiry, O.; Raula, M.; Le Ouai, B.; Stellaci, F.; Weinstock, I. A. *Nat. Nanotec.* **2017**, 12, 170.

Chapter 6:

General Conclusions

6.1- GENERAL CONCLUSIONS

The present thesis aimed at the preparation of new photoactive materials based on gold nanoparticles functionalized with cyclodextrins. For that purpose, thiolated derivatives of the chosen host were prepared for the subsequent functionalization of Au NPs with them and their application in the fields of photocatalysis and supramolecular association were tested.

Preparation of thiolated hosts and functionalization of Au NPs. The four target thiolated cyclodextrin derivatives were obtained with rather low yields, with the exception of the perthiolated derivative of γ-CD, for which higher reactivity was observed and also one step of the synthetic strategy could be skipped.

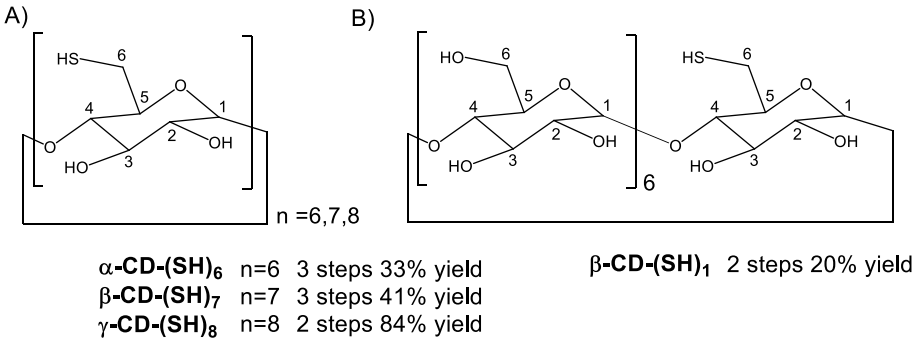

Figure 6.1. Chemical structure of the four different CD derivatives synthesized in these thesis.

Functionalization of Au NP was then carried out by different methods summarized in scheme 6.1. The direct method applied in this thesis provided small CD-capped particles with diameters below 10 nm which presented high polydispersities and it failed to provide bigger particles. Then, the implementation of a two-step procedure allowed the obtention of CD-functionalized NPs with big diameters via citrate stabilized Au NPs which were prepared by the Turkevick-Frens or seed-growth methods. The former methodology provided NPs with diameters around 15 nm with good polydispersities whereas the latter introduced the possibility to grow NPs up to 70 nm in diameter, presenting also good polydispersities. The final step implied the incorporation of the thiolated host to the surface of the NPs by a ligand exchange method, forming a robust monolayer around the particles as evidenced by their stability during the purification processes.

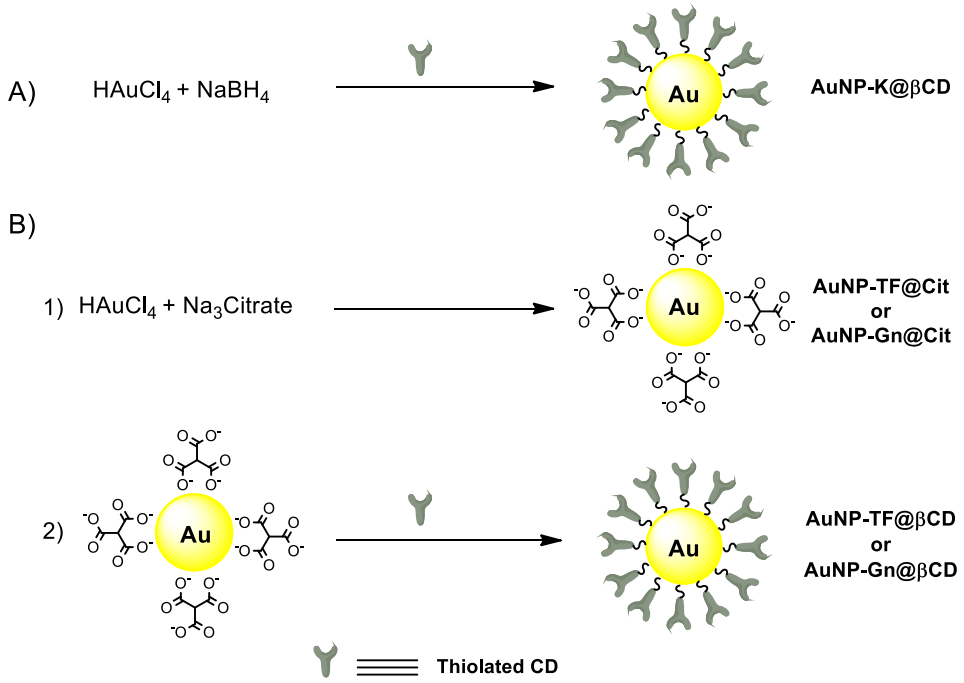

Scheme 6.1. Different methods applied in this thesis for the obtention of CD-functionalized Au NPs.

Gold Nanoparticle Photocatalysis. A new approach to enhance Au NP photocatalysis was developed in this thesis. As can be seen in scheme 6.2 both unimolecular and bimolecular processes were attempted owing to the distinct size of the CD used in each case. On the one hand the isomerization of stilbene derivatives was chosen as model unimolecular reaction to test the photocatalytic activity of **AuNP-TF@βCD** and on the other hand **2-AC** dimerization was attempted as a a bimolecular process model.

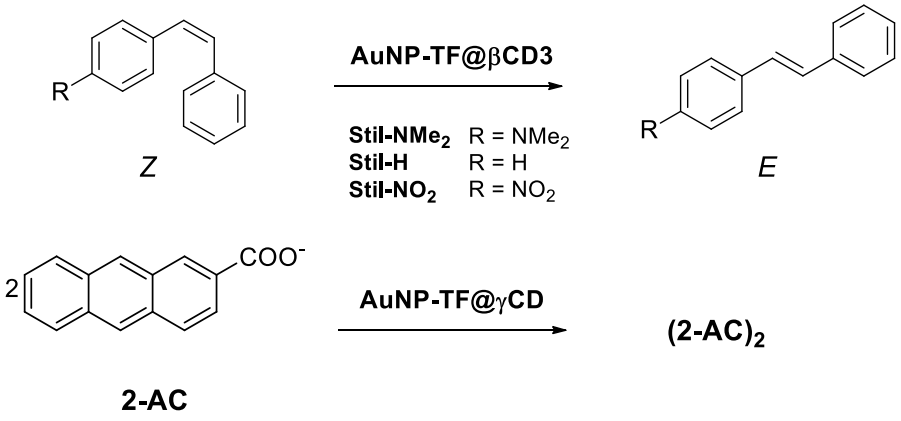

Scheme 6.2. Unimolecular and bimolecular processes photocatalyzed by CD-functionalized Au NPs attempted in this thesis.

In the case of stilbene isomerization, we demonstrated herein that the photocatalytic activity of Au NPs can be effectively enhanced by combining their plasmonic properties with supramolecular hosts like cyclodextrins. However, the photocatalytic performance is limited to the inherent capacity of Au NPs to perform the selected organic reaction. This was ilustrated in our results by the stricking contrast found between electron-rich and electron-poor stilbenes which showed remarkable differences in conversion, being higher for the former ones, for which we could propose a photocatalytic mechanism mediated by Au NPs. When trying to expand our results towards bimolecular processes though, were unable to obtain any conversion under NP excitation.

Gold Nanoparticle Heterroassembly. Our studies on the assembly of Au NPs by host guest complexation highlighted the importance of unspecific interactions that may overcome the capacity to form more steric demanding processes like host-guest recognition. Perhaps attributed to the faster kinetics of such unspecific interactions we could not obtain the target heteroassemblies and homoassemblies were majorly btained.

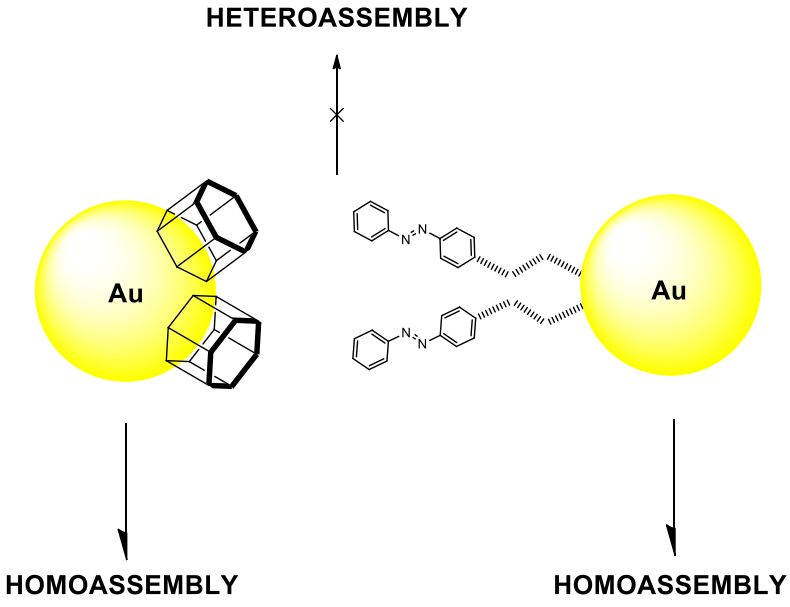

Scheme 6.2. Schematic representation showing the preferential homoassembly of Au NPs with respect to host-guest-driven association.

In conclusion, in the present thesis we have demonstrated the great potential of combining plasmonic nanostructures with supramolecular chemistry to develop new photoactive materials with improved properties, contributing with our work to the increasing knowledge in the expanding field of the nanosicience.

Chapter 7:

Experimental Section

7.1- GENERAL PROCEDURES

Reactants were purchased from Sigma-Aldrich and used without further purification. β-cyclodextrin was oven-dried for 12 h prior to its use. Solvents were purchased from Scharlab and use as received unless indicated. Dialysis processes were done using Cellu Step T1 cellullose membranes (3500 Da).

7.1.1- Spectroscopy

Nuclear magnetic resonance (NMR) spectra were recorded at *Servei de Ressonància Magnètica Nuclea*r of *Universitat Autònoma de Barcelona*. ^{1}H-NMR spectra were recorded on Bruker DPX250 (250 MHz for ^{1}H-NMR) Bruker DPX360 (360 MHz) and Bruker AV-III400 (400 MHz) spectrometers using the appropriate deuterated solvent. Proton chemical shifts (δ) are given in ppm and the signals are referenced to the residual solvent peak ^{13}C-NMR spectra were recorded with complete proton decoupling on Bruker DPX250 (62.5 MHz), Bruker DPX360 (90 MHz) and Bruker AV-III400 (100.6 MHz) spectrometers using the appropriate deuterated solvent. ^{13}C chemical shifts (δ) are given in ppm and the signals are referenced to the residual solvent peak. The abbreviations used to describe signal multiplicities are: s (singlet), br s (broad singlet), d (doublet), t (triplet), q (quartet), dd (double doublet), dt (double triplet), dq (double quartet), m (multiplet) and *J* (coupling constant).

Electronic Absorption and Extinction (UV-vis) spectra were measured in a HP 8453 spectrophotometer in 1-cm quartz cells and using HPLC or spectroscopic quality solvents.

7.1.2- Mass Spectrometry

High-resolution mass spectra (HRMS) were measured at *Servei de Genòmica i Proteòmica* of *Universitat Autònoma de Barcelona* in a MALDI-TOF UltrafleXtreme (Bruker Daltonics) spectrometer.

7.1.3- Chromatography

Thin layer chromatography was conducted over 0.25-cm thick *Alugram* foil *Sil G/UV*$_{254}$. Developing was made using a UV lamp operating at 254 nm and/or using $KMnO_4$/KOH aqueous solution. Flash column chromatography was performed using Silica 60 (0.04 – 0.06 mm) 230-240 mesh as stationary phase.

7.1.4- Transmission Electron Microscopy (TEM)

Transmission Electron Microscopy (TEM) images were recorded either in a Jeol JEM 1400 TEM electron microscope operating at 80 kV or in a Jeol JEM 2011 TEM electron microscope operating at 200 kV. For regular TEM measurements an aliquot of the sample was dropcasted over a copper grid and and after 1 minute, the excess solvent was removed and dried. For Cryo-TEM analysis a 3 μL drop of the sample was blotted onto holey carbon grids (Quantifoil Micro Tools, Großloübichau, Germany) previously glow discharged in a PELCO easiGlow glow discharger unit. They were subsequently plunged into liquid ethane at −180 °C using a Leica EM GP cryo workstation and observed in a Jeol JEM 2011 TEM electron microscope operating at 200 kV. During imaging, the samples were maintained at −181 °C, and pictures were taken using a CCD multiscan camera (Gatan).

7.1.5- Electrochemitry

Cyclic voltammograms were registered using a VSP 100 BIOLOGIC potentiostat. A three electrode conical electrochemical cell equipped with a glassy carbon electrode (WE, d = 1 mm), an auxiliary platinum electrode (CE, d = 1 mm), a saturated calomel electrode (SCE, RE) and an argon bubbling source was used. All the potentials are reported versus a SCE isolated from the working electrode by a salt bridge. All measurements were performed in anhydrous acetonitrile containing 0.1 M solution of *n*-Bu_4NPF_6, which acts as supporting electrolyte.

7.1.6- Fluorometry

Fluorescence emission spectra were recorded in a PerkinElmer LS 55 spectrofluorometer. All samples were measured in 1-cm quartz fluorescence cells at 25 ± 0.1 ºC using HPLC or spectroscopic quality solvents.

7.1.7- Excitation Sources

Different excitation sources were employed to induce *trans-cis* photoisomerization of stilbenes and azobenzene-based thiolated ligands: (i) a Vilber Lourmat UV lamp equipped with two 4W tubes emitting UV light at 254 and 365 nm; (ii) a diode cw laser emitting at 406 nm (SDL-BS-300, company). Gold nanopaticle plasmon excitation was done by irradiation with the second harmonic generation of a Nd:YAG (Brilliant, Quantel) pulsed laser (λ_{exc} = 532 nm) operating at a frequency of 10 Hz and with a round spot size of 0.8 cm in diameter

7.2- EXPERIMENTAL DESCRIPTION

7.2.1- Synthesis and characterization of host-functionalized gold nanoparticles

Synthesis of *per*-6-iodo-β-cyclodextrin (1)[1]

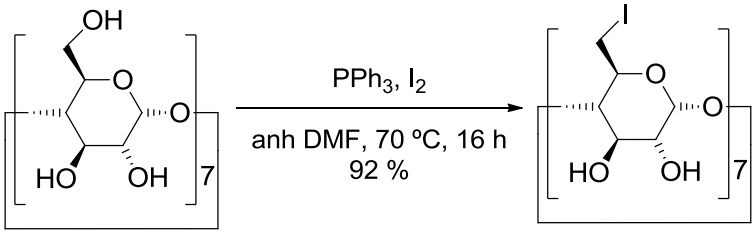

β-CD **1**

Triphenylphosphine (20.2 g, 77.0 mmol) was dissolved in dry DMF (80 mL) and iodine (20.2 g, 77.2 mmol) was carefully added during 10-15 minutes. Dry β-cyclodextrin (5 g, 4.4 mmol) was then added to the resulting dark-brown solution, which was stirred at 70 ºC under Ar atmosphere for 18 h. The resulting reaction mixture was concentrated under reduced pressure to half volume. The concentrated solution was adjusted to pH 9-10 by addition of 3 M sodium methoxide in methanol under cooling in an ice bath. Once at room temperature, the mixture was stirred for 30 minutes and was then poured over 400 mL of cold methanol under vigorous stirring to form a brownish precipitate. The precipitate was filtered, washed with methanol and air-dried. Soxhlet extraction with methanol of this solid was done until no more discoloration of the solvent could be seen, finally obtaining a clear brown solid (7.70 g, 92 % yield).

^{1}H-NMR (250 MHz, DMSO-d_6): δ 6.05 (d, *J* = 6.5 Hz, 7H), 5.94 (d, *J* = 2.0 Hz, 7H), 4.99 (d, *J* = 2.0 Hz, 7H) 3.80 (d, *J* = 9.0 Hz, 7H), 3.54-3.68 (m, 14H), 3.24-3.47 (m, 21H).

^{13}C-NMR (100.6 MHz, DMSO-d_6): δ 102.2, 86.0, 72.3, 72.0, 71.0, 9.5.

HRMS (MALDI-TOF): m/z; calcd. for [$C_{42}H_{63}I_7O_{28}$+Na^+] 1926.671, found 1926.690.

Synthesis of *per*-[(2,3-di-O-acetyl)-(6-iodo)]-β-cyclodextrin (2)[2]

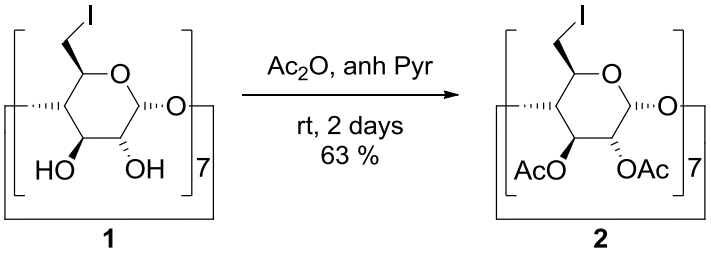

1 **2**

Per-6-iodo-β-cyclodextrin (5.0 g, 2.6 mmol) was dissolved in dry pyridine (15 mL, 186 mmol) and acetic anhydride (15 mL, 159 mmol) was added. The mixture was stirred under Ar atmosphere at room temperature for 2 days. Methanol (18 mL) was then added in 2 mL portions taking care that bubbling had finished before each new addition. The resulting mixture was poured over 500 mL 1.0 M HCl solution in water. The whole mixture was stirred for 5 min and then extracted with CH_2Cl_2 (4 x 75 mL), dried with Na_2SO_4, filtered and the solvent evaporated under reduced pressure to give a yellowish solid. Purification by flash column chromatography (Silica 60, 100 % EtOAc) furnished **2** as a white solid (3.98 g, 63 % yield).

^{1}H-NMR (250 MHz, DMSO-d$_6$): δ 5.34 (dd, J_1 = 8.1 Hz, J_2 = 9.9 Hz, 7H), 5.20 (d, J = 3.9 Hz, 7H), 4.84 (dd, J_1 = 3.9 Hz, J_2 = 9.9 Hz, 7H), 3.71-3.87 (m, 14H), 3.56-3.68 (m, 14H), 2.09 (s, 21H), 2.06 (s, 21H).

^{13}C-NMR (100.6 MHz, DMSO-d$_6$): δ 170.7, 169.5, 96.7, 80.7, 70.5, 70.4, 70.2, 20.9, 8.0.

HRMS (MALDI-TOF): m/z; calcd. for [$C_{70}H_{91}I_7O_{42}$+Na^+] 2514.820, found 2514.845.

Synthesis of *per*-6-thio-β-cyclodextrin (β-CD-(SH)$_7$)[1]

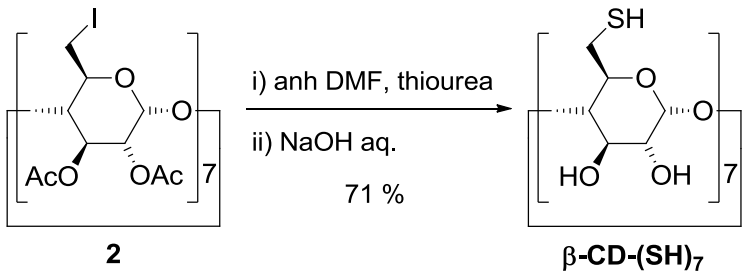

2 **β-CD-(SH)$_7$**

Per-[(2,3-di-*O*-acetyl)-(6-iodo)]-β-cyclodextrin (1.5 g, 0.6 mmol) was disolved in dry DMF (20 mL) and thiourea (0.35 g, 4.68 mmol) was added. The reaction mixture was stirred at 70 ºC under Ar atmosphere. After 19 h, DMF was removed under

reduced pressure to give a yellow-orange oil. The oil obtained was dissolved in water (50 mL) and sodium hydroxide (2.43 g, 61 mmol) was added. The resulting mixture was stirred at reflux under nitrogen atmosphere for 1 h, which resulted in a color change from pale yellow to pale orange. Once at room temperature, the resulting suspension was acidified with 1.0 M $KHSO_4$ and the precipitate filtered off, washed thoroughly with distilled water and dried under vacuum to obtain compound **β-CD-(SH)$_7$** as a white solid (0.53 g, 71 % yield).

^{1}H-NMR (250 MHz, DMSO-d$_6$): δ 5.94 (d, *J* = 6.5 Hz, 7H), 5.82 (s, 7H), 4.93 (d, *J* = 2.5 Hz, 7H), 3.50-3.87 (m, 14H), 3.05-3.50 (m, 21H), 2.75 (m, 7H), 2.13 (t, *J* = 8 Hz, 7H).

^{13}C-NMR (100.6 MHz, DMSO-d$_6$): δ 102.2, 84.9, 72.6, 72.3, 72.0, 26.0.

HRMS (MALDI-TOF): m/z; calcd. for [$C_{42}H_{70}O_{28}S_7$+Na^+] 1269.199, found 1269.217.

***Mono*-(6-O-*p*-toluensulfonyl)-β-cyclodextrin (3)**[3]

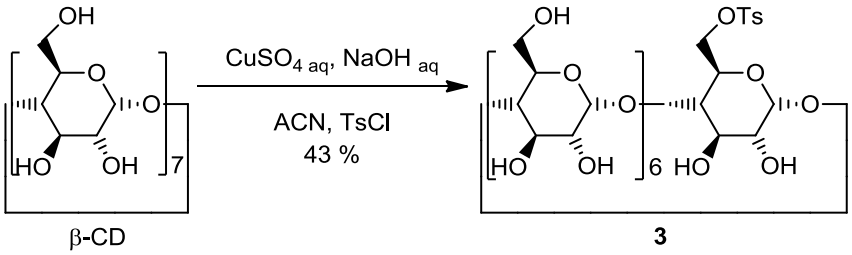

Dried β-cyclodextrin (8.5 g, 7.5 mmol) was suspended in water (100 mL) under stirring in a 1 L round bottom flask. To this suspension a solution of $CuSO_4$ 5 H_2O (6.7 g in 100 mL H_2O) was added. Then NaOH (8.9 g in 300 mL H_2O) was slowly added under stirring and the solution turned blue colored. A solution of *p*-toluenesulfonyl chloride (13.2 g, 69.2 mmol) in acetonitrile (100 mL) was added dropwise and the reaction mixture was allowed to stir at room temperature for 7 h. After that time, HCl was added until neutral pH and a light blue precipitate appeared. This precipitate was filtered off and the filtrate cooled down in the fridge for 24 h to obtain a white precipitate, which was finally filtered off and dried under vacuum (3.04 g, 30% yield). The product contains a small amount of the ditosylate product (~20%). Spectrometric data are only given for compound **3** based on previous reports.

^{1}H NMR (250 MHz, DMSO-*d*$_6$): δ 2.41 (s, 3H), 3.15-3.75 (m, overlapping with HDO), 4.15-4.62 (m, 6H), 4.75 (d, J = 3 Hz, 3H), 4.82 (d, J = 3 Hz, 4H), 5.60-5.88 (m, 14H), 7.41 (d, J = 8 Hz, 2H), 7.72 (d, J = 8 Hz, 2H).

^{13}C NMR (100.6 MHz, DMSO-d_6): δ 21.3, 59.3, 59.5, 60.0, 69.0, 69.8, 71.9, 72.1, 72.2, 72.4, 72.5, 72.8, 73.0, 73.1, 80.8, 81.2, 81.4, 81.5, 81.7, 101.3, 101.9, 102.0, 102.3, 127.6, 129.9, 132.7, 144.9.

HRMS (MALDI-TOF): m/z; calcld for [$C_{49}H_{76}O_{28}S_7$+Na^+] 1311.368, found 1311.390.

Synthesis of *mono*-6-thio-β-cyclodextrin (β-CD-(SH)$_1$)[4]

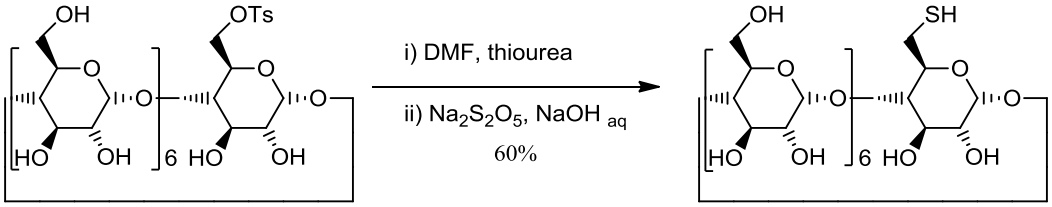

3 **β-CD-(SH)$_1$**

A mixture of 600 mg (0.5 mmol) of 3 and 300 mg (7.8 mmol) of thiourea in 24 mL dry DMF was heated to 75 ºC under Ar atmosphere for 48 h. After the reaction mixture had cooled down to room temperature, it was poured over 72 mL diethyl ether under stirring to form a precipitate. The precipitate was filtered, washed with acetone and vacuum dried. 602 mg of the corresponding isothiouronium salt were obtained (95% yield). The isothiouronium salt (242 mg, 0.18 mmol) was then dissolved in a solution of 12 mg sodium disulfite ($Na_2S_2O_5$) in 10 mL 1M aqueous NaOH and stirred for 30 min at room temperature. The solution was acidified with HCl until pH 3. Trichloroethylene (0.5 mL) was added and the mixture treated for 10 min in an ultrasonic bath. The precipitate was filtered, washed with acetone and vacuum dried to provide 143 mg of the target compound (66% yield).

^{1}H NMR (250 MHz, DMSO-d_6): δ 2.1 (br s, 1H), 2.75 (s, 1H), 2.95 (s, 1H), 3.19 - 3.45 (m, overlapping with HDO), 3.45 – 3.82 (m, 26H), 4.37 – 4.57 (br s, 6H), 4.82 (br s, 7H), 5.57 – 5.58 (m, 14H).

^{13}C NMR (100.6 MHz, DMSO-d_6): δ 25.7, 59.9, 71.2, 72.1, 72.5, 73.1, 81.57, 84.0, 101.9.

HRMS (MALDI-TOF): m/z; calcld for [$C_{42}H_{70}O_{34}S$+Na^+] 1173.337, found 1173.361.

Synthesis of *per*-6-iodo-α-cyclodextrin (4)[1]

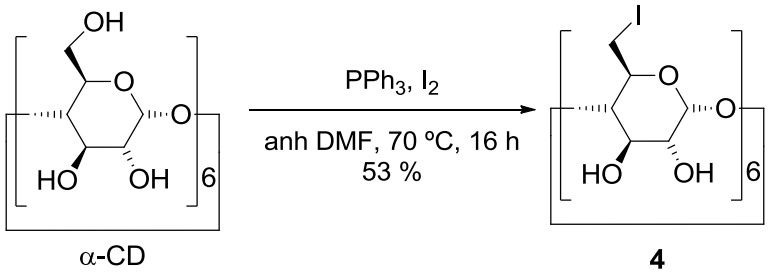

α-CD **4**

Triphenylphosphine (20.2 g, 77.0 mmol) was dissolved in dry DMF (80 mL) and iodine (19.58 g, 77.1 mmol) was carefully added during 10-15 minutes. Dry α-cyclodextrin (5 g, 5.14 mmol) was then added to the resulting dark-brown solution, which was stirred at 70 ºC under Ar atmosphere for 18 h. The resulting reaction mixture was concentrated under reduced pressure to half volume. The concentrated solution was adjusted to pH 9-10 by addition of 3 M sodium methoxide in methanol under cooling in an ice bath. Once at room temperature, the mixture was stirred for 30 minutes and was then poured over 400 mL of cold methanol under vigorous stirring to form a brownish precipitate. The precipitate was filtered, washed with methanol and air-dried. Soxhlet extraction with methanol of this solid was done until no more discoloration of the solvent could be seen, finally obtaining a clear brown solid (4.45 g, 53 % yield).

^{1}H-NMR (250 MHz, DMSO-d_6): δ 6.05 (d, *J* = 6.5 Hz, 7H), 5.94 (d, *J* = 2.0 Hz, 7H), 4.99 (d, *J* = 2.0 Hz, 7H) 3.80 (d, *J* = 9.0 Hz, 7H), 3.54-3.68 (m, 14H), 3.24-3.47 (m, 21H).

13C NMR (90 MHz, DMSO-d6): δ 101.84, 86.34, 72.24, 71.73, 70.69, 9.74.

Synthesis of *per*-[(2,3-di-O-acetyl)-(6-iodo)]-α-cyclodextrin (5)[2]

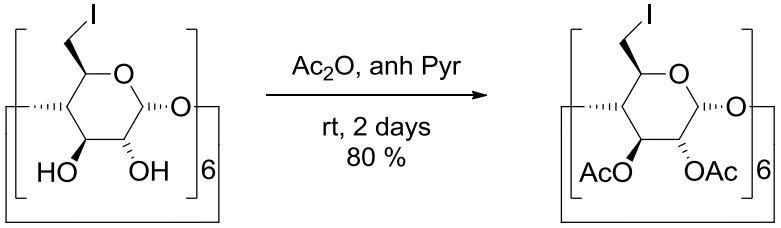

4 **5**

Per-6-iodo-α-cyclodextrin (5.24 g, 3.2 mmol) was dissolved in dry pyridine (17 mL, 211 mmol) and acetic anhydride (17.24 mL, 181.3 mmol) was added. The mixture was stirred under Ar atmosphere at room temperature for 2 days. Methanol (20 mL) was then added in 2 mL portions taking care that bubbling had finished before each new addition. The resulting mixture was poured over 1000 mL 0.5 M HCl solution in water. The whole mixture was stirred for 5 min and then extracted with CH_2Cl_2 (4 x 75 mL), dried with Na_2SO_4, filtered and the solvent evaporated under reduced pressure to give a yellowish solid. Purification by flash column chromatography (Silica 60, 100 % EtOAc) furnished **5** as a white solid (4.56 g, 80 % yield).

1H NMR (360 MHz, $CDCl_3$): δ 5.50 (dd, 6H, J1 = 10.2 Hz, J2 = 8.0 Hz), 5.14 (d, 6H, J = 3.6 Hz), 4.84 (dd, 6H, J1 = 10.2 Hz, J2 = 3.6 Hz), 3.83-3.58 (m, 24H), 2.05 (s, 18H), 2.03 (s, 18H).

13C NMR (90 MHz, $CDCl_3$): δ 170.68, 169.38, 96.98, 81.24, 70.89, 70.73, 70.04, 20.93, 20.87, 8.61.

Synthesis of *per*-6-thio-α-cyclodextrin (α-CD-$(SH)_6$)[1]

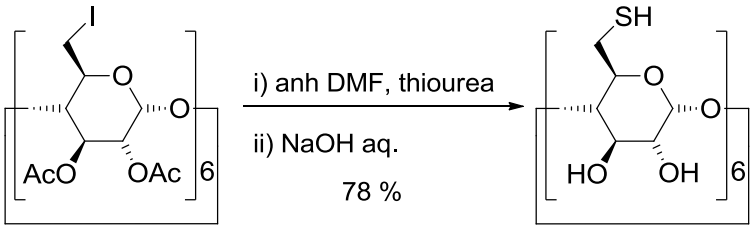

5 **α-CD-$(SH)_6$**

Per-[(2,3-di-*O*-acetyl)-(6-iodo)]-α-cyclodextrin (1.5 g, 0.6 mmol) was disolved in dry DMF (20 mL) and thiourea (0.35 g, 4.68 mmol) was added. The reaction mixture was stirred at 70 ºC under Ar atmosphere. After 19 h, DMF was removed under reduced pressure to give a yellow-orange oil. The oil obtained was dissolved in water (50 mL) and sodium hydroxide (2.43 g, 61 mmol) was added. The resulting mixture was stirred at reflux under nitrogen atmosphere for 1 h, which resulted in a color change from pale yellow to pale orange. Once at room temperature, the resulting suspension was acidified with 1.0 M $KHSO_4$ and the precipitate filtered off, washed thoroughly with distilled water and dried under vacuum to obtain **α-CD-$(SH)_6$** as a white solid (0.53 g, 78 % yield).

^{1}H-NMR (250 MHz, DMSO-d_6): δ 5.94 (d, *J* = 6.5 Hz, 7H), 5.82 (s, 7H), 4.93 (d, *J* = 2.5 Hz, 7H), 3.50-3.87 (m, 14H), 3.05-3.50 (m, 21H), 2.75 (m, 7H), 2.13 (t, *J* = 8 Hz, 7H).

^{13}C NMR (90 MHz, DMSO-d6): δ 102.58, 85.62, 73.66, 72.70, 72.57, 26.48.

Synthesis of *per*-6-iodo-γ-cyclodextrin (6)[1]

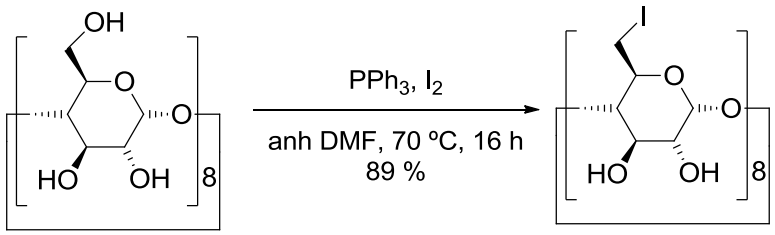

γ-CD **6**

Triphenylphosphine (17.40 g, 65.7 mmol) was dissolved in dry DMF (70 mL) and iodine (16.67 g, 65.7 mmol) was carefully added during 10-15 minutes. Dry γ-cyclodextrin (4.52 g, 3.4 mmol) was then added to the resulting dark-brown solution, which was stirred at 70 ºC under Ar atmosphere for 18 h. The resulting reaction mixture was concentrated under reduced pressure to half volume. The concentrated solution was adjusted to pH 9-10 by addition of 3 M sodium methoxide in methanol under cooling in an ice bath. Once at room temperature, the mixture was stirred for 30 minutes and was then poured over 400 mL of cold methanol under vigorous stirring to form a brownish precipitate. The precipitate was filtered, washed with methanol and air-dried. Soxhlet extraction with methanol of this solid was done until no more discoloration of the solvent could be seen, finally obtaining a clear brown solid (6.62 g, 89 % yield).

^{1}H-NMR (400 MHz, DMSO-d_6): δ 3.21-3.59 (m, overlapped with HDO signal), 3.50-3.73 (m, 16H), 3.82 (d, J = 9 Hz, 8H), 5.03 (d, J = 3.5 Hz, 8H), 5.95 (bs, 16H).

13C NMR (90 MHz, DMSO-d6): δ 102.09, 85.91, 72.14, 71.91, 70.89, 9.42.

Synthesis of *per*-6-thio-γ-cyclodextrin (γ-CD-(SH)$_8$)[1]

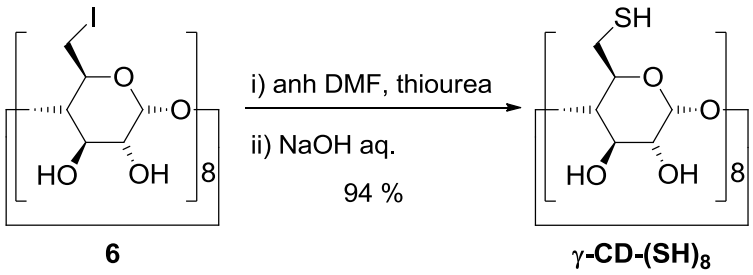

6 **γ-CD-(SH)$_8$**

Per-6-iodo-γ-cyclodextrin (3.71 g, 1.7 mmol) was disolved in dry DMF (50 mL) and thiourea (1.30 g, 17.1 mmol) was added. The reaction mixture was stirred at 70 ºC under Ar atmosphere. After 19 h, DMF was removed under reduced pressure to give a yellow-orange oil. The oil obtained was dissolved in water (200 mL) and sodium hydroxide (1.37 g, 34.2 mmol) was added. The resulting mixture was stirred at reflux under nitrogen atmosphere for 1 h, which resulted in a color change from pale yellow to pale orange. Once at room temperature, the resulting suspension was acidified with 1.0 M $KHSO_4$ and the precipitate filtered off, washed thoroughly with distilled water and dried under vacuum to obtain **γ-CD-(SH)$_8$** as a white solid (2.28 g, 94 % yield).

^{1}H-NMR (250 MHz, DMSO-d$_6$): δ 6.12 (d, J = 6.3 Hz, 7H), 6.00 (bs, 7H), 5.07 (d, *J* = 3.9 Hz, 7H), 3.83 (bt, J = 7.4 Hz, 7H), 3.77 (t, *J* = 9 Hz, 7H), 3.59-3.42 (m, 14H), 3.31 (dd, J1 = 9.4 Hz, J2 = 14.5 Hz, 7H), 2.90-2.83 (m, 7H), 2.13 (t, *J* = 8.3 Hz, 7H).

^{13}C NMR (90 MHz, DMSO-d$_6$): δ 102.93, 85.18, 73.36, 73.04, 72.54, 26.26.

Synthesis of AuNP-K@β-CD1 by the Kaifer's method[5]

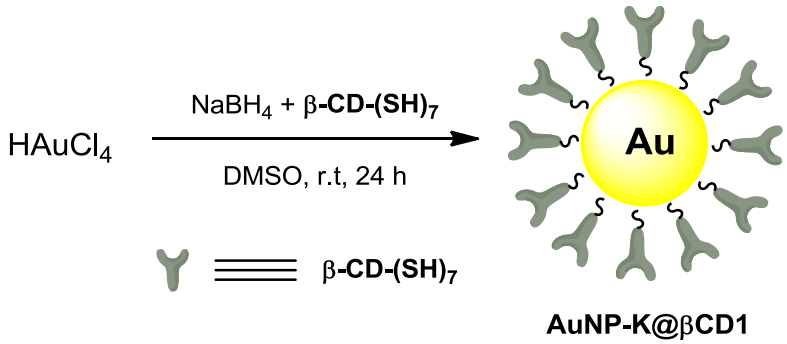

AuNP-K@βCD1

Solutions of chloroauric acid (50 mg) in DMSO (20 mL) were quickly mixed with another solution containing $NaBH_4$ (75.5 mg) and variable amounts **β-CD-(SH)$_7$** corresponding to **β-CD-(SH)$_7$**:Au molar ratios ($r_{CD/Au}$) of 0.00625, 0.0125, 0.018, 0.025,

0.050, 0.075. The reaction mixture changed in color and turned deep brown immediately but the reaction was allowed to stir for 24 h. Then acetonitrile was added (40 mL) and the precipitated gold colloid was centrifuged at 10000 rpm during 5 minutes. The pelleted Au NPs were redissolved in DMSO (20 mL), precipitated again by the addition of acetonitrile (20 mL) and centrifuged at 10000 rpm for 10 minutes. Finally, the pelleted Au NPs were resuspended in ethanol (60 mL), isolated by centrifugation at 10000 rpm during 10 minutes and dried under vacuum at room temperature. **AuNP-K@β-CD1** were characterized by means of UV-Vis spectroscopy and TEM.

Synthesis of AuNP-TF@Cit1 by the Turkevich-Frens method:[6]

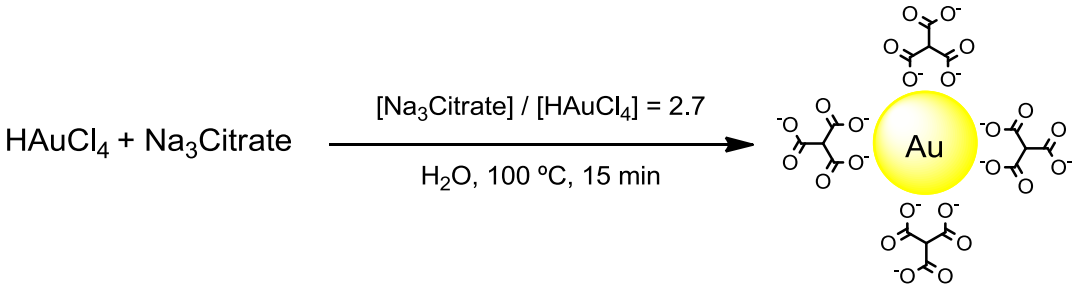

AuNP-TF@Cit1

A solution of chloroauric acid (1.25 mM) in deionized water (180 mL) was heated to boiling under stirring. To this solution, a pre-heated solution (95 ºC) of trisodium citrate (30 mM) in deionized water (20 mL) was rapidly added maintaining a gentle boiling. Rapidly, the color changed from light yellow to deep-wine red. Boiling was maintained for 10-15 minutes and the reaction mixture was allowed to cool down to room temperature. Finally, the colloidal suspension of **AuNP-TF@Cit1** was stored at 4 ºC in the fridge. **AuNP-TF@Cit1** were characterized by means of UV-Vis spectroscopy and TEM.

Synthesis of AuNP-TF@Cit2 by the Turkevich-Frens method[6]

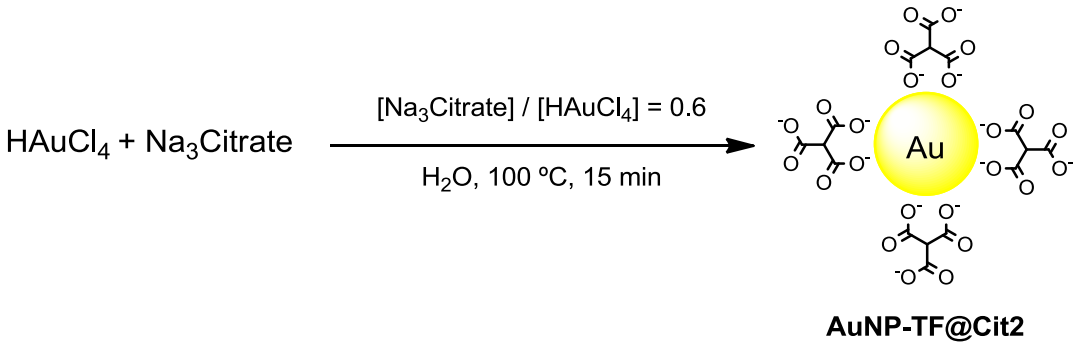

AuNP-TF@Cit2

The synthesis of **AuNP-TF@Cit2** was performed using the method described by Frens.[7] An aqueous solution of $HAuCl_4$ (50 mL, 0.01% w/v) was prepared and heated to boiling. Then, of an aqueous solution of trisodium citrate (300 mL, 1% w/v) was quickly added. In about 25-30 seconds the boiling solution turned faintly blue-gray due to the formation of small nuclei, and in time, its color changed into a brilliant red, finally brownish-red indicating the formation of large particles. After 10 minutes the reaction was stopped. The obtained particles were characterized by UV-vis spectroscopy and TEM.

Synthesis of AuNP-Gn@Cit by the seed-growth method[8]

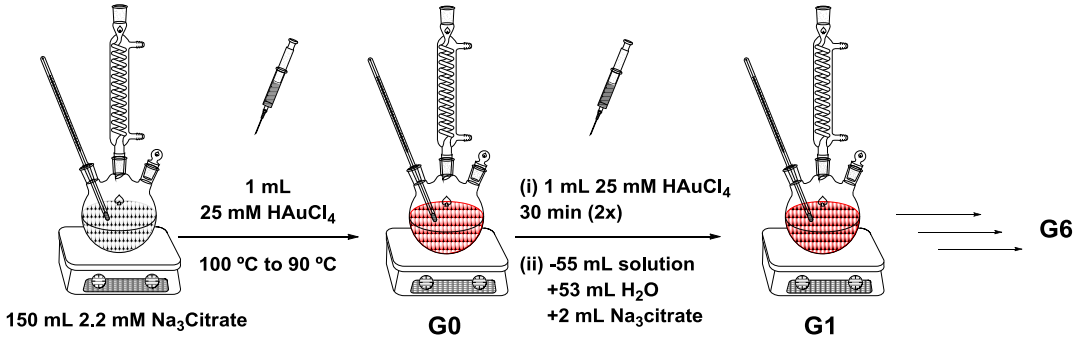

AuNP-Gn@Cit were synthesized by the seed-growth method developed by Puntes *et al.* First, gold seeds (G0) were prepared injecting 1 mL of an aqueous solution of $HAuCl_4$ (25 mM) into 150 mL of an aqueous solution of trisodium citrate (2.2 mM) under vigorous stirring at 100 ºC. In few minutes the formation of small seeds was confirmed by the red wine color of the suspension and, then, the reaction mixture was cooled until the temperature reached 90 ºC to prevent the formation of new cores. After that, six equivalent growth steps (G1-G6) were conducted consisting in the injection of 1 mL of an aqueous solution of $HAuCl_4$ (25 mM) and 30 minutes of reaction at 90 ºC, a

process that was repeated twice for every growth step. In addition, for G2-G6, the initial solution was diluted by extracting 55 mL of the final mixture of the previous growth step and adding 53 mL of water and 2 mL of an aqueous solution of trisodium citrate (60 mM).

Synthesis of AuNP-TF@β-CD1 by ligand exchange[9]

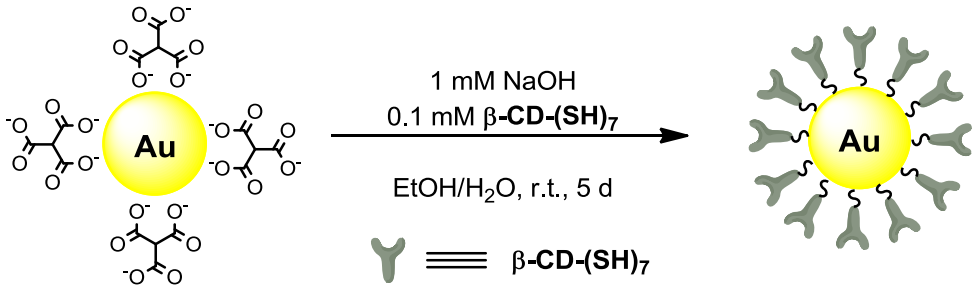

AuNP-TF@Cit1 **AuNP-TF@βCD1**

To an aqueous colloidal suspension of **AuNP-TF@Cit1** (*c* = 8.27 nM), a mixture of **β-CD-(SH)$_7$** and NaOH in ethanol was added so that their final concentrations were 0.1 mM and 1 mM, respectively (e.g. 20 mL of a 1.0 mM ligand and 10 mM NaOH suspension per 180 mL **AuNP-TF@Cit1** colloid). The resulting mixture was left to stir at room temperature for 5 days. Afterwards, the mixture was diluted to one half with acetonitrile and the resulting **AuNP-TF@β-CD1** suspension was centrifuged at 11500 rpm during 15 minutes. The pelleted Au NPs were resuspended in DMF (15 mL) and dialyzed against this solvent during 3 days changing the solvent every 24 h. Acetonitrile was then added (150 mL) and the colloidal suspension was centrifuged at 12000 rpm during 20 minutes. The pelleted AuNPs were resuspended in deionized water (10 mL) upon sonication. **AuNP-TF@β-CD1** were characterized by means of UV-Vis spectroscopy, ^{1}H NMR and TEM.

Synthesis of AuNP-TF@βCD2 by ligand exchange

These NPs were prepared as already described for **AuNP-TF@β-CD1** (see above). **AuNP-TF@βCD2** were characterized by UV-vis spectroscopy and TEM.

Synthesis of AuNP-G6@β-CD by ligand exchange[9]

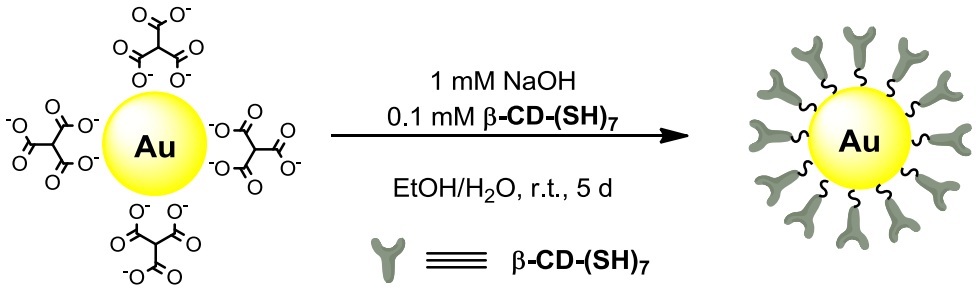

AuNP-G6@Cit **AuNP-G6@β-CD**

To an aqueous colloidal suspension of **AuNP-G6@Cit** (*c* ~0.6 nM), a mixture of **β-CD-(SH)$_7$** and NaOH in ethanol was added so that their final concentrations were 0.1 mM and 1 mM, respectively (e.g. 20 mL of a 1.0 mM ligand and 10 mM NaOH suspension per 180 mL **AuNP-G6@Cit** colloid). The resulting mixture was left to stir at room temperature for 5 days. Afterwards, the mixture was diluted to one half with acetonitrile and the resulting **AuNP-G6@β-CD** suspension was centrifuged at 10000 rpm during 15 minutes. The pelleted Au NPs were resuspended in DMF (15 mL) and dialyzed against this solvent during 3 days changing the solvent every 24 h. Acetonitrile was then added (150 mL) and the colloidal suspension was centrifuged at 11000 rpm during 20 minutes. The pelleted AuNPs were resuspended in deionized water (10 mL) upon sonication. **AuNP-G6@β-CD1** were characterized by means of UV-Vis spectroscopy and TEM.

Determination of Au NP concentration in aqueous suspension

From the extinction spectrum of Au NPs and the extinction coefficient of the maximum of the surface plasmon resonance band, the concentration of AuNPs in aqueous suspension was determined using the following double logarithm equation:[10]

$$\ln \varepsilon = k \ln D + a \qquad (7.1)$$

In this expression, ε is the extinction coefficient (given in M^{-1} cm^{-1}), D is the core diameter of the nanoparticles (given in nm and determined from TEM measurements),

and k = 3.32111 and a = 10.80505 are pre-established parameters determined for citrate-stabilized spherical Au NPs in water. As an approximation,[10] we also took these parameter values for the rest of nanoparticles investigated in this thesis when suspended in aqueous media.

7.2.2- Photocatalysis with gold nanoparticles

General procedure for the synthesis of (Z)-Stil-NMe_2, (Z)-Stil-H, (Z)-Stil-NO_2 and (Z)-Stil-OH

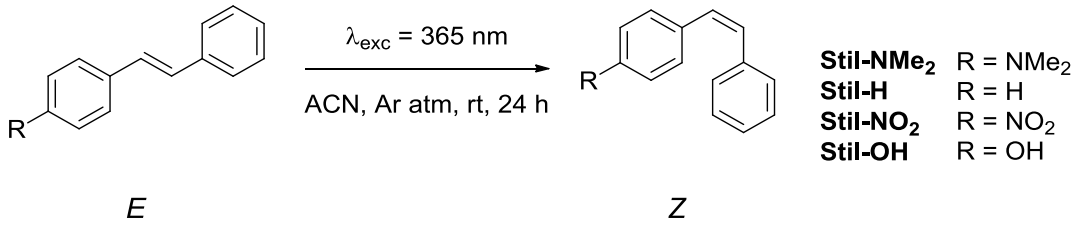

Commercially available (*E*)-**Stil-NMe_2**, (*E*)-**Stil-H**, (*E*)-**Stil-NO_2** and (*E*)-**Stil-OH** (80 mg) were dissolved in acetonitrile (10 mL). The resulting solutions were degassed with Ar and irradiated at 365 nm with a 4 W UV lamp during 24 h to achieve the photostationary state. The solvent was evaporated under reduced pressure and the solid obtained was purified.

Purification of (Z)-Stil-NMe_2

(*Z*)-**Stil-NMe_2** was purified from the reaction mixture by successive fractional precipitation of the (*E*)-**Stil-NMe_2** isomer. After evaporation of the solvent the residue was resuspended in 10 mL of *n*-hexane and digested at -32 ºC for 24 h. The suspension obtained was filtered through a tight cotton plug and the solvent evaporated under reduced pressure. The residue was again resuspended in 5 mL of *n*-hexane and digested at -32 ºC for 24 h. The precipitate was filtered, the solvent evaporated and the resuspension-precipitation operation was repeated one more time with 2 mL of *n*-hexane. After evaporation of the final filtrate, an amber oil was obtained (35 mg, 44 % yield) with a 98:2 (*Z*)-**Stil-NMe_2**:(*E*)-**Stil-NMe_2** ratio. Further purification of this mixture could not be achieved by flash column chromatography.

^{1}H-NMR (400 MHz, DMSO-d_6): δ 7.30-7.24 (m, 4H), 7.20 (m, 1H), 7.06 (m, 2H), 6.57 (m, 2H), 6.46 (d, *J* = 12.0 Hz, 1H), 6.38 (d, *J* = 12.0 Hz, 1H), 2.87 (s, 6H).

^{13}C-NMR (100.6 MHz, DMSO-d_6): δ 149.48, 137.83, 130.22, 129.51, 128.31, 128.30, 126.74, 126.17, 124.05, 111.67, 39.85.

Purification of (Z)-Stil-H

(*Z*)-**Stil-H** was purified from the reaction mixture by flash column chromatography (Silica 60, *n*-hexane:$CHCl_3$ 10:1), obtaining a colorless oil (20 mg, 25 % yield).

^{1}H-NMR (400 MHz, DMSO-d_6): δ 7.31-7.19 (m, 10H), 6.65 (s, 2H).

^{13}C-NMR (100.6 MHz, DMSO-d_6): δ 136.82, 130.08, 128.48, 128.34, 127.28.

Purification of (Z)-Stil-NO_2

(*Z*)-**Stil-NO_2** was purified from the reaction mixture by successive fractional precipitation of the (*E*)-**Stil-NO_2** isomer. After evaporation of the solvent the residue was resuspended in 10 mL of *n*-hexane and digested at -32 ºC for 24 h. The suspension obtained was filtered through a tight cotton plug and the solvent evaporated under reduced pressure. The residue was again resuspended in 5 mL of *n*-hexane and digested at -32 ºC for 24 h. The precipitate was filtered, the solvent evaporated and the resuspension-precipitation operation was repeated one more time with 2 mL of *n*-hexane. After evaporation of the final filtrate, a yellow oil was obtained (18 mg, 22 % yield) with a 97:3 (*Z*)-**Stil-NO_2**:(*E*)-**Stil-NO_2** ratio. Further purification of this mixture could not be achieved by flash column chromatography.

^{1}H-NMR (400 MHz, DMSO-d_6): δ 8.13 (d, *J* = 8.9 Hz, 2H), 7.47 (d, *J* = 8.9 Hz, 2H), 7.34-7.27 (m, 3H), 7.22 (m, 2H), 6.88 (d, *J* = 12.35 Hz, 1H), 6.76 (d, *J* = 12.35 Hz, 1H).

^{13}C-NMR (100.6 MHz, DMSO-d_6): δ 146.52, 136.31, 133.90, 130.11, 129.01, 128.98, 128.54, 128.35, 124.02, 118.42.

Purification of (Z)-Stil-OH

(*Z*)-**Stil-OH** was purified from the reaction mixture by successive fractional precipitation of the (*E*)-**Stil-OH** isomer. After evaporation of the solvent the residue was resuspended in 10 mL of *n*-hexane and digested at -32 ºC for 24 h. The suspension obtained was filtered through a tight cotton plug and the solvent evaporated under reduced pressure. The residue was again resuspended in 5 mL of *n*-hexane and digested at -32 ºC for 24 h. The precipitate was filtered, the solvent evaporated and the resuspension-precipitation operation was repeated one more time with 2 mL of *n*-hexane. After evaporation of the final filtrate, a colorless oil was obtained (15 mg, 19 % yield) with a 98:2 (*Z*)-**10**:(*E*)-**10** ratio. Further purification of this mixture could not be achieved by flash column chromatography.

^{1}H-NMR (400 MHz, DMSO-d_6): δ 9.50 (s, 1H), 7.30-7.16 (m, 5H), 7.04 (d, J = 8.45 Hz, 2H), 6.62 (d, J = 8.45 Hz, 2H), 6.50 (d, J = 12.35 Hz, 1H), 6.45 (d, J = 12.35 Hz, 1H).

^{13}C-NMR (100.6 MHz, DMSO-d_6): δ 157.09, 137.74, 130.41, 130.25, 128.78, 128.70, 127.93, 127.72, 127.34, 115.48.

Supramolecular host-guest characterization of Stil-NMe_2, Stil-H, Stil-NO_2 and Stil-OH

The supramolecular association constants (K_a) of the different stilbenes studied were determined by fluorescence measurements according to a previously reported procedure.[11] The association constant of the 1:1 CD-stilbene complexes can be defined as the equilibrium constant of the following reaction:

$$\text{CD} + \text{stilbene} \rightleftharpoons \text{CD:stilbene}$$

$$K_a = \frac{[\text{CD:stilbene}]}{[\text{CD}][\text{stilbene}]} \qquad (7.2)$$

The K_a values were obtained from the observed fluorescence enhancement (or quenching) (F/F_0) as a function of the concentration of β-CD added ($[CD]_0$ = 0, 0.1, 0.5, 1, 2, 3, 5, 7 and 10 mM) to solutions of constant concentration of the stilbene of interest ($2 \cdot 10^{-5}$ M).

$$F/F_0 = 1 + (F_\infty/F_0 - 1)\frac{[CD]_0 K_a}{1 + [CD]_0 K_a} \quad (7.3)$$

In this expression F is the fluorescence intensity in the presence of CD for a certain CD:stilbene mixture, F_0 is the fluorescence intensity in the absence of CD, and F_∞ is the fluorescence intensity when all guest molecules are complexed (i.e. at infinite concentration of CD).

Synthesis of AuNP-TF@Cit3 by the Turkevich-Frens method[6]

AuNP-TF@Cit3 were prepared as previously described for **AuNP-TF@Cit1** (see above). **AuNP-TF@Cit3** were characterized by means of UV-Vis spectroscopy and TEM.

Synthesis of AuNP-TF@β-CD3 by ligand exchange[9]

AuNP-TF@β-CD3 were prepared as previously described for **AuNP-TF@βCD1** (see above). **AuNP-TF@β-CD3** were characterized by means of UV-Vis spectroscopy and TEM.

Synthesis of PVP-capped gold nanopartilces: AuNP-TF@PVP[12]

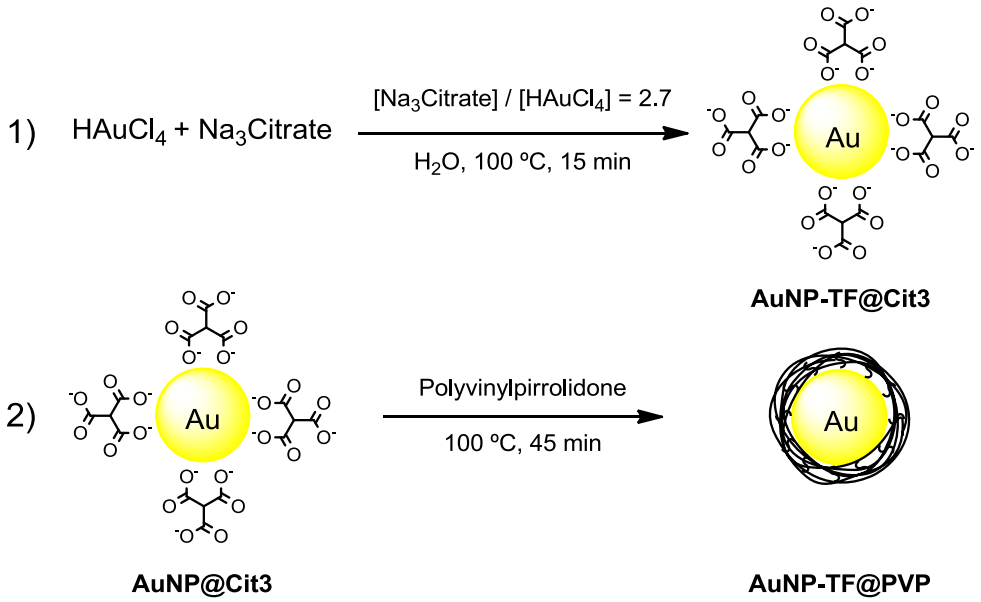

To a boiling aqueous colloidal suspension of freshly prepared **AuNP-TF@Cit3** (50 mL, *c* = 8.27·nM), 2.5 mL of a 0.2 mg/mL polyvinylpyrrolidone solution were added. The reaction mixture was allowed to boil for additional 35-45 minutes. The final colloidal suspension was allowed to cool down to room temperature, concentrated by centrifugation at 4000 rpm during 1 h and stored at 4ºC in the fridge. **AuNP-TF@PVP** were characterized by means of UV-Vis spectroscopy and TEM.

Photochemical stilbene isomerization

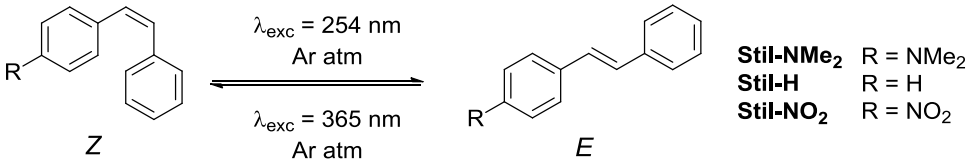

Solutions of the *Z*- and *E*-isomers of **(*Z*)-Stil-NMe$_2$**, **(*Z*)-Stil-H** and **(*Z*)-Stil-NO$_2$** in water:acetonitrile 94:6 (c = 2 10^{-6} M) were purged with Ar and irradiated with a UV-lamp (4 W) until obtaining the corresponding photostationary states (PSS). Owing to the different UV-vis absorption spectra of these compounds, $Z \rightarrow E$ photoisomerization was induced by irradiation at 254 nm, while $E \rightarrow Z$ photoisomerization was investigated by irradiation at 365 nm. After illumination, the photoisomerization conversions were determined by comparison of the UV-vis absorption spectra of the PSS mixtures with those of the pure *Z*- and *E*-isomers.

Thermal stilbene isomerization

Samples containing *ca.* 1 mg of the corresponding *Z*- or *E*-stilbene suspended in 500 μL of D_2O:CD_3CN 94:6 were purged with Ar and heated in an oil bath under reflux (~373 K) for 2 h. (i.e. the same duration as in our photocatalytic experiments). Afterwards the samples were cooled in an ice bath, 500 μL of DMSO-d_6 were added to completely dissolve the solid and they were analyzed by ^{1}H-NMR. The conversion of the *Z* isomer to the *E* form was determined from the integration of the signals for the protons at the *ortho* position of the substituted phenyl ring.

Photocatalytic studies with Au NPs

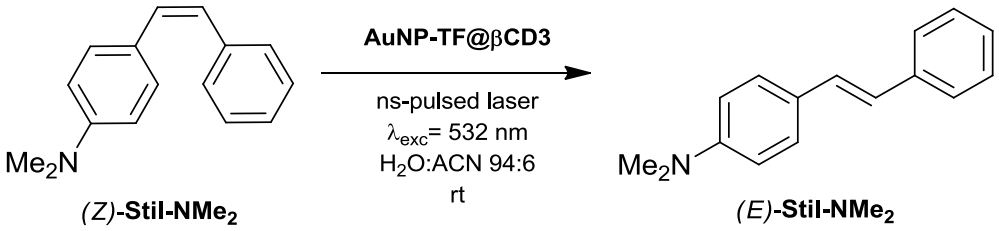

(Z)-**StiI-NMe$_2$** *(E)*-**StiI-NMe$_2$**

Photocatalysis experiments were carried out using the second harmonic of a Nd:YAG pulsed laser as excitation source (λ_{exc} = 532 nm) operating at a frequency of 10 Hz and with a round spot size of 0.8 cm in diameter.

Sample preparation and reaction

500 μL of an aqueous Au NP suspension (prepared from concentrated stock suspensions) were put in a GC vial equipped with a septum stopper. The suspension was purged with Ar and irradiated at 100 mW (10 mJ/pulse) during 30 minutes prior to the addition of the reactant molecules. Afterwards, the stilbene derivative of interest was added (30 μL from a 200 mM stock solution in acetonitrile). The resulting mixture was irradiated under stirring at 532 nm during 30, 60 or 120 minutes. All blank samples for control experiments were pre-treated in the same way (100 mW, 30 min) before the addition of the reactant molecules. When required, other compounds were added to the reaction mixtures before irradiation (e.g. Ad-NH_2 or β-CD).

Sample work-up

After irradiation, the reaction mixture was diluted with acetonitrile (6 mL) and centrifuged at 12000 rpm during 15 minutes. The supernatant was isolated and evaporated under reduced pressure. The final residue was dissolved in deuterated DMSO for further ^{1}H-NMR analysis. Determination of the final $Z \rightarrow E$ (or $E \rightarrow Z$) isomerization conversion for the photocatalytic studies was determined by integration of the signals for the protons at the *ortho* position of the substituted phenyl ring.

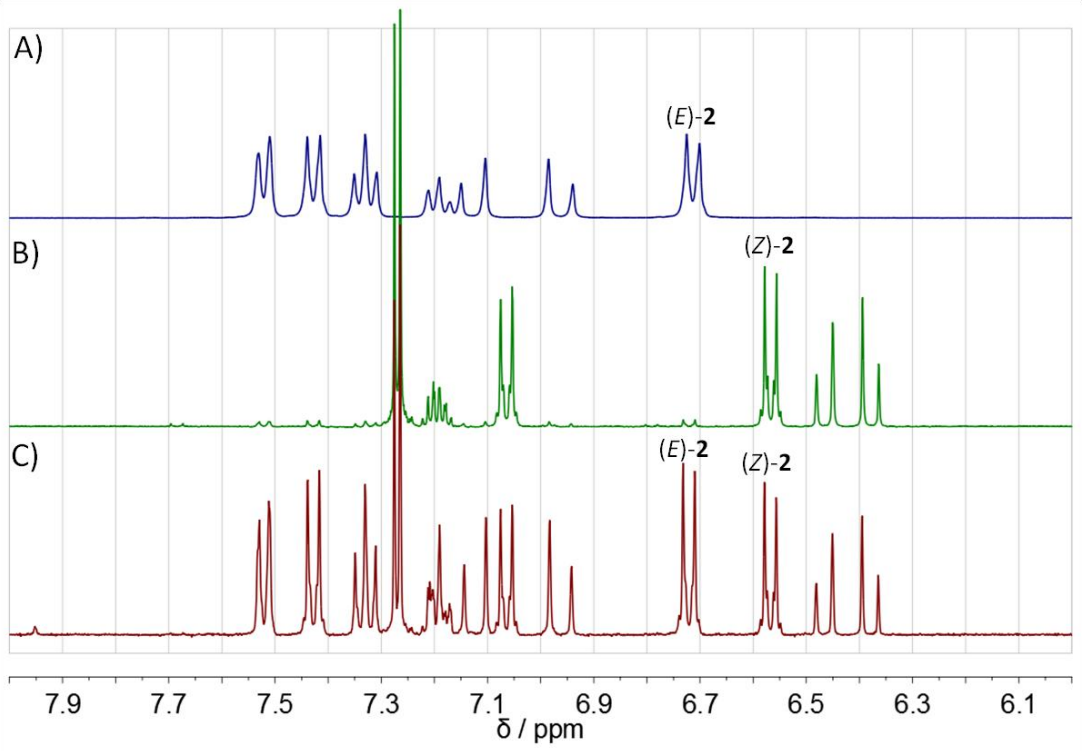

Figure 7.1. ^{1}H-NMR spectra (400 MHz, DMSO-d_6) of A) (*E*)-**StilNMe$_2$** and B) (*Z*)-**StilNMe$_2$**. C) ^{1}H-NMR spectrum (400 MHz, DMSO-d_6) of the reaction mixture obtained after irradiation of (*Z*)-**Stil-NMe$_2$** at λ = 532 nm in the presence **of AuNP-TF@βCD3** The *Z* → *E* conversion obtained for this experiment was 55% as calculated from the integrals corresponding to the proton signals indicated in the spectrum.

Recycling experiments

At the end of a photocatalytic experiment, the reaction mixture was diluted with acetonitrile (1 mL) and centrifuged in an *eppendorf* tube at 11000 rpm during 8 min. The supernatant was isolated for further ^{1}H-NMR analysis of the reaction conversion and the pelleted **AuNP-TF@β-CD3** were resuspended in deionized water (500 μL) under sonication for the next photocatalytic cycle.

7.2.3- Photocatalysis of bimolecular reactions

Photoinduced [4+4] cycloaddition of 2-anthracenecarboxylate[13]

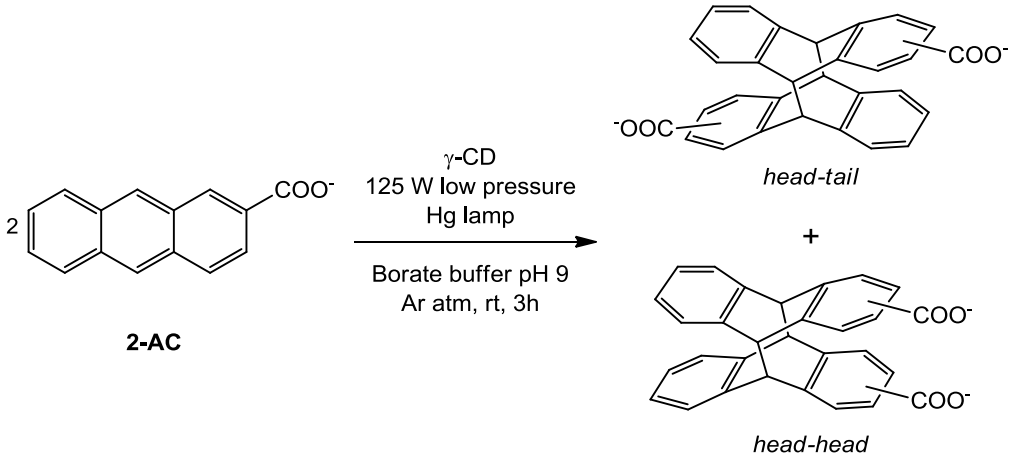

2-AC **$(2\text{-AC})_2$**

γ-cyclodextrin (0.65 g, 0.5 mmol) were dissolved in borate buffer (700 mL) pH = 9.2. 2-anthracene carboxylic acid (0.23, 1.1 mmol) was then added and the resulting solution was stirred at room temperature for 90 minutes. Afterwards, the resulting pale yellow solution was irradiated with a low pressure Hg lamp (125 W, λ = 250-400 nm) n a quartz reactor under stirring and argon atmosphere during 3 h. Then, the solution was acidified until pH = 2 by the drop wise addition of concentrated HCl and a brown-orange precipitate appeared, which was filtered and discarded. The filtrate was extracted with diethyl ether 4x100 mL, dried over Na_2SO_4 and the solvent was removed evaporated under reduced pressure to provide 0.893 g of a white solid (38 % yield).

1H-NMR (400 MHz, DMSO-d_6): δ 7.54 (dd, J_1 = 9.1 Hz, J_2 = 1.6 Hz), 7.40 (dd, J_1=7.6 Hz, J_2=1.6 Hz), 7.05-7.14 (m, 3H), 6.93-7.02 (m, 4H), 6.76-6.84 (m, 4H), 4.77 (m, 4H).

Thermal retro-cycloaddition of 2-anthracenecarboxylate dimers

$(2\text{-AC})_2$ **2-AC**

(2-AC)$_2$ (15 mg, 0.035 mmol) was dissolved in DMSO-d_6 (0.6 mL) and the resulting solution was transferred to an NMR tube. Afterwards the solution was purged thoroughly with Ar. The sample was sealed (rubber stopper and laboratory film) and heated at 150 ºC in an oil bath. The sample was monitored by ^{1}H-NMR every 24 h during two days, by inspection of the signal at δ = 4.77 ppm corresponding to the alkyl protons of **(2-AC)$_2$**.

Synthesis of AuNP-TF@Cit4 by the Turkevich-Frens method

AuNP-TF@Cit4 were prepared as previously described for **AuNP-TF@Cit1** (see above). **AuNP-TF@Cit4** were characterized by means of UV-Vis spectroscopy and TEM.

Synthesis of AuNP-TF@γCD by ligand exchange

AuNP-TF@γCD were prepared as previously described for **AuNP-TF@βCD1** (see above). **AuNP-TF@γCD** were characterized by means of UV-Vis spectroscopy and TEM.

Photocatalytic dimerization of 2-antracenecarboxylate with gold nanoparticles

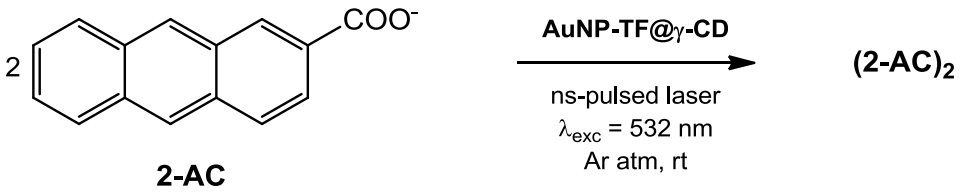

2-AC

Photocatalysis experiments were carried out using the second harmonic of a Nd:YAG pulsed laser as excitation source (λ_{exc} = 532 nm) operating at a frequency of 10 Hz and with a round spot size of 0.8 cm in diameter.

Sample preparation and reaction

500 μL of an aqueous **AuNP-TF@γ-CD** suspension (prepared from concentrated stock suspensions) were put in a GC vial equipped with a septum stopper. The suspension was purged with Ar and irradiated at 150 mW (15 mJ/pulse) during 30 minutes prior to the addition of the reactant molecules. Afterwards, **2-AC** was

added (30 μL from a 200 mM stock solution in DMSO). The resulting mixture was irradiated under stirring at 532 nm during 120 minutes. When required borate buffer was added to the reaction mixture.

Sample work-up

After irradiation, the reaction mixture was diluted with hydrochloric acid (0.5 mL, 0.1 M) and acetonitrile was added (6 mL). The resulting mixture was centrifuged at 12000 rpm during 15 minutes. The supernatant was isolated and evaporated under reduced pressure. The final residue was dissolved in deuterated DMSO for further ^{1}H-NMR analysis. Determination of the conversion for the photocatalytic studies was determined according to ^{1}H NMR by inspection of the signals corresponding to the alkyl protons on **(2-AC)$_2$**.

7.2.4- Controlled assembly of gold nanoparticles using cyclodextrin-based supramolecular chemistry

Synthesis of 2-(2-(2-(2-hydroxyethoxy)ethoxy)ethoxy)ethyl-4-methyl-benzenesulfonate (8)

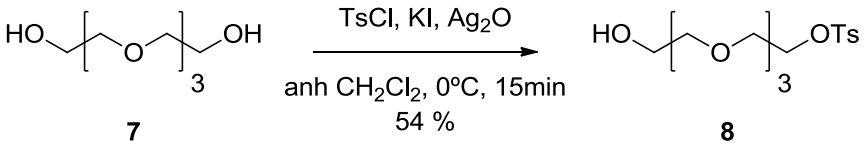

7 **8**

This product was synthesized adapting the procedure described by Bouzide and Sauvé.[14] Briefly, a mixture containing tetraethylene glycol (5.00 g, 26 mmol), Ag_2O (8.95 g, 39 mmol) and KI (0.863 g, 5 mmol) in dry dichloromethane (60 mL) under Ar atmosphere was cooled to 0 ºC. Then *p*-toluensulfonyl chloride (5.45 g, 29 mmol) was added at once. The obtained mixture was allowed to stir at 0 ºC under Ar atmosphere for 15 min. The whole mixture was filtered through a pad of Celite and the filter cake was washed with a 12/1 CH_2Cl_2/CH_3OH solution (4 x 25 mL). The solvent was removed under vacuum and the residue was purified by flash column chromatography in Silica 60 with ethyl acetate to provide 4.88 g of a colorless oil (54 % yield).

^{1}H NMR (360 MHz, $CDCl_3$): δ 7.82 (d, 2H, *J* = 8.0 Hz), 7.36 (d, 2H, *J* = 8.0 Hz), 4.18 (m, 2H), 3.76-3.58 (m, 14H), 2.46 (s, 3H).

^{13}C NMR (90 MHz, $CDCl_3$): δ 144.96, 133.08, 129.97, 128.13, 72.58, 70.88, 70.79, 70.60, 70.46, 69.38, 61.88, 21.79.

HRMS (ESI+)**:** m/z calcd. for [$C_{15}H_{24}O_7S$+Na^+] 371.1135, found 371.1136.

Synthesis of S-(2-(2-(2-(2-hydroxyethoxy)ethoxy)ethoxy)ethyl) ethanethioate (10)[15]

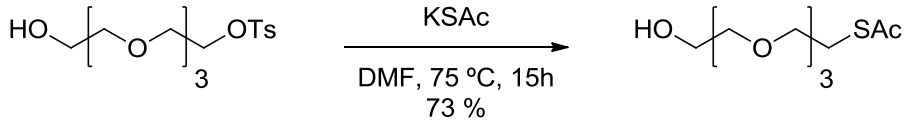

8 **10**

Monotosylated tetraethylene glycol **8** (3.00 g, 8.6 mmol) and potassium thioacetate (2.20 g, 19.3 mmol) were dissolved in dry DMF (30 mL). The resulting mixture was stirred at 75ºC during 15 h. After evaporating the solvent under reduced pressure, the residue was diluted in ethyl acetate (25 mL), and water (25 mL) was added. The water phase was extracted with ethyl acetate (3 x 10 mL). The combined organic phase was dried over Na_2SO_4, filtered and evaporated under reduced pressure and a dark brown oil was obtained. Purification by flash column chromatography in Silica 60 with hexanes:EtOAc (2:1) → EtOAc → 10% MetOH in EtOAc provided 1.59 g of an amber oil (73 % yield).

^{1}H NMR (360 MHz, $CDCl_3$): δ 3.80-3.54 (m, 14H), 3.11 (t, 2H, *J* = 6.4 Hz), 2.50 (broad s, 1H) 2.35 (s, 3H).

^{13}C NMR (90 MHz, $CDCl_3$): δ 195.65, 72.48, 70.68, 70.51, 70.38, 70.29, 69.80, 61.79, 30.60, 28.79.

Synthesis of 2-(2-(2-(2-mercaptoethoxy)ethoxy)ethoxy)ethanol (OEG-SH)

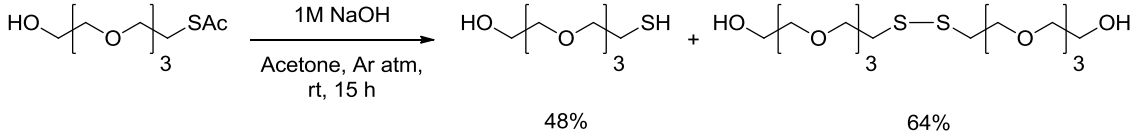

48% 64%

10 **OEG-SH** **11**

The synthetic procedure was adapted from reference 15. Compound **10** (400 mg, 1.6 mmol) was dissolved in acetone (5 mL) at 0ºC and under Ar atmosphere. Then

5 mL 1 M NaOH in MetOH was added and the obtained solution was stirred at 0ºC under Ar atmosphere during 7 h. The reaction mixture was quenched by the addition of water (50 mL) and acidified with 0.1 M HCl solution. The aqueous solution was then extracted with CH_2Cl_2 (4 x 20 mL). The combined organic layers were dried over Na_2SO_4 and filtered. Evaporation of the solvent followed by purification by flash column chromatography in Silica 60 with 5 % MeOH in CH_2Cl_2 provided 161 mg of a color-less oil (48 % yield) identified as **OEG-SH**. In addition, 215 mg of disulfide **11** were also isolated (64 % yield).

^{1}H NMR (400 MHz, $CDCl_3$): δ 3.84-3.59 (m, 14H), 2.70 (dt, 2H, J_1 = 8.3 Hz, J_2 = 6.5 Hz).

^{13}C NMR (90 MHz, $CDCl_3$): δ 73.06, 72.63, 70.79, 70.65, 70.50, 70.34, 61.91, 24.38.

Spectroscopic data of compound **11**:

^{1}H NMR (360 MHz, $CDCl_3$): δ 3.79-3.58 (m, 28H), 2.9 (t, 4H, J = 6.5 Hz).

^{13}C NMR (90 MHz, $CDCl_3$): δ 72.66, 70.76, 70.62, 70.45, 70.44, 69.73, 61.84, 38.45, 31.08.

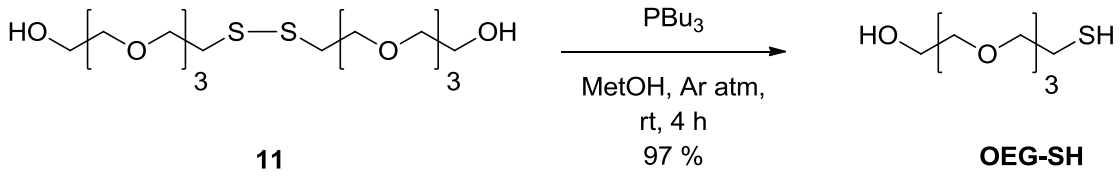

11 **OEG-SH**

In order to improve the overall yield for this reaction, disulfide **10** was submitted to reducing conditions. Briefly, to a solution of **11** (62 mg, 0.15 mmol) in degassed MeOH (5mL), PBu_3 was added (155 µL, 0.62 mmol) and the mixture was stirred at room temperature under Ar atmosphere for 4 h. Then the reaction was quenched by the addition of water (20 mL) and the obtained solution was extracted with EtOAc (3 x 3 mL). The combined organic fractions were dried over Na_2SO_4, filtered and concentrated under reduced pressure. The crude reaction mixture was purified in Silica 60 with 1% MetOH in $CHCl_3$ to provide 60 mg of **OEG-SH** (97 % yield).

Synthesis of (*E*)-(4-(phenyldiazenyl)phenyl)methanol (13)[16]

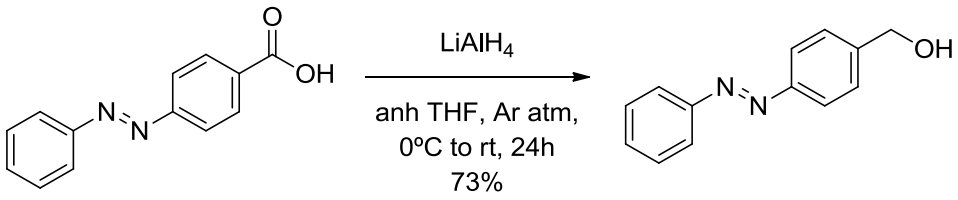

12 **13**

A solution of 4-(phenyldiazenyl)benzoic acid (2.50 g, 11 mmol) in anhydrous THF (60 mL) was added in small portions to a suspension of $LiAlH_4$ (550 mg, 14.5 mmol) in anhydrous THF (40 mL) kept at 0 ºC under Ar atmosphere. The reaction mixture was allowed to warm to room temperature and stirred for 24 h under Ar atmosphere. Then, the reaction mixture was cooled to 0 ºC and water (0.6 mL) was added slowly, followed by 10 % aqueous NaOH (1.2 mL) and additional water (2 mL). The obtained suspension was filtered through a pad of Celite and the filter cake washed with THF (3 x 20 mL). The combined filtrates were evaporated under reduced pressure to provide an orange solid. The crude product obtained by evaporation was purified by flash column chromatography in Silica 60 with hexanes/EtOAc (6/4) to provide 1.7 g of a light orange solid (73 % yield).

^{1}H NMR (360 MHz, $CDCl_3$): δ 7.97-7.89 (m, 4H), 7.57-7.47 (m, 5H), 4.81 (d, 2H, *J* = 5.8 Hz), 1.78 (t, 1H, *J* = 5.8 Hz).

^{13}C NMR (90 MHz, $CDCl_3$): δ 72.67, 70.76, 70.63, 70.46, 70.44, 69.72, 61.84, 38.46.

Synthesis of (*E*)-4-(phenyldiazenyl)benzyl 4-methylbenzenesulfonate (14)

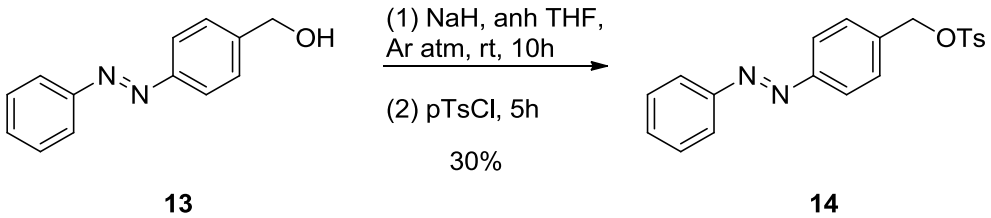

13 **14**

To a solution of *p*-(phenyldiazenyl)benzyl alcohol (**13**) (500 mg, 2.4 mmol) in dry THF/DMF (3:1) (30 mL) under Ar atmosphere, NaH (175 mg, 4.4 mmol) was added. The mixture was stirred at room temperature and in the absence of light for 10 hours, during which the colour of the solution changed from light orange to deep dark orange. Tosyl chloride (1.00 g, 5.2 mmol) was then added with an immediate recovery of the initial orange color. The reaction mixture was stirred at room temperature under Ar

atmosphere for 12 hours. Then, the reaction mixture was poured over saturated $NaHCO_3$ solution in water (50 mL). The aqueous phase was extracted with CH_2Cl_2 (3 x 25 mL). The combined organic layers were dried over Na_2SO_4, filtered and their solvent evaporated under reduced pressure. The obtained orange solid was purified by flash column chromatography in Silica 60 with hexanes/EtOAc (4/1) and, then, hexanes/EtOAc (2/1) to yield 264 mg of an orange solid (30 % yield).

^{1}H NMR (360 MHz, $CDCl_3$): δ 7.96–7.89 (m, 2H), 7.87 (d, 2H, *J* = 8.0 Hz), 7.83 (d, 2H, *J* = 8.0 Hz), 7.58-, 7.46 (m, 3H), 7.41 (d, 3H, *J* = 8 Hz), 7.35 (d, 2H, *J* = 8 Hz), 5.15 (s, 2H), 2.45 (s, 3H).

^{13}C NMR (90 MHz, $CDCl_3$): δ 72.67, 70.76, 70.63, 70.46, 70.44, 69.72, 61.84, 38.46.

ESI-HRMS: m/z; calcltd for $[C_{16}H_{34}O_8S_2+Na]^+$: 441.1587, found 441.1589.

Synthesis of (*E*)-1-(4-(phenyldiazenyl)phenyl)-5,8,11-trioxa-2-thiatridecan-13-yl acetate (XV)

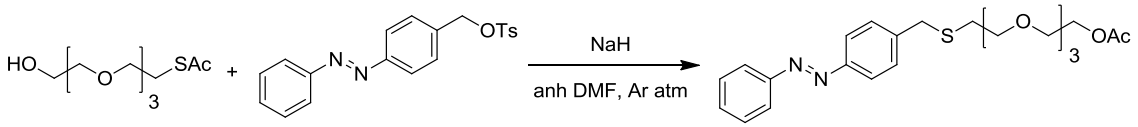

10 **14** **XV**

To a solution of thioacetate **10** (115 mg, 0.45 mmol) and *p*-(phenyldiazenyl)benzyltosylate **14** (74 mg, 0.2 mmol) in dry THF/DMF (3:1) NaH (24 mg, 0.59 mmol) was added. The mixture was stirred at room temperature in the absence of light under Ar atmosphere for 36 hours. Then, the reaction mixture was poured over saturated $NaHCO_3$ solution in water (50 mL). The aqueous phase was extracted with CH_2Cl_2 (3 x 25 mL). The combined organic layers were dried over Na_2SO_4, filtered and their solvent evaporated under reduced pressure. The obtained orange oil was purified by flash column chromatography in Silica 60 CH_2Cl_2, then 3% MetOH in CH_2Cl_2 and then 10% MetOH in CH_2Cl_2 to yield 24 mg of an orange oil (27% yield).

^{1}H NMR (360 MHz, $CDCl_3$): δ 7.96–7.89 (m, 2H), 7.87 (d, 2H, *J* = 8.0 Hz), 7.83 (d, 2H, *J* = 8.0 Hz), 7.58-, 7.46 (m, 3H), 7.41 (d, 3H, *J* = 8 Hz), 7.35 (d, 2H, *J* = 8 Hz), 5.15 (s, 2H), 2.45 (s, 3H).

^{13}C NMR (90 MHz, $CDCl_3$): δ 72.67, 70.76, 70.63, 70.46, 70.44, 69.72, 61.84, 38.46.

ESI-HRMS: m/z; calcltd for $[C_{23}H_{30}N_2O_5S+Na]^+$: 469.1768, found 441.1589.

Synthesis of (*E*)-3,6,9,16,19,22-hexaoxa-12,13-dithiatetracosane-1,24-diyl bis(4-((*E*)-phenyldiazenyl)benzoate) (16)

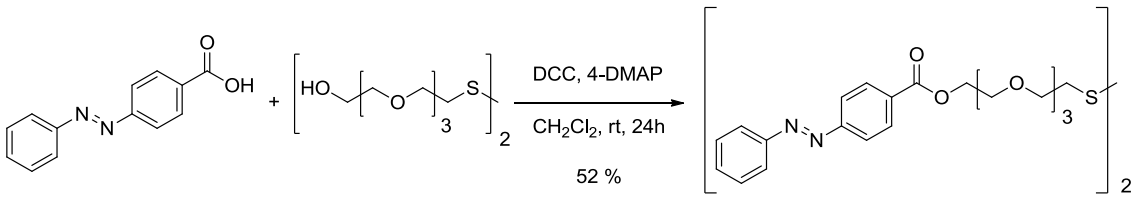

12 **11** **16**

To a solution of 4-(phenylazo)carboxylic acid (76 mg, 0.335 mmol), 4-dimethylaminopyridine (41 mg, 0.335 mmol) and **11** (70 mg, 0.167 mmol) in dry CH_2Cl_2 (20 mL), DCC (670 µL 1.0 M in CH_2Cl_2, 0.67 mmol) was added. The resulting mixture was stirred at room temperature during 24 h. Then water was poured (25 mL), and the organic phase was washed with water (3 x 15 mL), dried with Na_2SO_4, filtered and concentrated under reduced pressure. The product obtained was dissolved in the minimum amount of acetone to dissolve the orange oil rather than the colourless crystals. The mixture was cooled at -32 ºC and filtered through a tight cotton plug. The redisolution-precipitation cycle was repeated twice. After evaporation of the final solvent, the oil was purified by flash column chromatography in Silica 60 with CH_2Cl_2/acetone (10/1) to provide 75 mg of an orange oil (52 % yield).

^{1}H NMR (360 MHz, $CDCl_3$): δ 8.20 (d, 4H, *J* = 8.8 Hz), 7.98-7.91 (m, 8H), 7.57-7.49 (m, 6H), 4.51 (m, 4H), 3.86 (m, 4H), 3.75-3.58 (m, 20H), 2.86 (t, 4H, *J* = 6.6 Hz)..

^{13}C NMR (90 MHz, $CDCl_3$): δ 166.11, 155.28, 152.66, 131.88, 130.90, 129.33, 123.31, 122.79, 70.85, 70.80, 70.73, 70.51, 69.74, 69.32, 64.53, 38.44.

ESI-HRMS: m/z; calcltd for $[C_{42}H_{50}N_4O_{10}S_2+H]^+$: 835.3041, found 835.3053.

Synthesis of (*E*)-2-(2-(2-(2-mercaptoethoxy)ethoxy)ethoxy)ethyl 4-(phenyldiazenyl)benzoate (Azo-OEG-2)

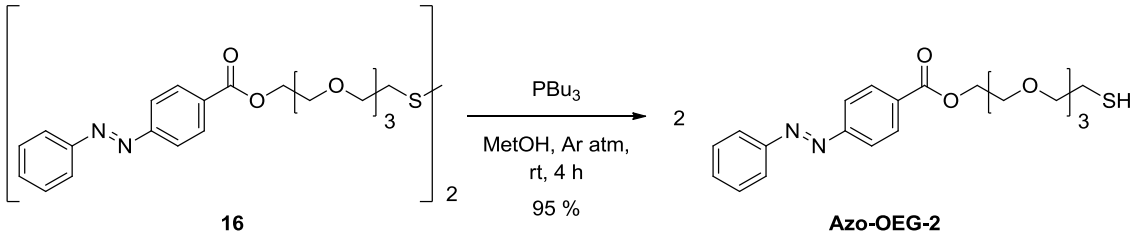

16 **Azo-OEG-2**

To a solution of **16** (58 mg, 0.07 mmol) in degassed methanol (5 mL) and acetone (3 mL), PBu_3 (70 µL, 0.28 mmol) was added and the mixture was stirred at 0 ºC under Ar atmosphere for 4 h. Then the reaction was quenched by the addition of water (30 mL) and the obtained solution was extracted with diethylether (3 x 5 mL). The combined organic fractions were dried over Na_2SO_4, filtered and concentrated under reduced pressure. The crude reaction mixture was purified in Silica 60 with 1% MeOH in $CHCl_3$ to provide 56 mg of **Azo-OEG-SH2** (95 % yield).

^{1}H NMR (400 MHz, $CDCl_3$): δ 8.21 (d, 2H, *J* = 8.6 Hz), 7.98-7.92 (m, 4H), 7.58-7.48 (m, 3H), 4.52 (m, 2H), 3.87 (m, 2H), 3.77-3.58 (m, 10H), 2.69 (dt, 2H, J_1 = 8.2 Hz , J_2 = 6.4 Hz), 1.58 (t, 1H, *J* = 8.2 Hz).

^{13}C NMR (100.6 MHz, $CDCl_3$): δ 166.14, 155.34, 152.71, 131.93, 131.87, 130.90, 129.35, 123.31, 122.78, 73.05, 70.92, 70.87, 70.79, 70.40, 69.37, 64.54, 24.42.

ESI-HRMS: m/z; calcltd for $[C_{21}H_{26}N_2O_5S+Na]^+$: 441.1460, found 441.1467.

Photochemical and thermal characterization of AZO-OEG-2

Absorption spectra

The absorption spectrum of ***(E)*-AZO-OEG-2** was measured from a 19 µM **AZO-OEG-2** solution in 1 % ACN in water. This sample was prepared by the appropriate dilution of a 1.9 mM ***(E)*-AZO-OEG-2** stock solution in ACN. From this UV-Vis absorption spectrum, a molar absorptivity of 20210 $M^{-1}\cdot cm^{-1}$ at 325 nm was calculated.

The absorption spectrum of ***(Z)*-AZO-OEG-2** was derived from the spectral data for the corresponding initial *E* isomer and of the photostationary state mixture achieved in ACN at 365 nm, the composition of which was determined from ^{1}H NMR analysis.

The molar absorptivity at 263 nm estimated for the derived spectrum was 9369 $M^{-1} \cdot cm^{-1}$.

E-Z photoisomerization of AZO-OEG-2

A 19 μM solution of **(*E*)-AZO-OEG-2** in 1 % ACN in water was degassed with Ar and irradiated at 365 nm with a monochromatic UV lamp (4 W) until no significant changes in the UV Vis spectra could be observed. UV Vis absorption spectra were recorded every 10 seconds of irradiation. An estimated 90 % conversion was derived from ^{1}H NMR analysis. In addition, a 10^{-2} M **(*E*)-AZO-OEG-2** in ACN-d_3 sample was degassed with Ar and irradiated with monochromatic light at 365 nm until no changes were observed by UV-Vis absorption spectroscopy. Then, the ^{1}H NMR of the PSS mixture was registered to determine its composition. Simultaneously, and aliquot of this sample was diluted in a 1% mixture of ACN in water to determine its absorption spectrum. All this data was used to estimate the UV Vis absorption spectrum of **(*Z*)-AZO-OEG-2** in water, which was subsequently applied to the determination of the composition of the PSS mixtures obtained in this solvent.

Z-E photoisomerization of AZO-OEG-2

An *E*/*Z* **AZO-OEG-2** mixture, corresponding to the PSS obtained by irradiation at 365 nm, with a total concentration of 19 μM **AZO-OEG-2** in 1 % ACN in water was degassed with Ar and illuminated with a cw laser at 406 nm until no significant changes in the UV Vis spectra could be observed. UV Vis absorption spectra were recorded every 2 seconds of irradiation. An estimated 65% conversion was derived by comparison of the spectra corresponding to the PSS and those of pure *Z* and *E* isomers.

Thermal Z→E back isomerization

Thermal *Z→E* back isomerization rate constant was determined by monitoring the time-dependence of the absorption spectra of an E/Z **AZO-OEG-2** mixture (corresponding to the PSS upon 365 nm irradiation) with a total concentration of 19 μM **AZO-OEG2** in 1 % ACN in water in the dark at 25 ºC. UV Vis absorption spectra were recorded every 10 minutes and the time dependence of the spectral data fitted to a monoexponential growth function.

Supramolecular Host-Guest characterization of (E)-Azo-OEG-2

The supramolecular K_a value between α-CD and **(*E*)-Azo-OEG-2** was determined using Benesi-Hildebrand plots according to reference 17. Briefly, different samples containing equal amounts of **(*E*)-Azo-OEG-2** (0.5 mM) and increasing amounts of a-CD from 0 to 10 mM in D_2O were prepared and their ^1H NMR spectra were subsequently analyzed. Afterwards the degree of complexation (α) was calculated from the observed change of the signals in the aromatic region corresponding to complexed and uncomplexed molecules of **(*E*)-Azo-OEG-2**. The K_a values were derived from the slope of the corresponding Benesi-Hildebrand plot (Figure 7.2).

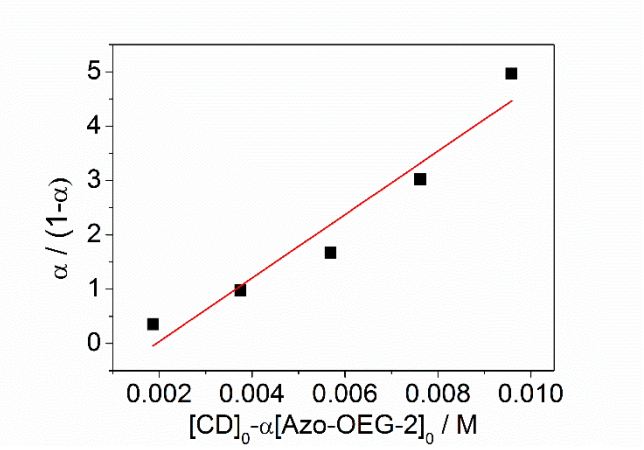

Figure 7.2. Benesi-Hildebrand plot of (α/1−α) vs ([CD]$_0$−α[**AZO-OEG-2**]$_0$). Black squares correspond to the experimental data and the red line to the least squares fit. A K_a value for the α-CD:(E)-**AZO-OEG-2** complex of 584 ± 83 corresponding to the slope of the fitted equation was determined.

Synthesis of Au NP-Gn@Cit

Citrate-stabilized Au NPs were prepared according to the seed-growth method described by Bastús et al.[8]

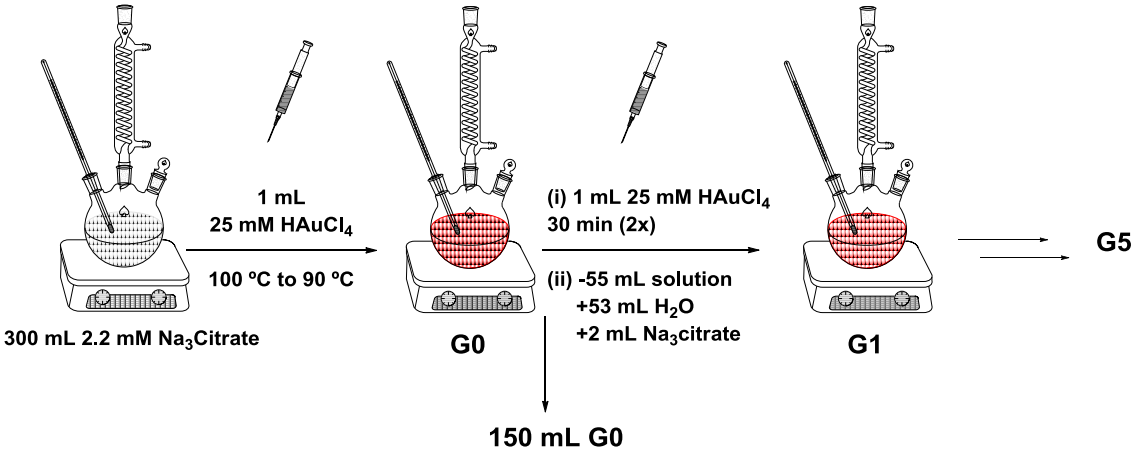

*Synthesis of Au seeds (**G0**)*

A 2.2 mM solution of sodium citrate in deionized water (300 mL) was heated in an oil-bath in a 500 mL round-bottomed flask. After boiling had commenced, 2 mL of $HAuCl_4$ (25 mM) were injected. The colour of the solution changed from initial yellow to bluish gray and then soft pink in few minutes. 150 mL of the seed solution were immediately transfered to a 250 mL three-necked round-bottomed flask equipped for the next step with a thermometer in one of the small necks, a reflux condenser in the central one and a septum stopper in the remaining one.

Seeded growth of Au NPs up to the 5th Generation

Right after the synthesis of the Au seeds (**G0**), the solution was allowed to reach 90 ºC. Then, 1 mL of $HAuCl_4$ solution (25 mM) was injected. After 30 min the reaction was finished. This process was repeated twice. After that the reaction was diluted by extracting a 55 mL sample, which was stored as the **G1** sample, and adding 53 mL of deionized water and 2 mL of 60 mM sodium citrate. This solution was then used as a seed solution for the synthesis of the next generation of nanoparticles and the process was repeated 4 more times to reach **G5** The obtained colloidal dispersions of citrate-stabilized Au NPs were characterized by means of UV-Vis spectroscopy and TEM.

Synthesis of AuNP-G0@αCD by the ligand exchange method

150 mL of an Au NP seed suspension were stirred at room temperature. To this colloidal dispersion, 16.5 mL of 1 mM **α-CD-$(SH)_6$** and 10 mM NaOH solution in ethanol were added and the mixture was stirred for 3 days. Then ACN (150 mL) was added and the resulting mixture stirred for 30 min. The resulting colloidal dispersion was centrifuged at 10000 rpm during 20 min. The supernatant was removed and the pelleted NPs were resuspended in 8 mL of DMF and dialyzed against this solvent for 3 days changing the solvent bath every 24 h. The solution was then diuted with ACN (80 mL) and the mixture stirred for 30 min. The resulting colloidal dispersion was centrifuged at 10000 rpm during 20 min. The supernatant was removed and the pelleted **AuNP-G0@αCD** were resuspended in the minimum amount of deionized water with the help of an ultrasonic bath. These NPs were characterized by means of TEM and UV-Vis spectroscopy.

Synthesis of AuNP-G5@αCD by the ligand exchange method

50 mL of a citrate-stabilized **G5** suspension were stirred at room temperature. To this colloidal dispersion, 5.5 mL of 1 mM **α-CD-SH$_6$** and 10 mM NaOH solution in ethanol were added and the mixture was stirred for 3 days. Purification and characterization of these NPs was carried out as previously described for **AuNP-G0@αCD**.

Synthesis of method AuNP-G3@AZO-OEG/OEG by the ligand exchange

50 mL of a citrate-stabilized **G3** suspension were stirred at room temperature. To this colloidal dispersion, 5.5 mL of 0.2 mM **AZO-OEG-SH2**,, 0.8 mM **OEG-SH** and 10 mM NaOH solution in ethanol were added and the mixture was stirred for 3 days. After this time, the reaction mixture was centrifuged at 4000 rpm during 1 hour. The supernatant was discarded and the concentrated NPs were resuspended in deionized water. This centrifugation-resuspension cycle was repeated 2 more times and the final concentrated Au NPs were resuspended in water.

Synthesis of method AuNP-G2@AZO-OEG/OEG by the ligand exchange method

50 mL of a citrate-stabilized **G2** suspension were stirred at room temperature. To this colloidal dispersion, 5.5 mL of 0.25 mM **AZO-OEG-SH2**, 0.75 mM **OEG-SH** and 10 mM NaOH solution in ethanol were added and the mixture was stirred for 3 days. ACN was added to dilute the reaction mixture to one half. The NP dispersion was then centrifuged at 3000 rpm during 40 minutes. The supernatant was removed and the concentrated Au NPs were resuspended in deionized water with the help of an ultrasonic bath. The colloidal dispersion was diluted with an equal amount of ACN and centrifuged at 3000 rpm during 40 minutes. The supernatant was removed and the pelleted Au NPs were removed from the glass tube with the minimum amount of deionized water using an ultrasonic bath. After testing the solubility of the obtained colloid in different solvents the stock solution was finally resuspended in DMF.

Synthesis of method AuNP-G1@AZO-OEG/OEG by the ligand exchange method

As described for **AuNP-G2@AZO-OEG/OEG**, but starting from a citrate-stabilized **G1** suspension and a 0.15 mM **Azo-OEG-2**, 0.85 mM **OEG-SH** and 10 mM NaOH solution in ethanol. The obtained nanoparticles were characterized by TEM and UV-vis spectroscopy.

Synthesis of method AuNPG5@AZO-OEG/OEG_1 by the ligand exchange method

As described for **AuNP-G2@AZO-OEG/OEG**, but starting from a citrate-stabilized **G5** suspension and a 0.05 mM **Azo-OEG-2**, 0.95 mM **OEG-SH** and 10 mM NaOH solution in ethanol. The obtained nanoparticles were characterized by TEM and UV-vis spectroscopy.

Synthesis of method AuNP-G5@AZO-OEG/OEG_2 by the ligand exchange method

As described for **AuNP-G2@AZO-OEG/OEG**, but starting from a citrate-stabilized **G5** suspension and a 0.15 mM **Azo-OEG-2**, 0.85 mM **OEG-SH2** and 10 mM NaOH solution in ethanol. The obtained nanoparticles were characterized by TEM and UV-vis spectroscopy.

Synthesis of method AuNP-G4@OEG-SH by the ligand exchange method

As described for **AuNP-G2@AZO-OEG/OEG**, but starting from a citrate-stabilized **G2** suspension and a 1 mM **OEG-SH2** and 10 mM NaOH solution in ethanol. The obtained nanoparticles were characterized by TEM and UV-vis spectroscopy.

Ligand induced assembly of AuNP-G4@OEG

Samples containing equal amounts of **AuNP-G4@OEG** and increasing amounts of ditopic azobenzene ligand **11** in 1% acetonitrile in water were prepared and monitored by UV-vis spectroscopy during 6 days.

Ligand induced assembly of AuNP-G0@αCD

Samples containing equal amounts of **AuNP-G0@αCD** and increasing amounts of ditopic azobenzene ligand **11** in 1% acetonitrile in water were prepared and monitored by UV-vis spectroscopy during 10 days.

Preparation of Au NP heteroaggregates

Samples containing mixtures of host- and guest- functionalized Au NPs were prepared by mixing appropriate quantities of their corresponding stock solutions. The ratio between small and big NP was adjusted to 10 and the resulting mixtures were stirred at room temperature in the dark during 24h. Afterwards the Au NP mixtures were analyzed by Cryo-TEM.

7.5- BIBLIOGRAPHY

[1] Rojas, M. T.; Königer, R.; Stoddart, J. F. Kaifer, A. E. *J. Am. Chem. Soc.* **1995**, 117, 336.

[2] Wang, H. M.; Wenz,G. *Chem. Asian J.* **2011**, 6, 2390.

[3] Defaye, G.; Crouzy, S.; Evrard, N.; Law, H. *WO9961483 (A1)*.

[4] Nelles, G.; Weisser, M.; Back, R.; Wolhfart, P.; Wenz, G.; Mittler-Neher, S. *J. Am. Chem Soc.* **1996**, 118, 5039.

[5] Kaifer, *Langmuir*, **2000**, 16, 3000.

[6] Kimling, J.; Maier, M.; Okenve, B.; Kotadis, V.; Ballot, H.; Plech, A. *J. Phys. Chem B* **2006**, 110, 15700.

[7] Frens, G. *Nature Phys. Sci.* **1973**, 241, 20.

[8] Bastús, N. G.; Comenge, J.; Puntes, V. *Langmuir* **2011**, 27, 11098.

[9] Weibecker, C. S.; Merrit, M. V.; Whitesides, G. M. *Langmuir*, **1996**, 12, 3763.

[10] X. Liu, M. Atwater, J. Wang, and Q. Huo, *Coll. Surf. B Biointerfaces*, 2007, **58**, 3-7.

[11] Wagner, B. D.; Fitzpatrick, S. *J. Inclus. Phen. Macrocyclic Chem.*, **2000**, 38, 467.

[12] Gangwar, K. R.; Dhumale, V. A.; Kumari, D.; Nakate, U. T.; Gosavi, S. W.; Sharma, R. B.; Kale, S. N.; Datar, S. *Mater. Sci. Eng. C*, **2012**, 32, 2659.

[13] Nakamura, A.; Inoue, Y. *J. Am. Chem. Soc.* **2003**, 125, 966.

[14] Bouzide, A.; Sauvé G. *Org Lett* **2002**, 4, 2329.

[15] Frisch, H.; Fritz, E.-V.; Stricker, F.; Schmüser, L.; Spitzer, D.; Weidner, T.; Ravoo, B. J.; Besenius, P. *Angew. Chem. Int. Ed.* **2016**, 55, 7242.

[16] Fatás, P.; Longo, E.; Rastrelli, F.; Crisma, M.; Toniolo, C.; Jiménez, A. I.; Cativiela, C.; Moretto, A. *Chem. Eur. J.* **2011**, 17, 12606-12611.

[17] Yamaguchi, H.; Kobayashi, Y.; Kobayashi, R.; Takashima, Y.; Hashidzume, A.; Harada, A. *Nat. Commun.* **2012**, 3:603.

Formula Index

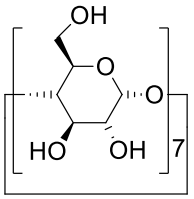

β-CD

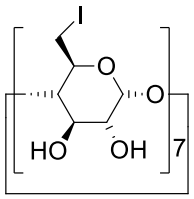

1

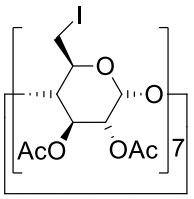

2

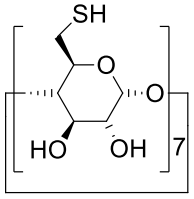

β-CD-(SH)$_7$

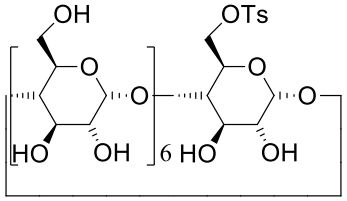

3

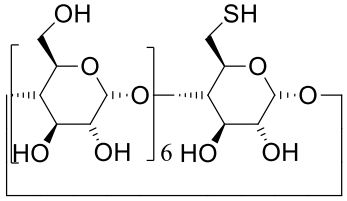

β-CD-(SH)$_1$

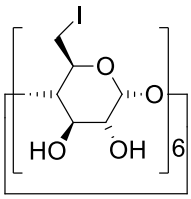

α-CD

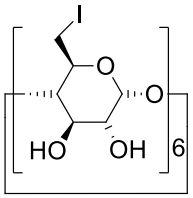

4

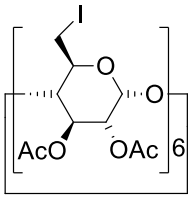

5

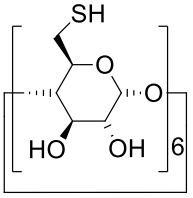

α-CD-(SH)$_6$

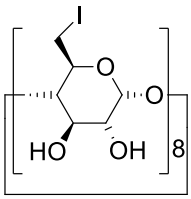

γ-CD

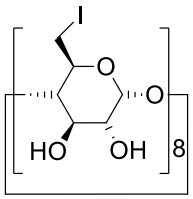

6

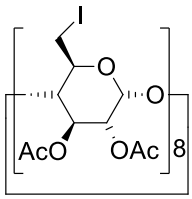

7

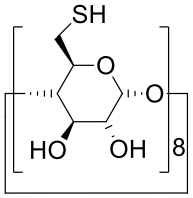

γ-CD-(SH)$_8$

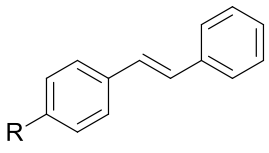

StiI-NMe$_2$ R = NMe_2
StiI-H R = H
StiI-NO$_2$ R = NO_2
StiI-OH R = OH

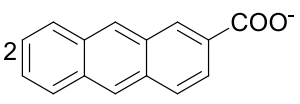

2-AC

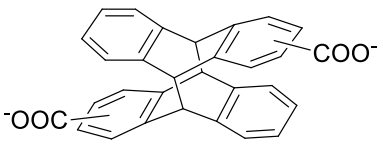

head-tail

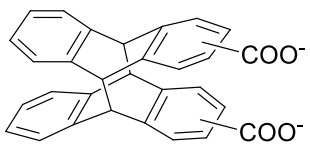

head-head

(2-AC)$_2$

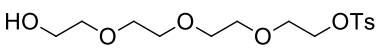

8

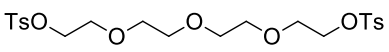

9

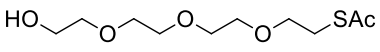

10

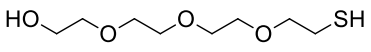

OEG-SH

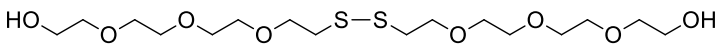

11

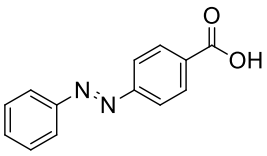

12

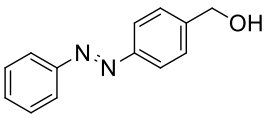

13

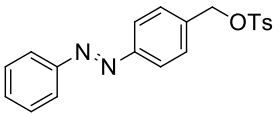

14

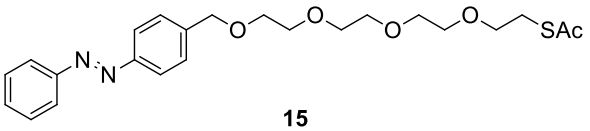

15

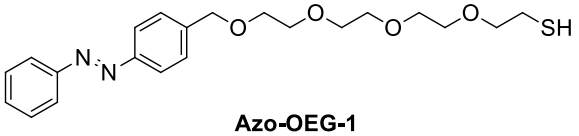

Azo-OEG-1

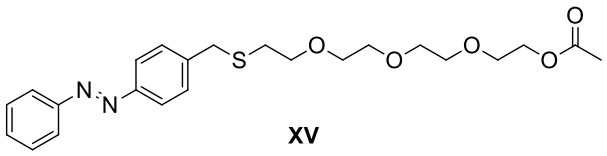

XV

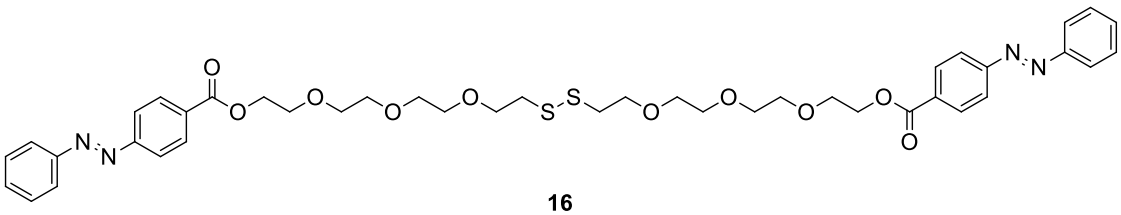

16

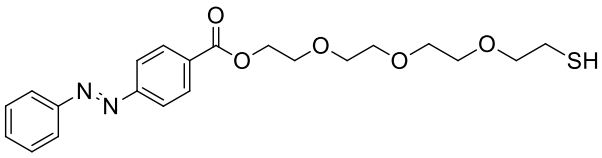

Azo-OEG-2

Annex NMR Spectra of Selected Compounds

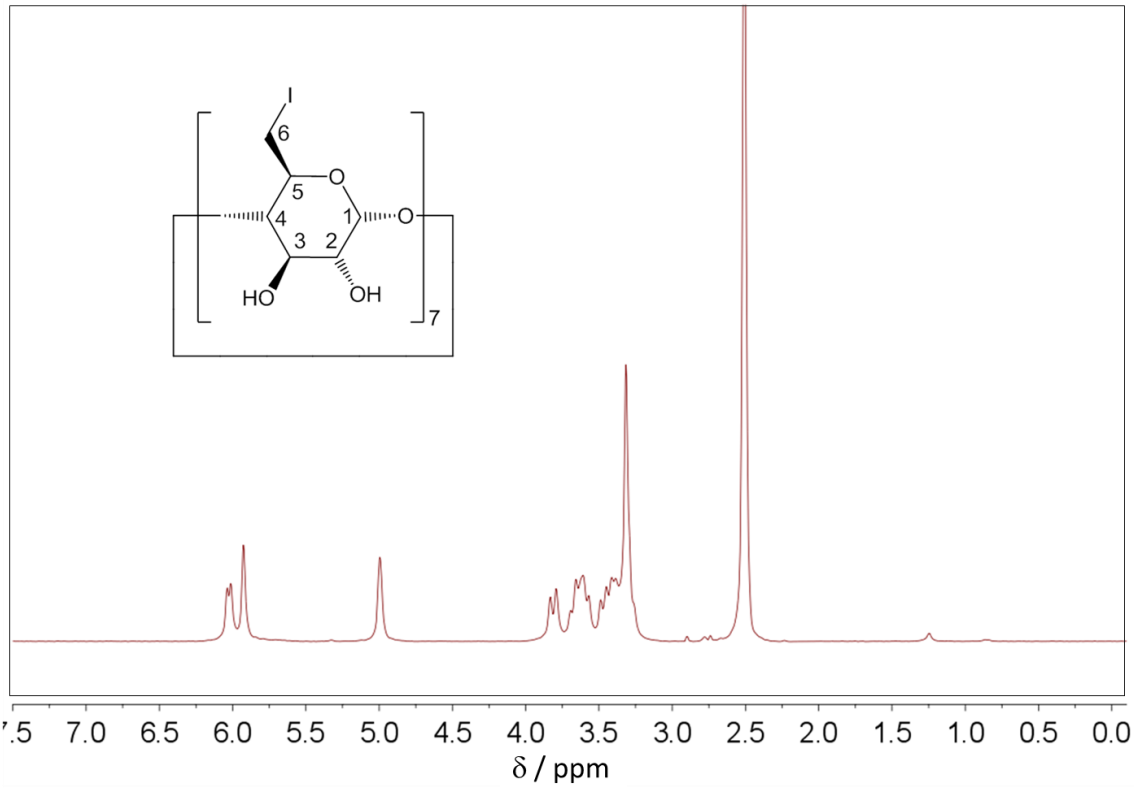

^{1}H-NMR (250 MHz, DMSO-d_6)

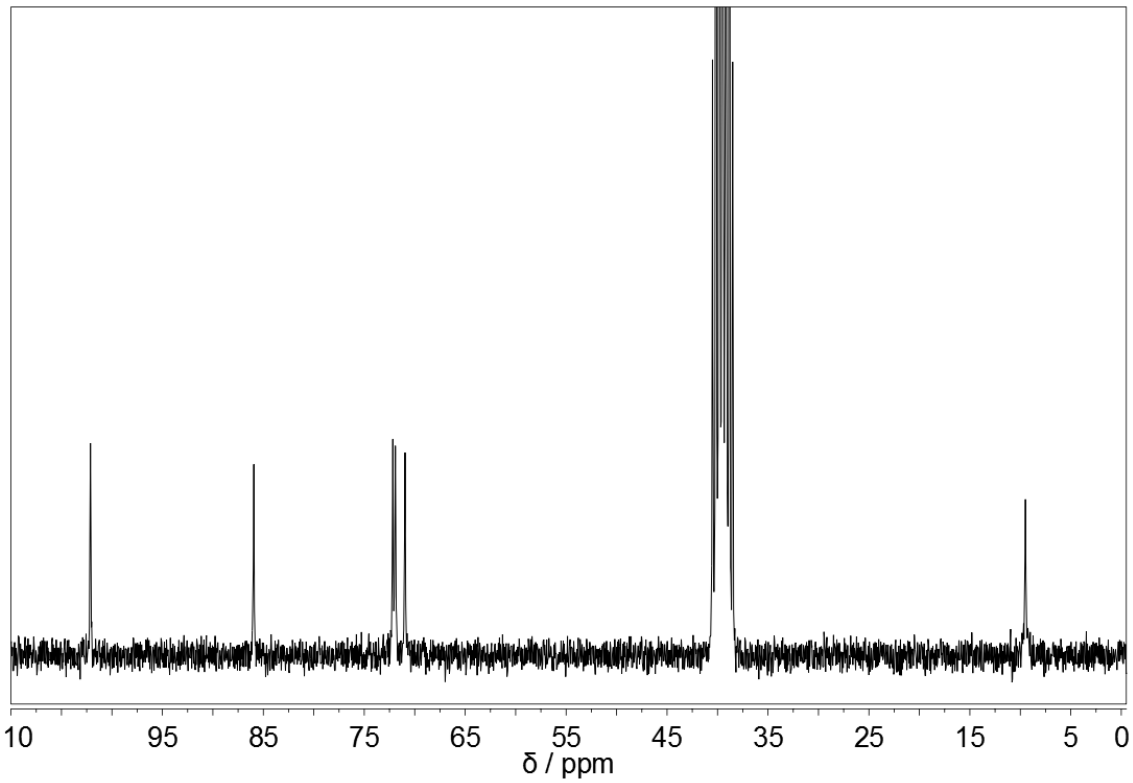

^{13}C-NMR (100.6 MHz, DMSO-d_6)

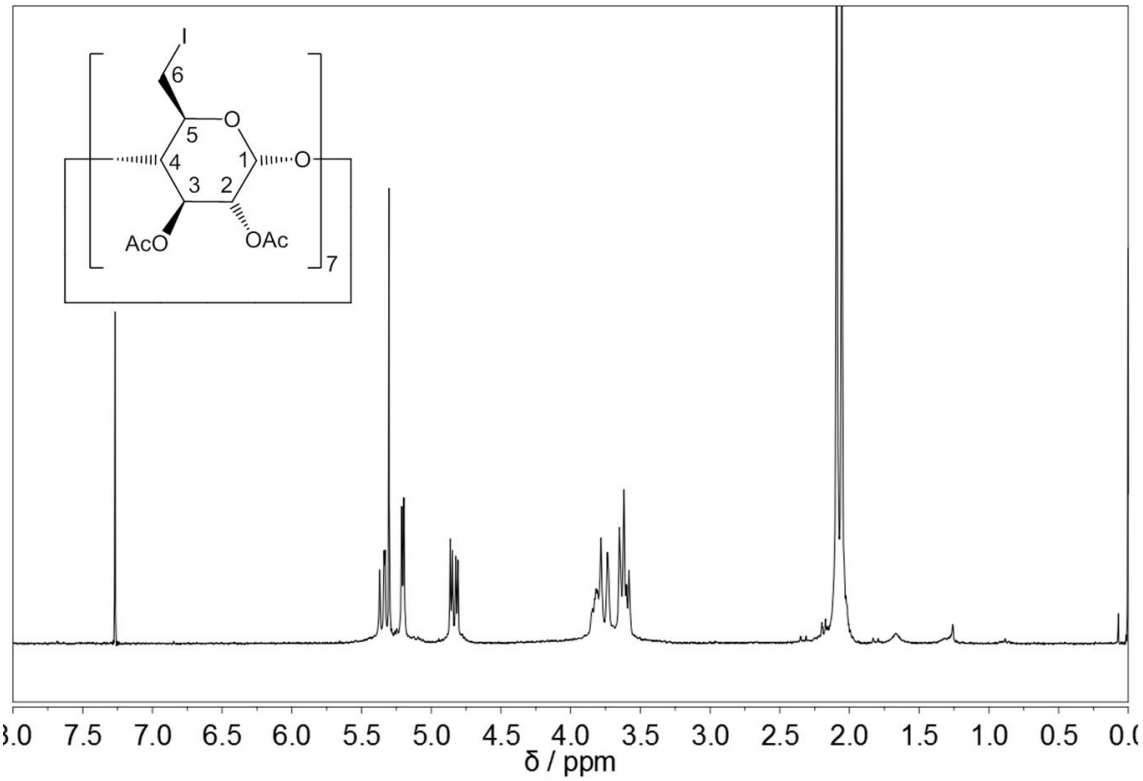

^{1}H-NMR (250 MHz, $CDCl_3$)

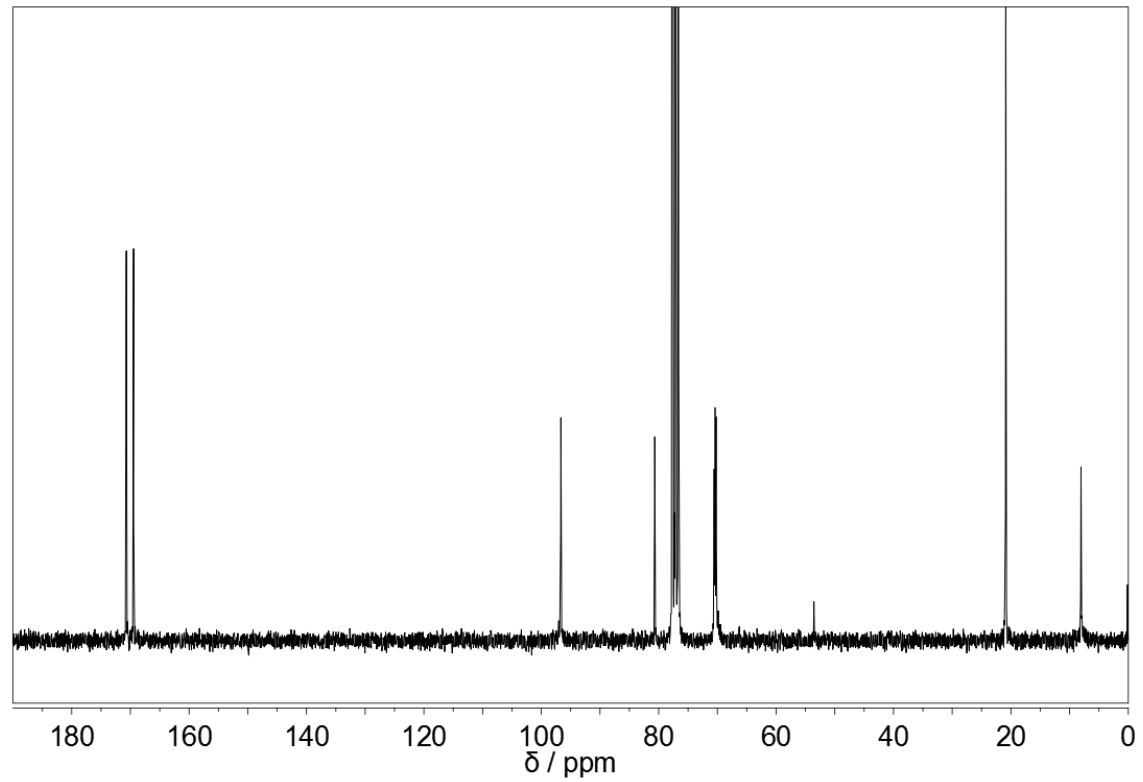

^{13}C-NMR (100.6 MHz, $CDCl_3$)

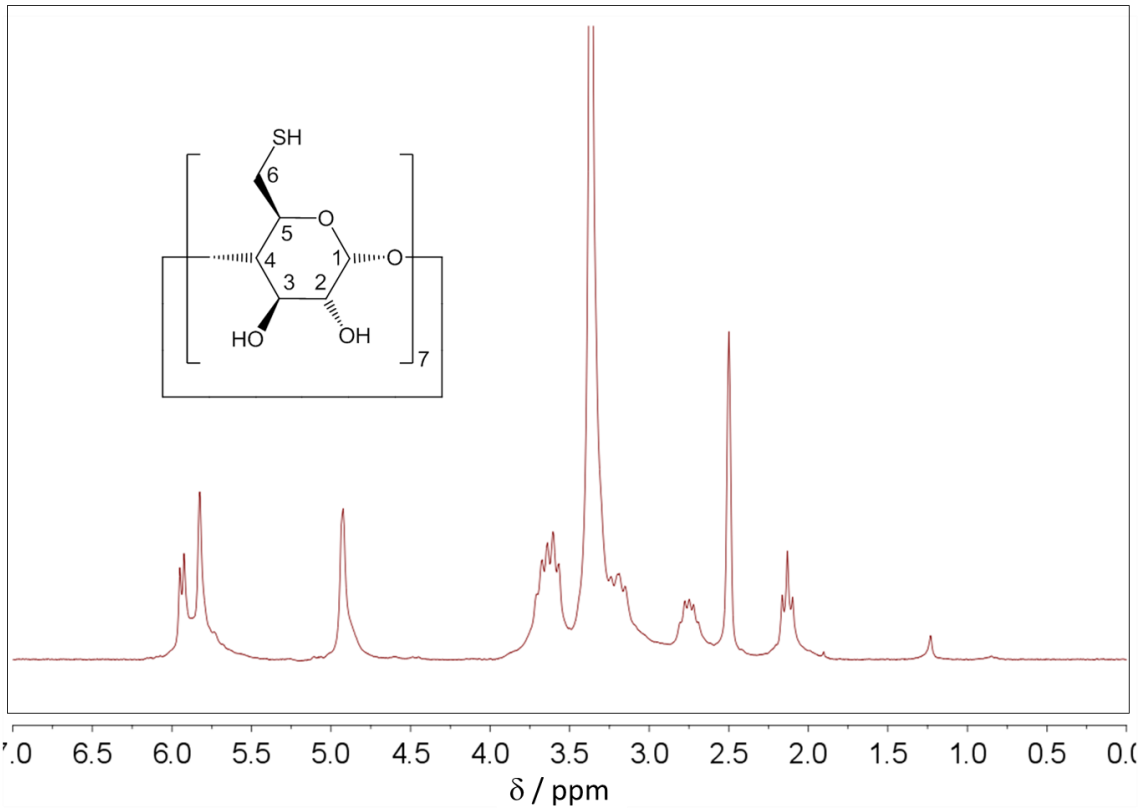

^{1}H-NMR (250 MHz, DMSO-d_6)

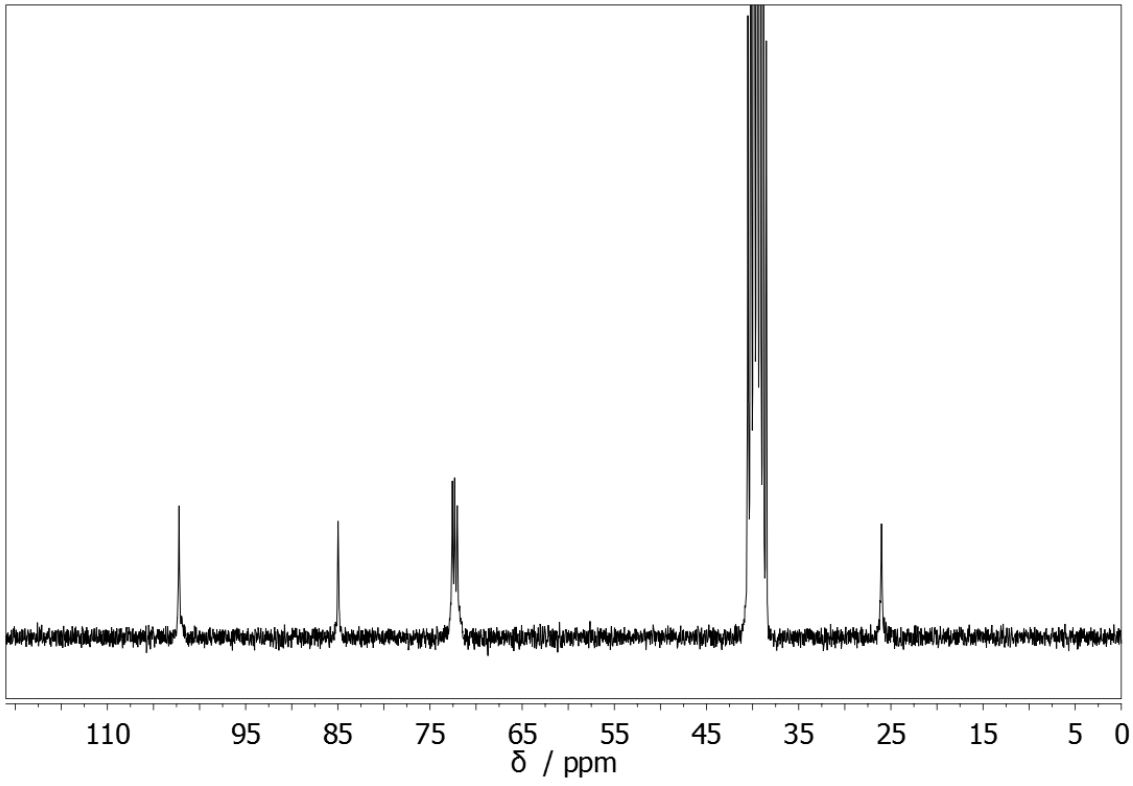

^{13}C-NMR (100.6 MHz, DMSO-d_6)

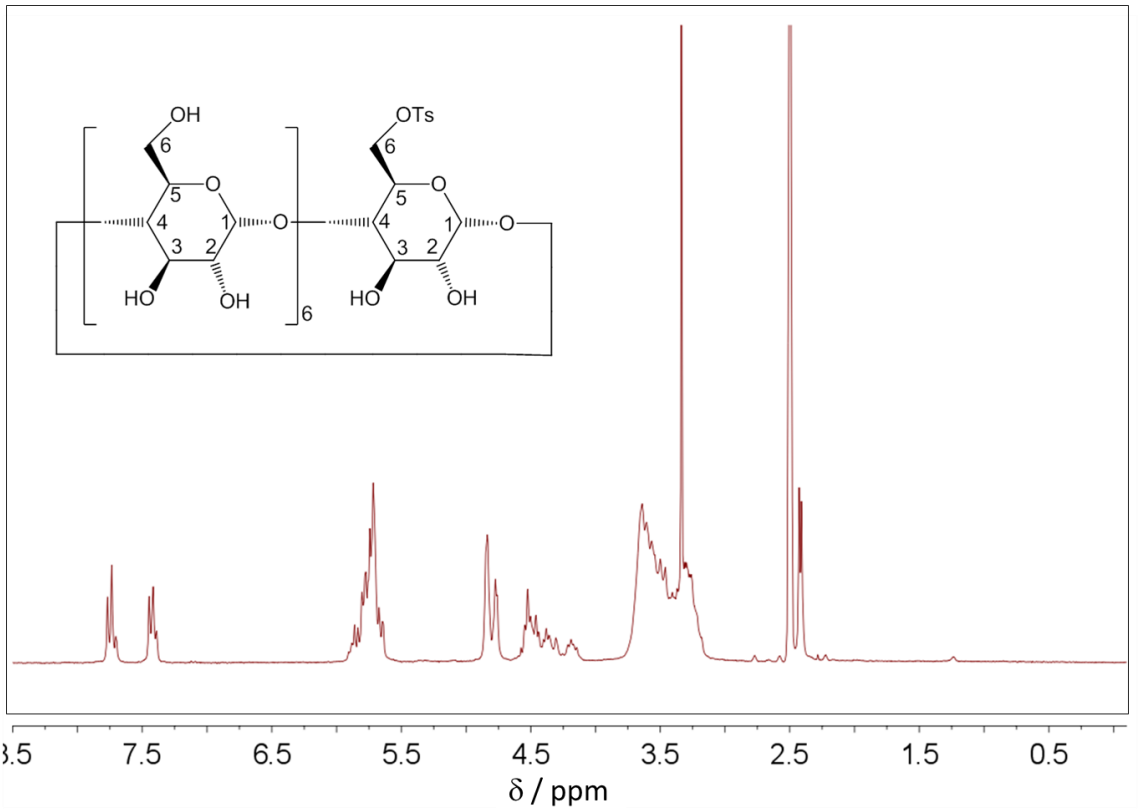

^{1}H-NMR (250 MHz, DMSO-d_6)

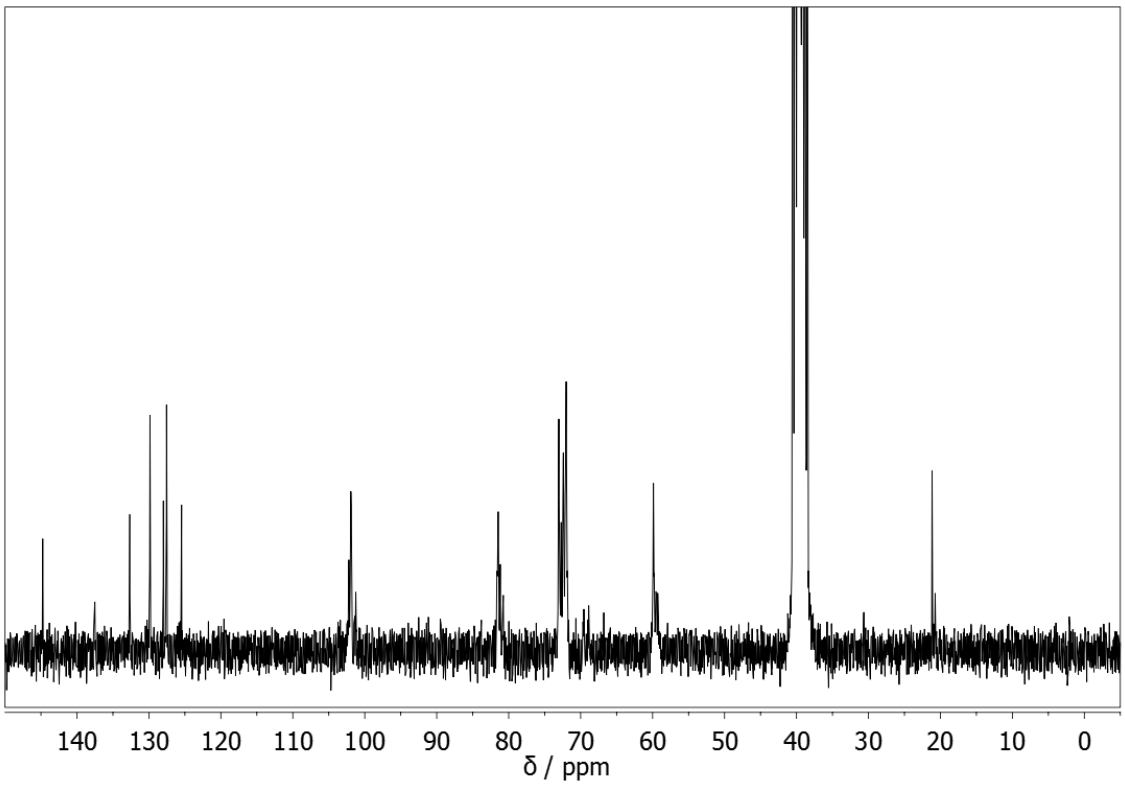

^{13}C-NMR (100.6 MHz, DMSO-d_6)

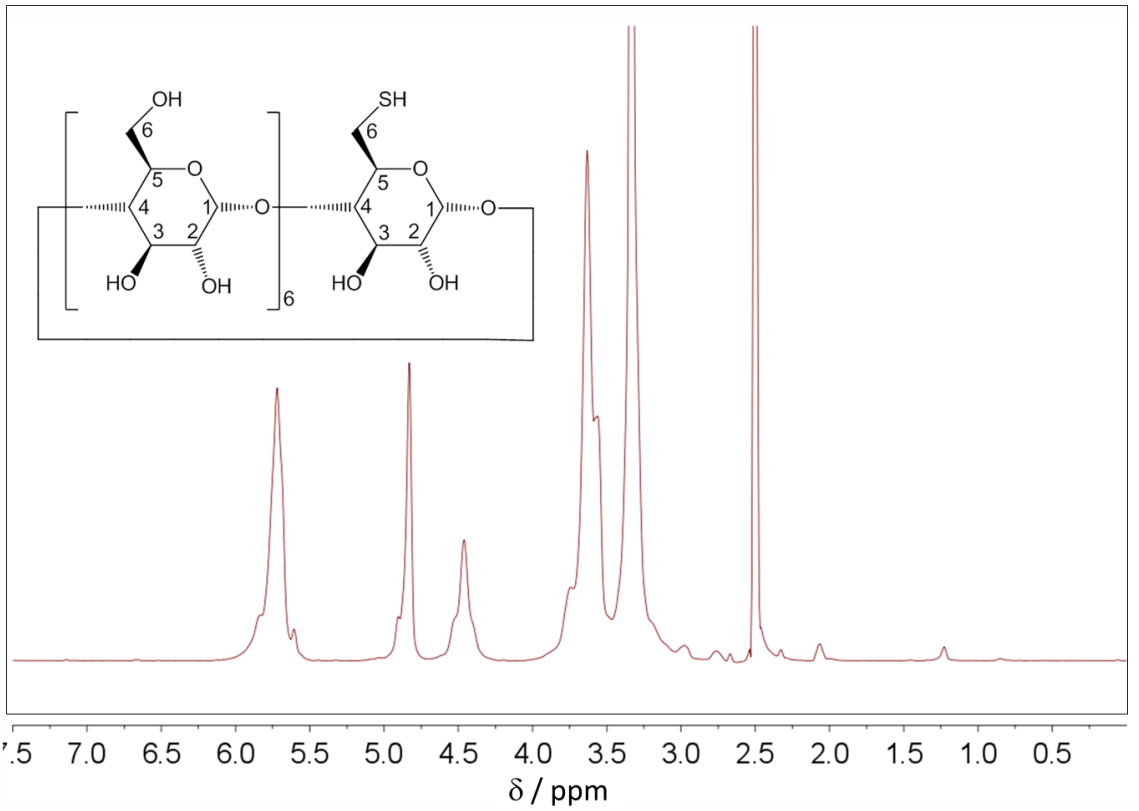

^{1}H-NMR (250 MHz, DMSO-d_6)

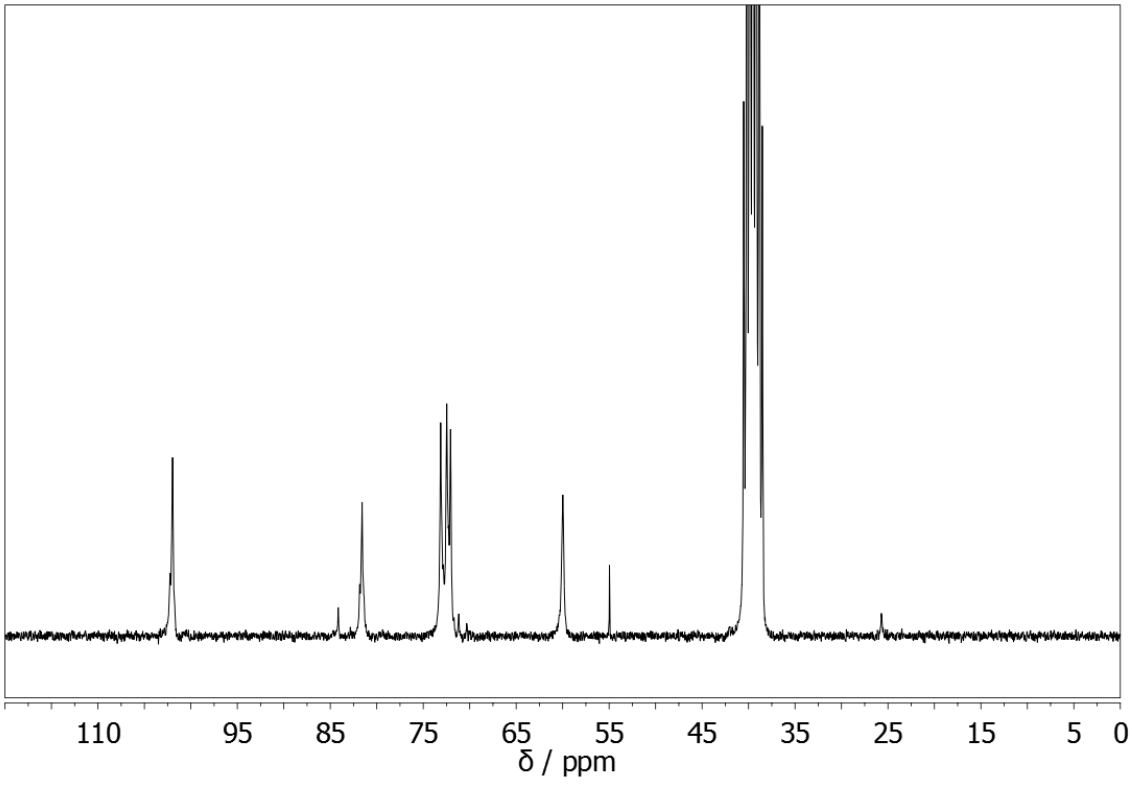

^{13}C-NMR (100.6 MHz, DMSO-d_6)

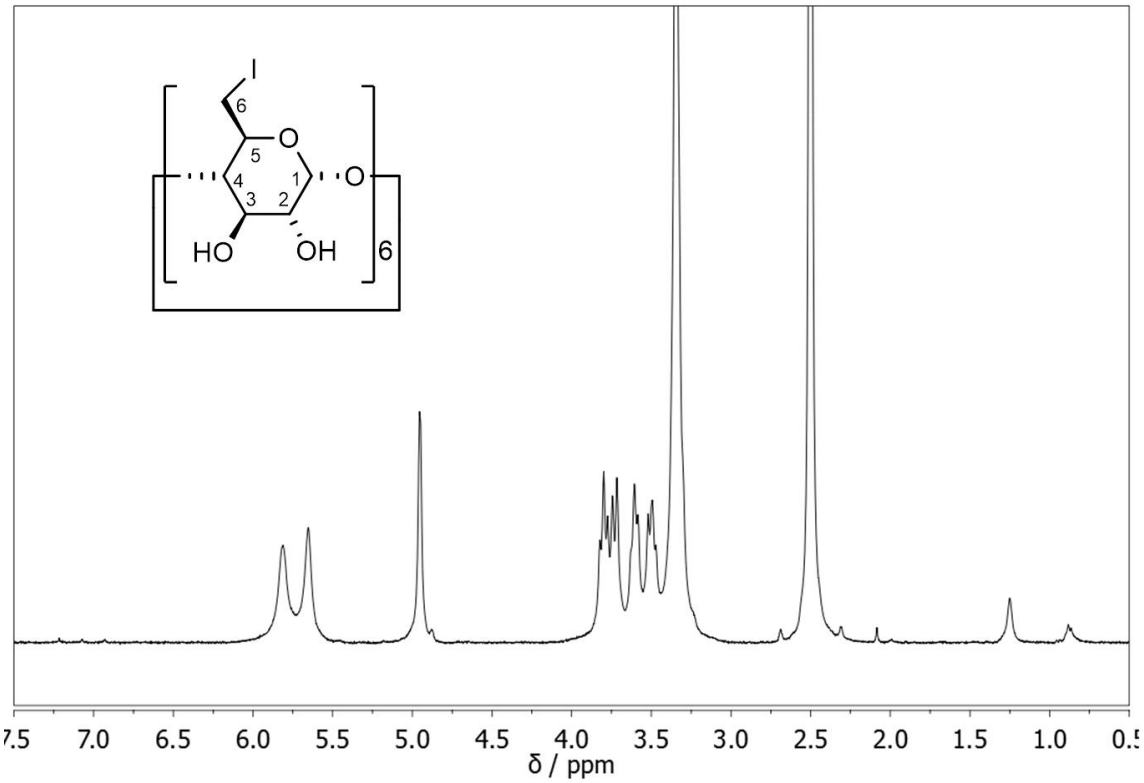

^{1}H-NMR (250 MHz, DMSO-d_6)

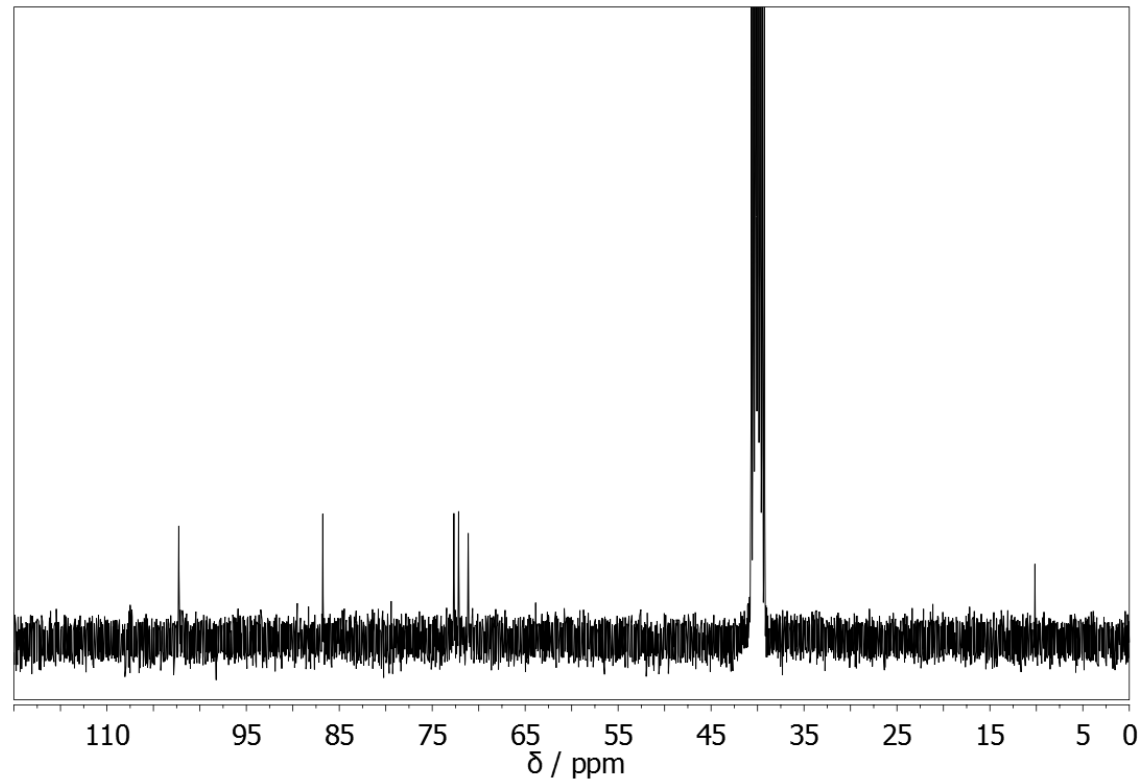

^{13}C-NMR (90 MHz, DMSO-d_6)

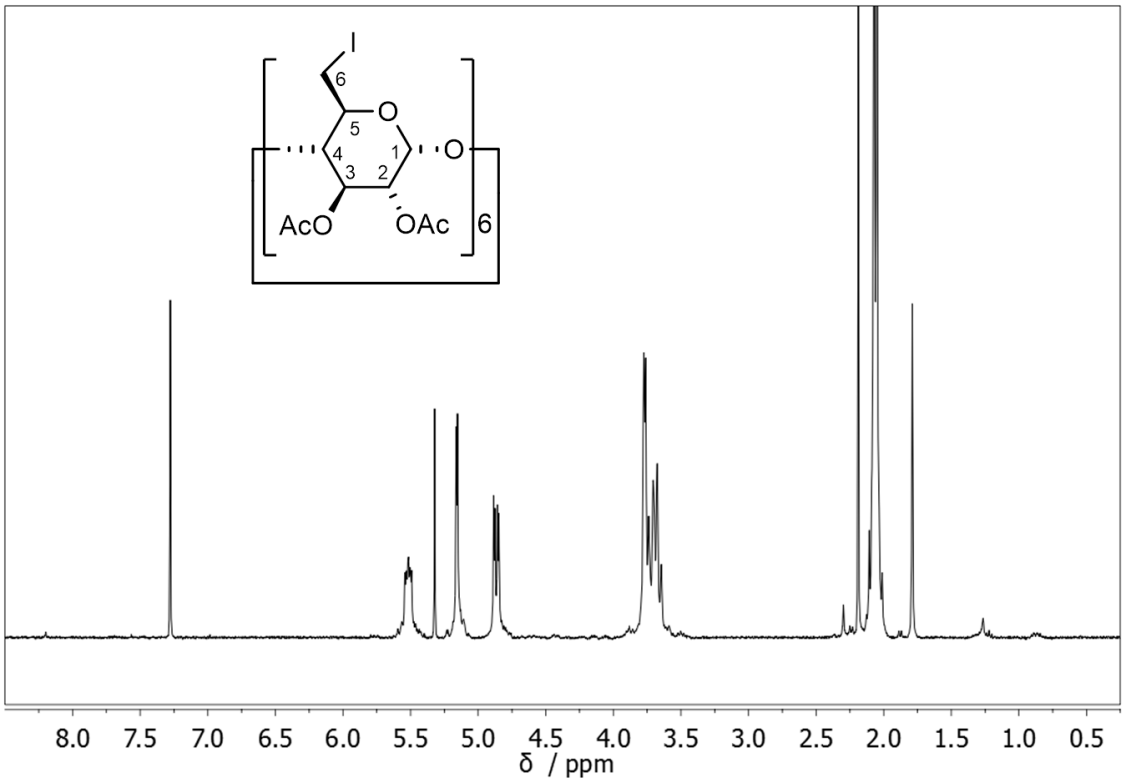

^{1}H-NMR (360 MHz, DMSO-d_6)

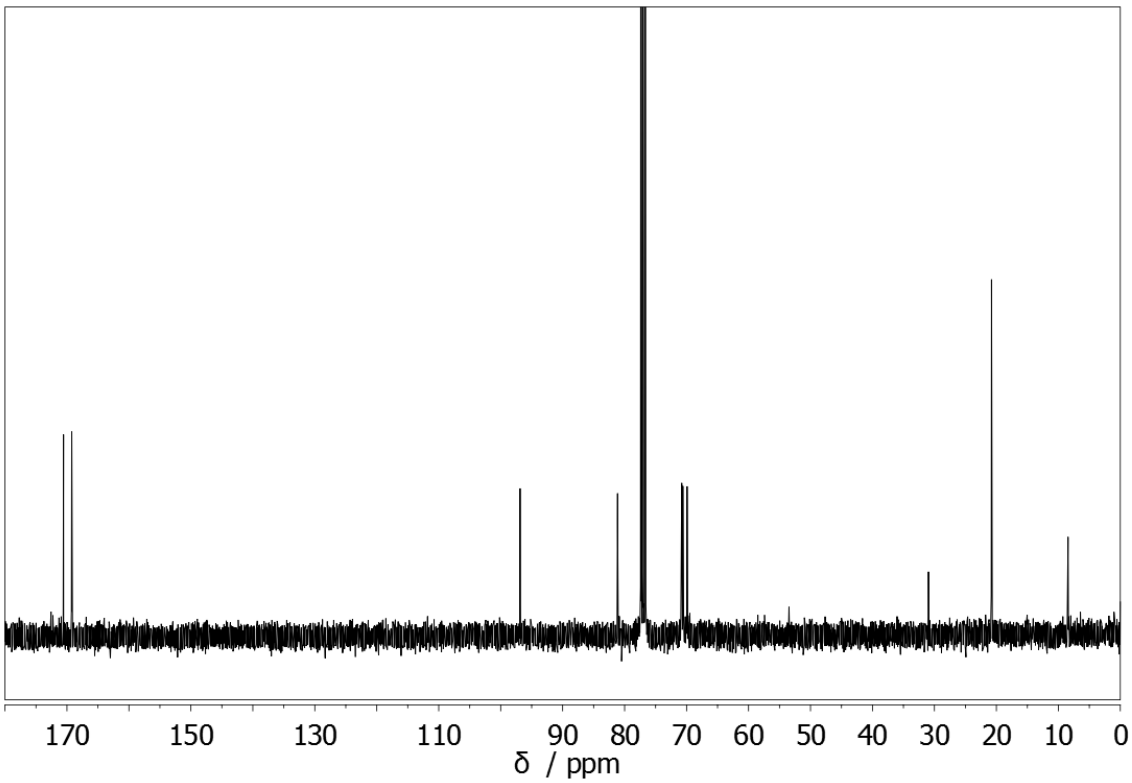

^{13}C-NMR (90 MHz, $CDCl_3$)

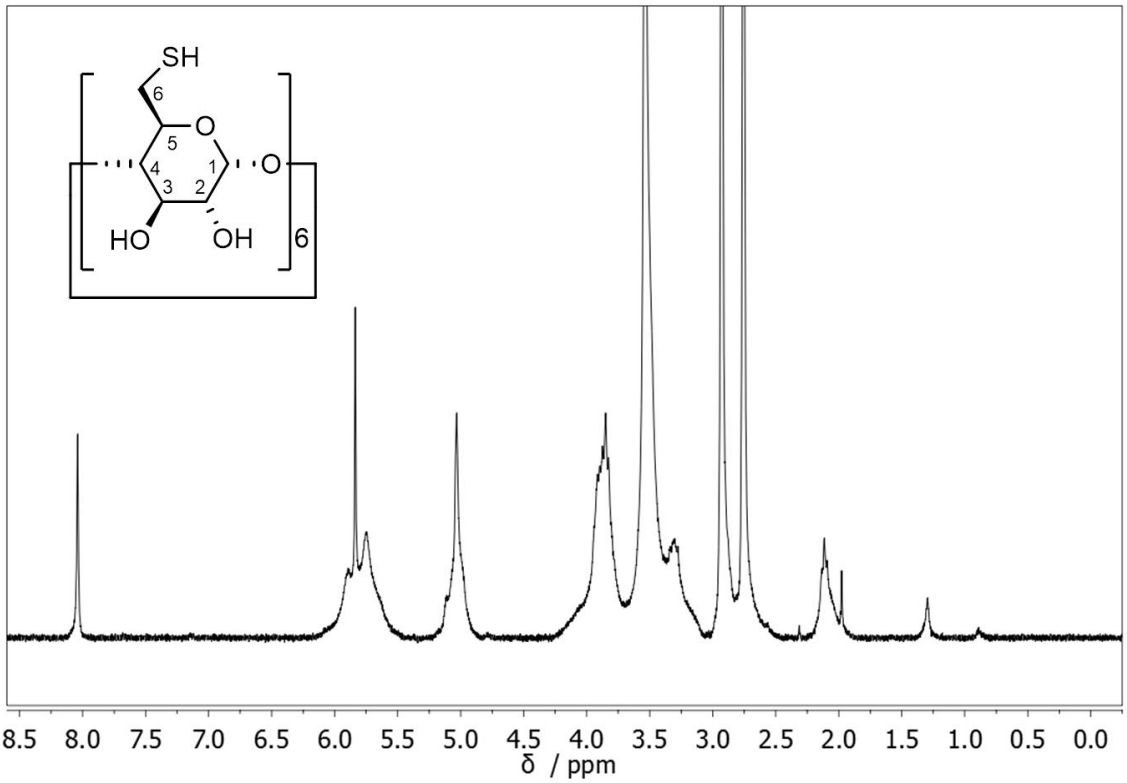

^{1}H-NMR (250 MHz, DMF-d_7)

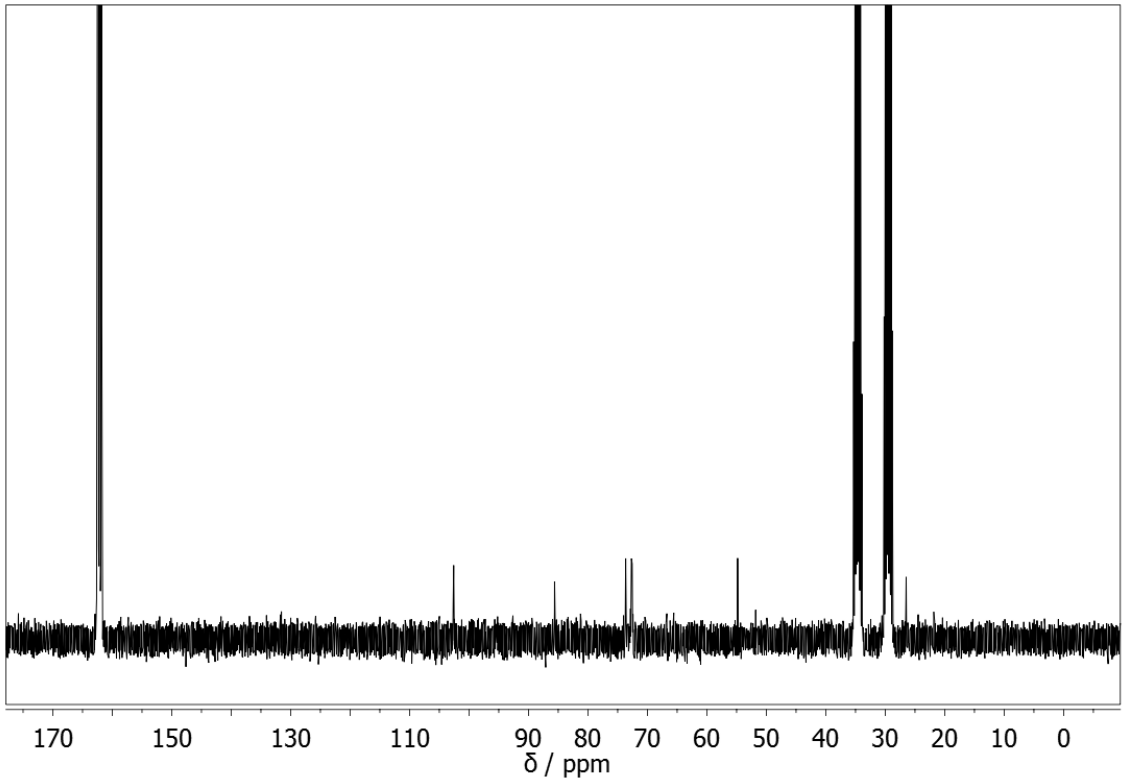

^{13}C-NMR (90 MHz, DMF-d_7)

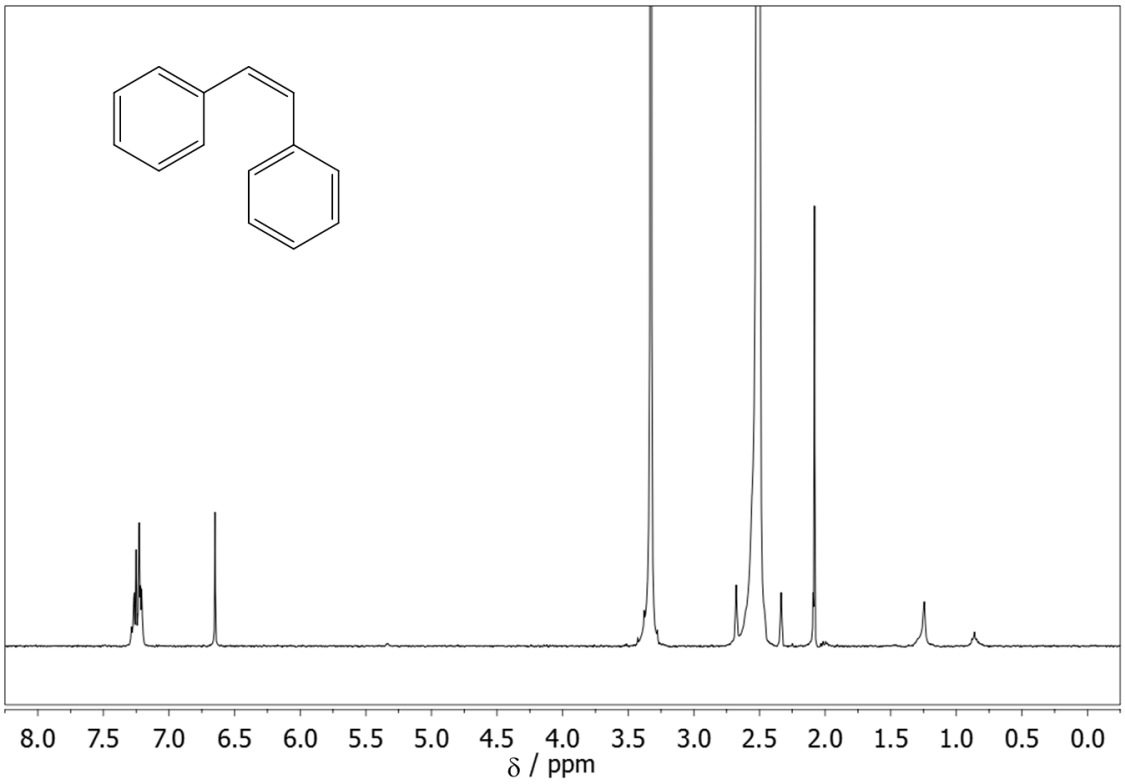

^{1}H-NMR (400 MHz, DMSO-d_6)

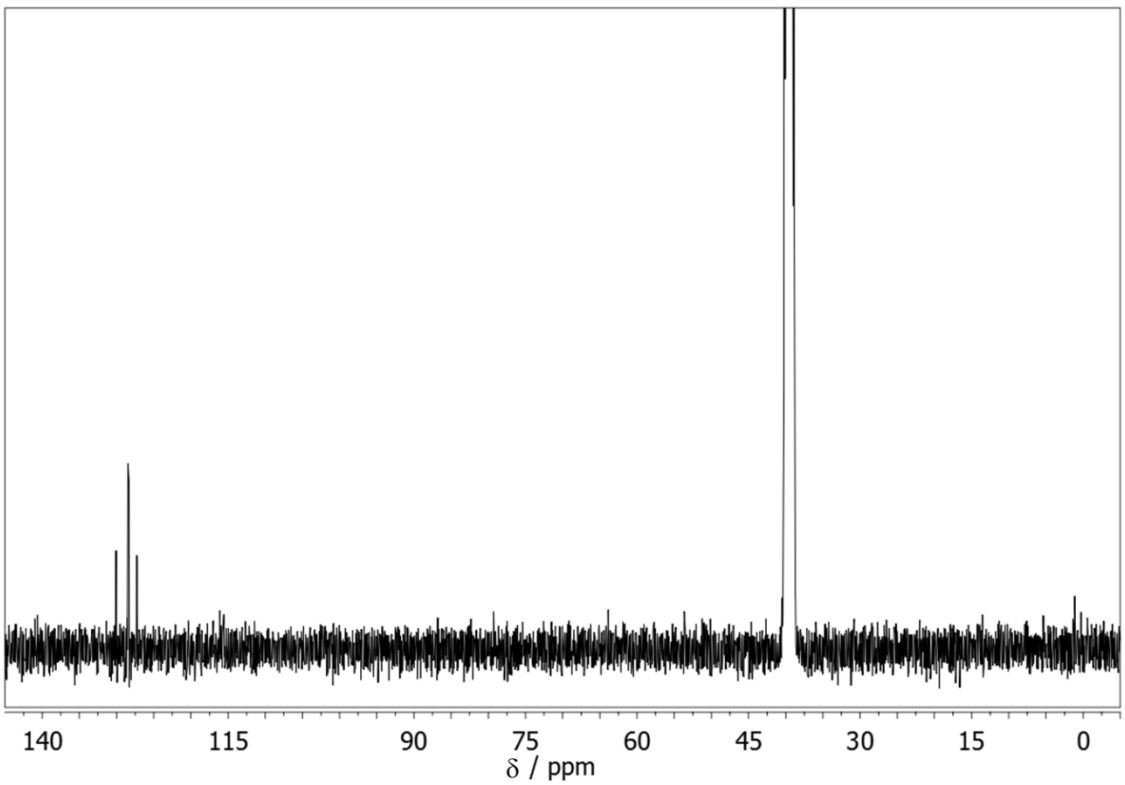

^{13}C-NMR (100.6 MHz, DMSO-d_6)

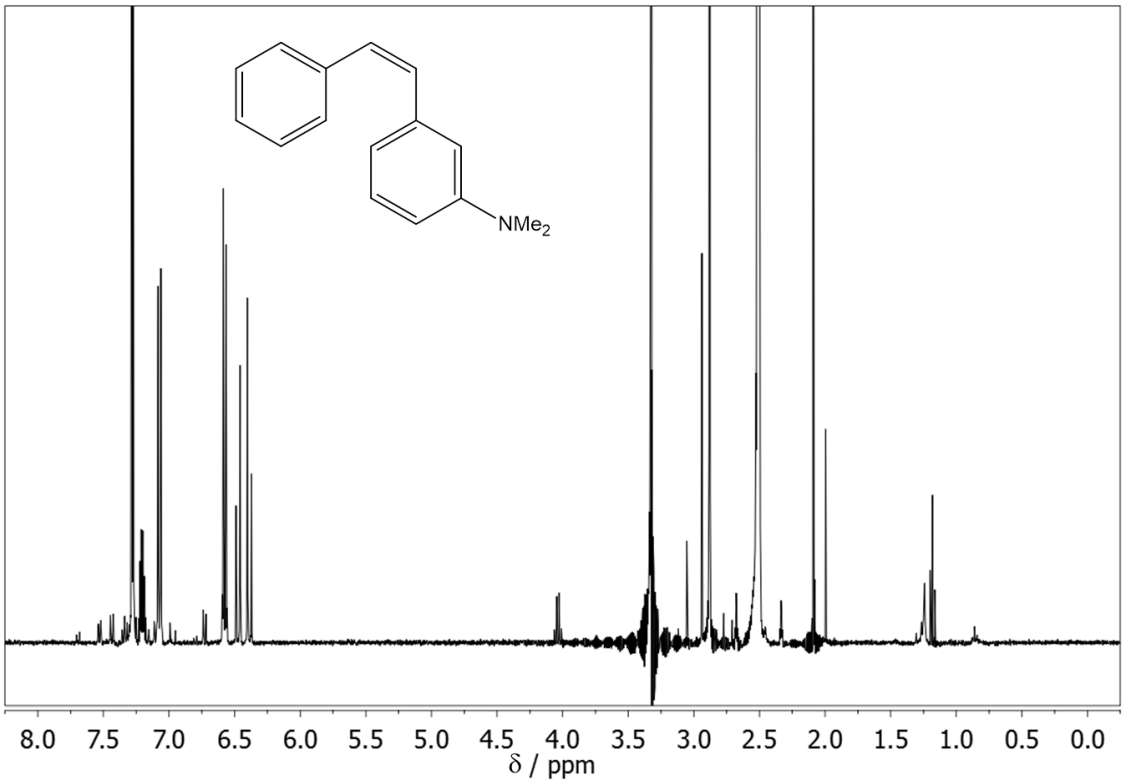

^{1}H-NMR (400 MHz, DMSO-d_6)

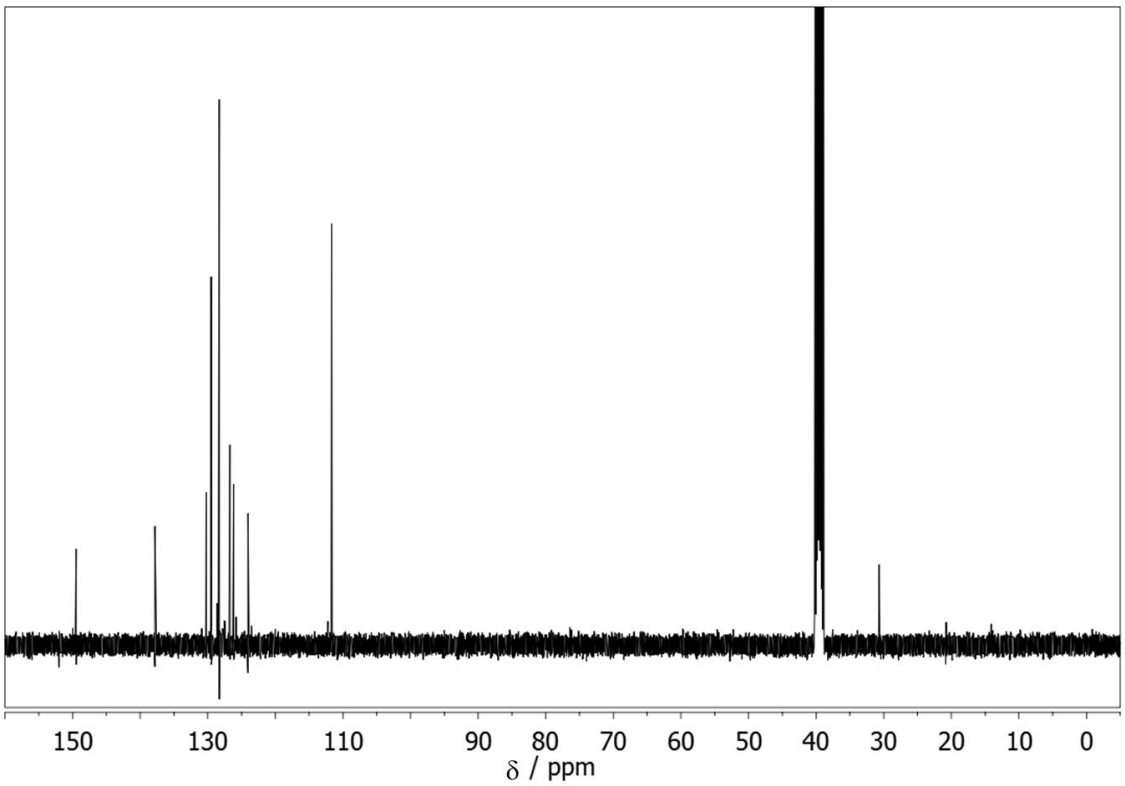

^{13}C-NMR (100.6 MHz, DMSO-d_6)

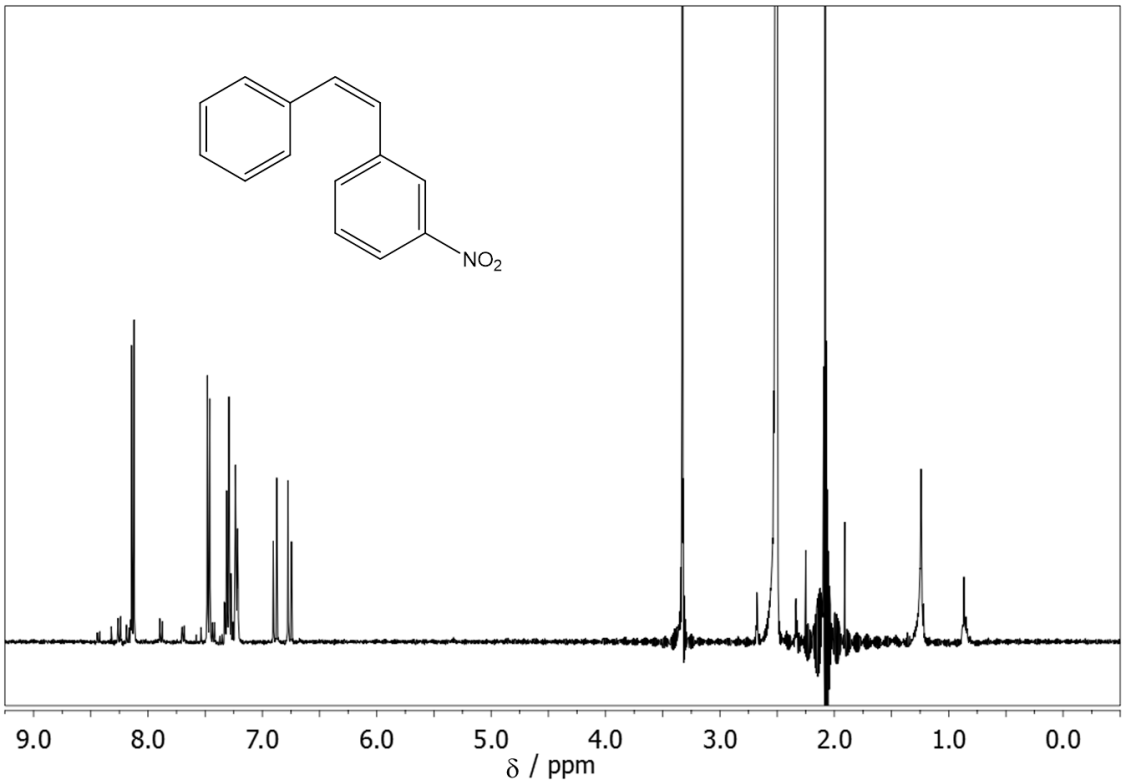

^{1}H-NMR (400 MHz, DMSO-d_6)

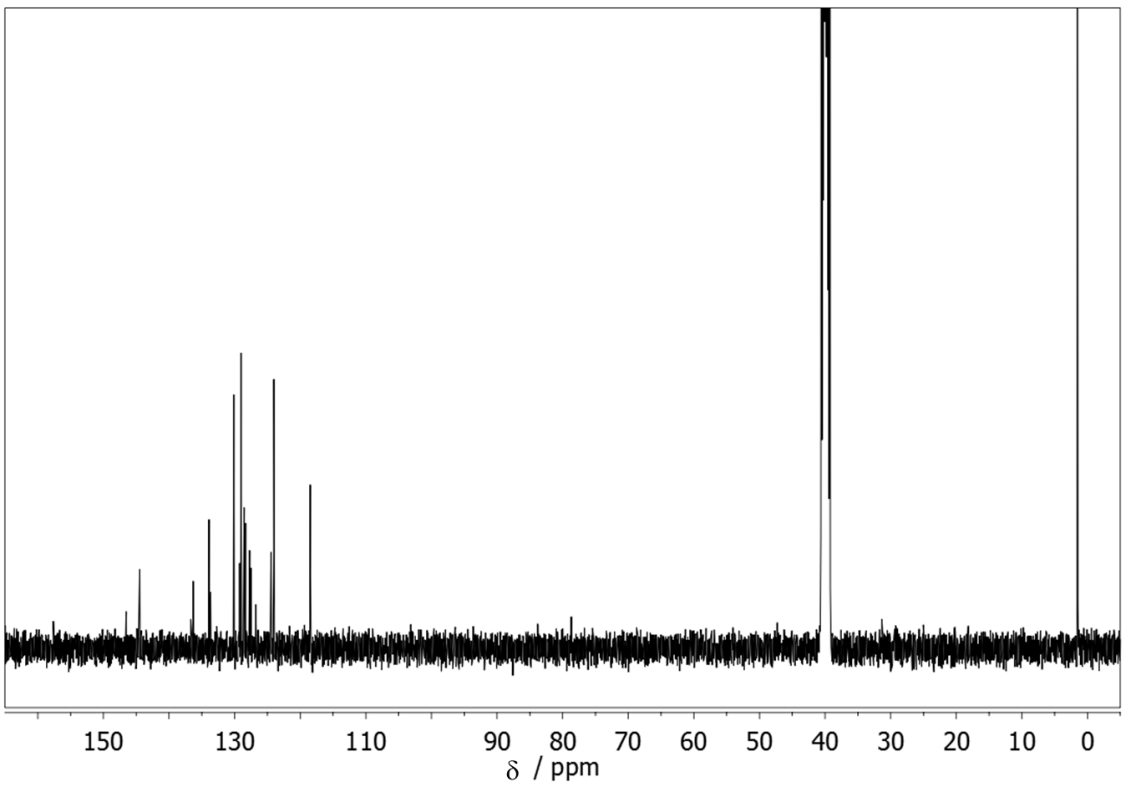

^{13}C-NMR (100.6 MHz, DMSO-d_6)

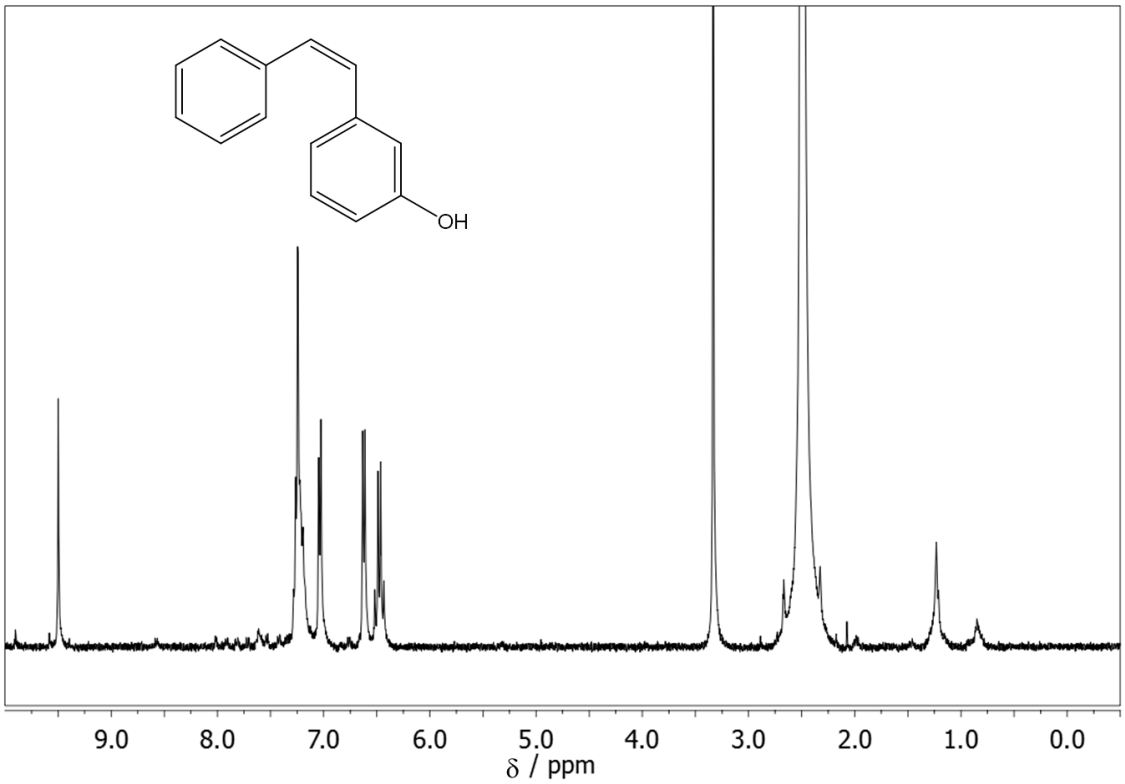

^{1}H-NMR (400 MHz, DMSO-d_6)

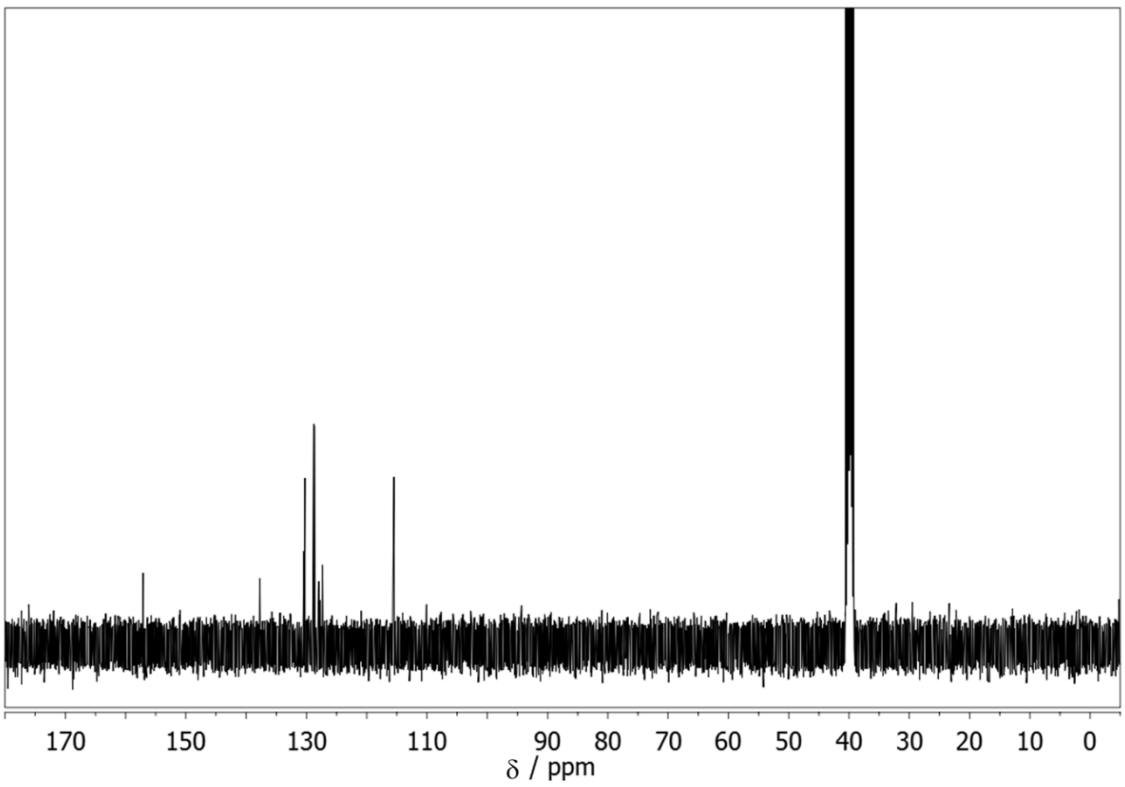

^{13}C-NMR (100.6 MHz, DMSO-d_6)

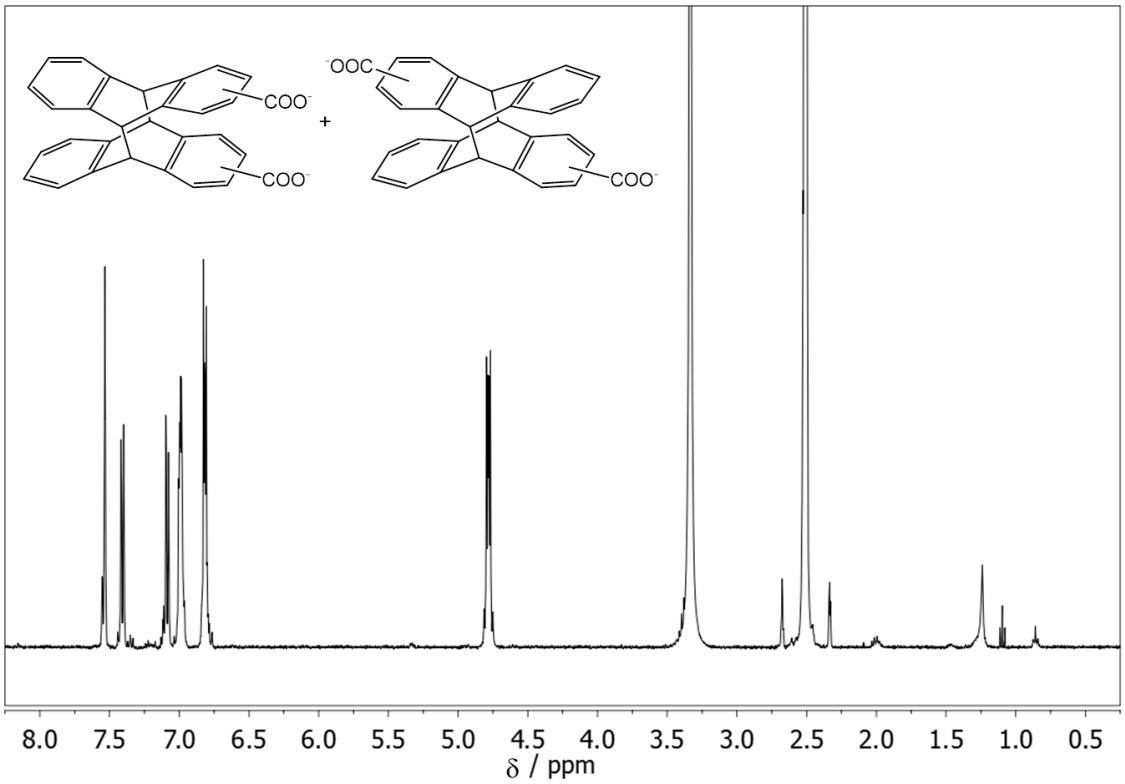

^{1}H-NMR (400 MHz, DMSO-d_6)

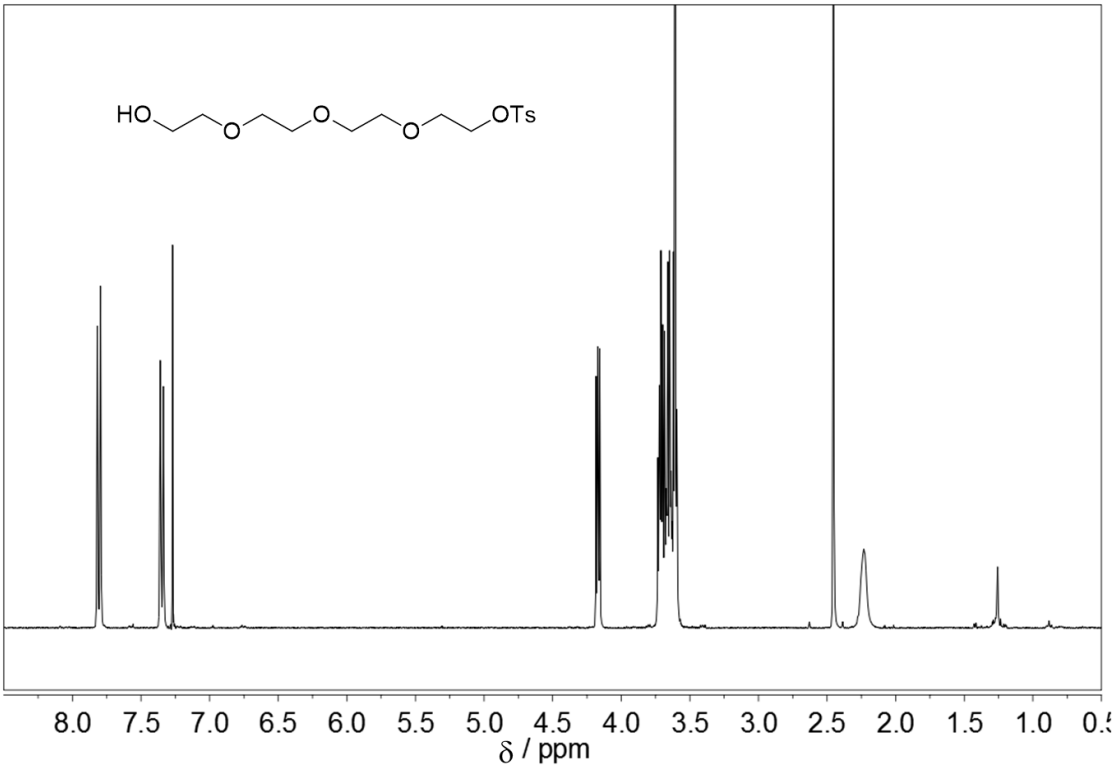

^{1}H-NMR (360 MHz, $CDCl_3$)

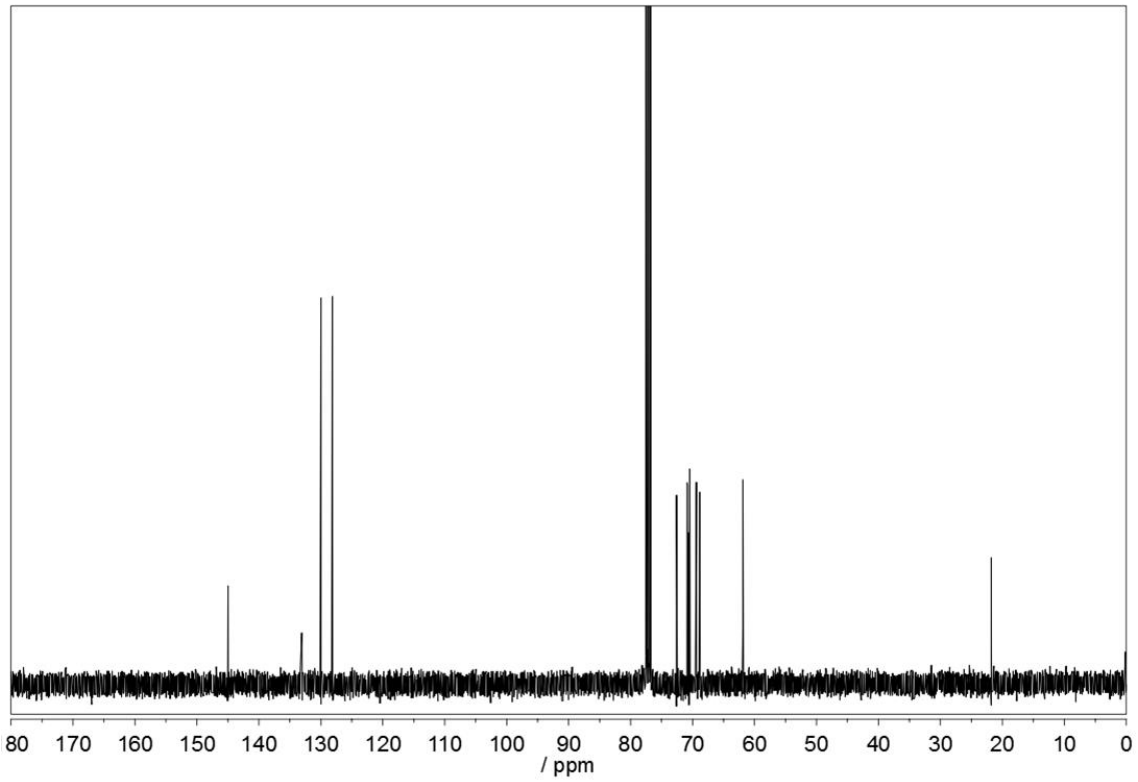

^{13}C-NMR (90 MHz, $CDCl_3$)

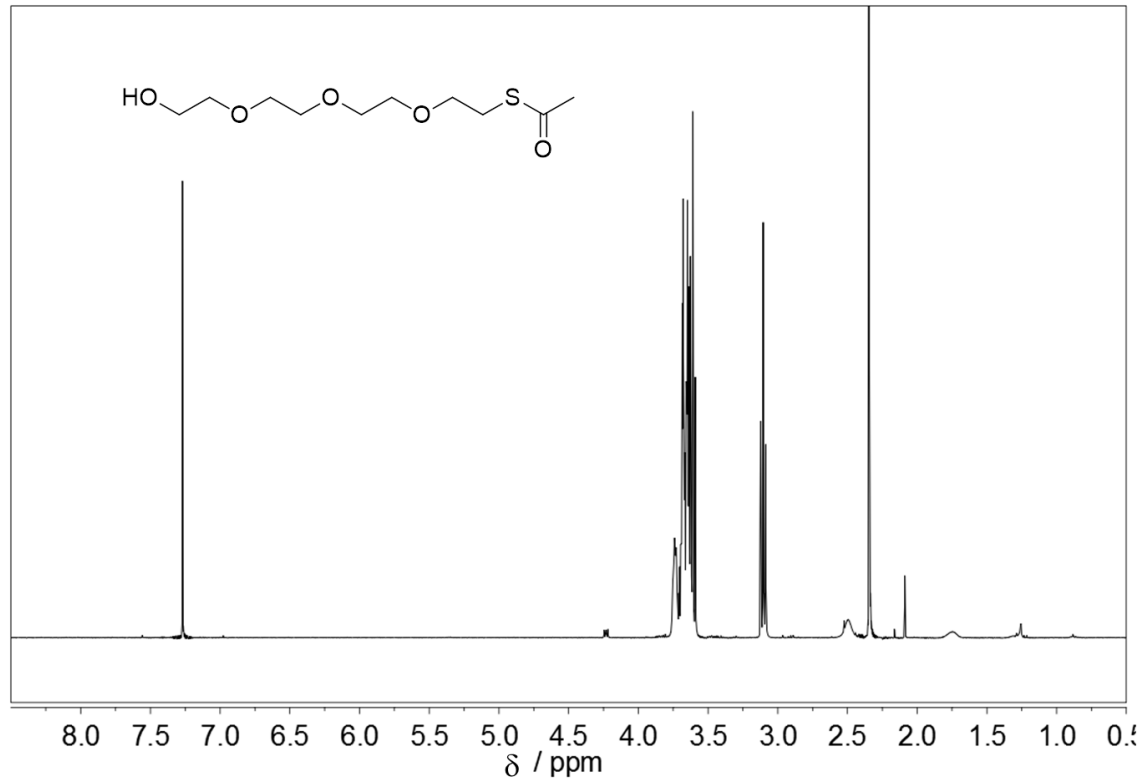

^{1}H-NMR (3600 MHz, $CDCl_3$)

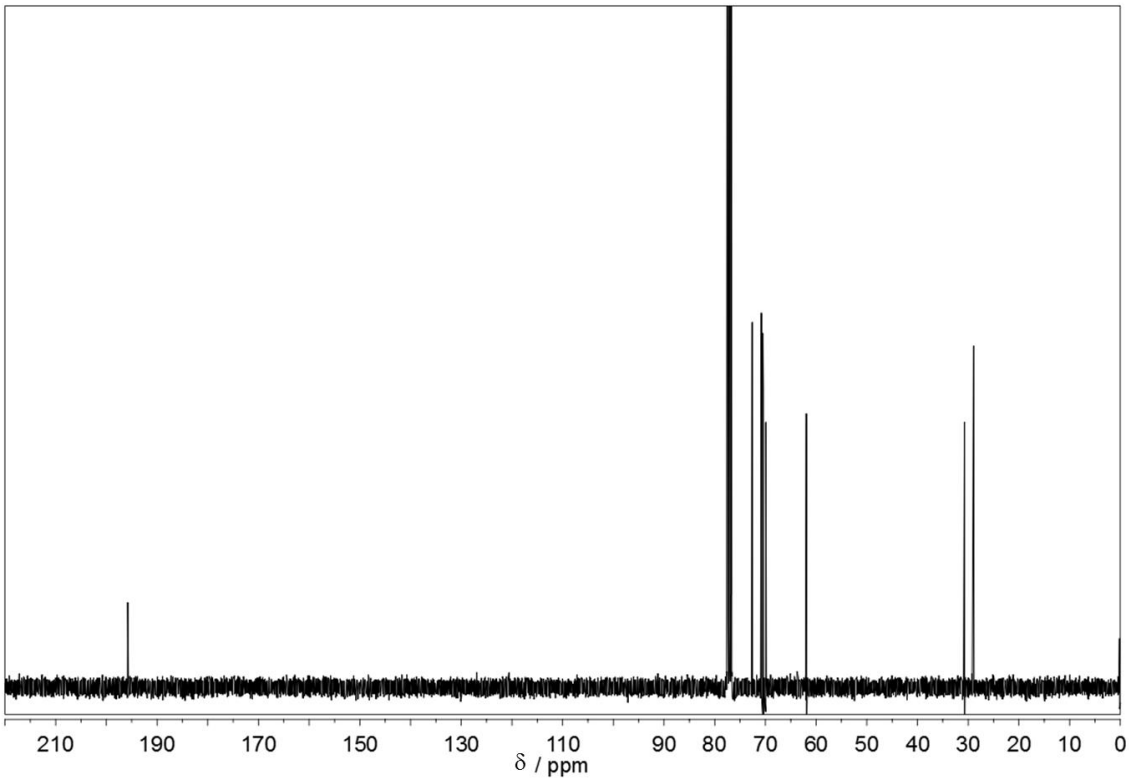

^{13}C-NMR (90 MHz, $CDCl_3$)

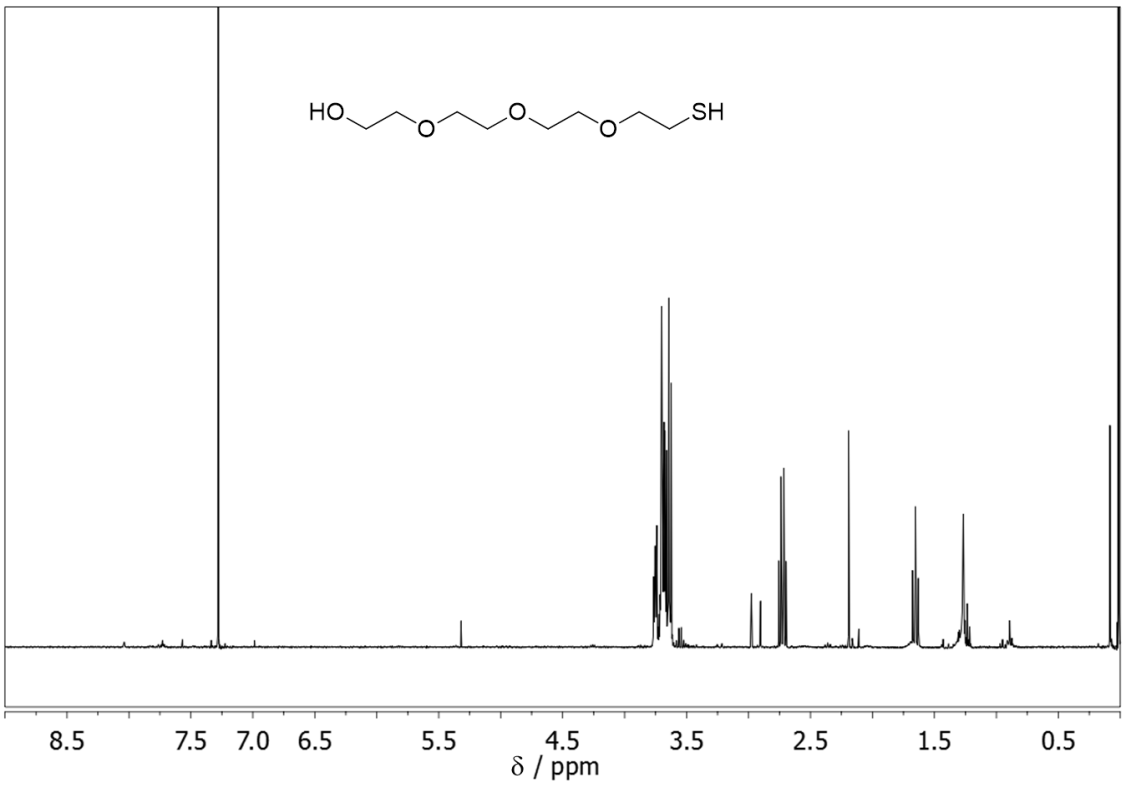

^{1}H-NMR (400 MHz, $CDCl_3$)

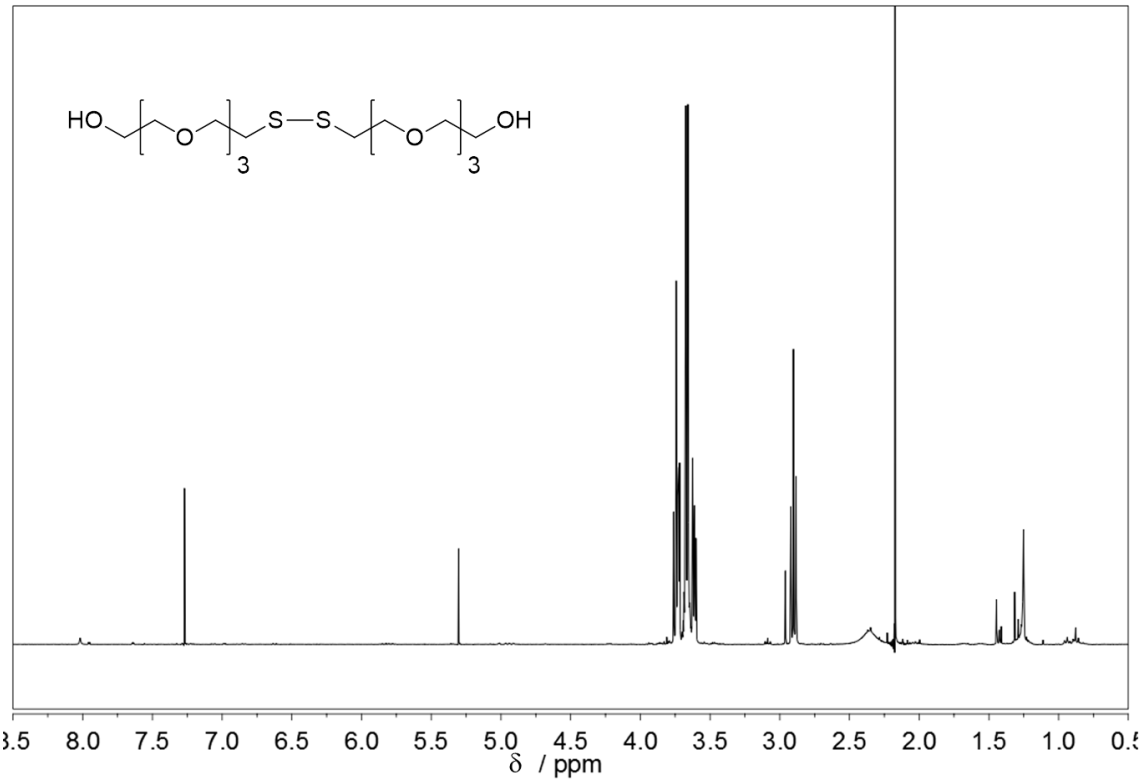

^{1}H-NMR (360 MHz, $CDCl_3$)

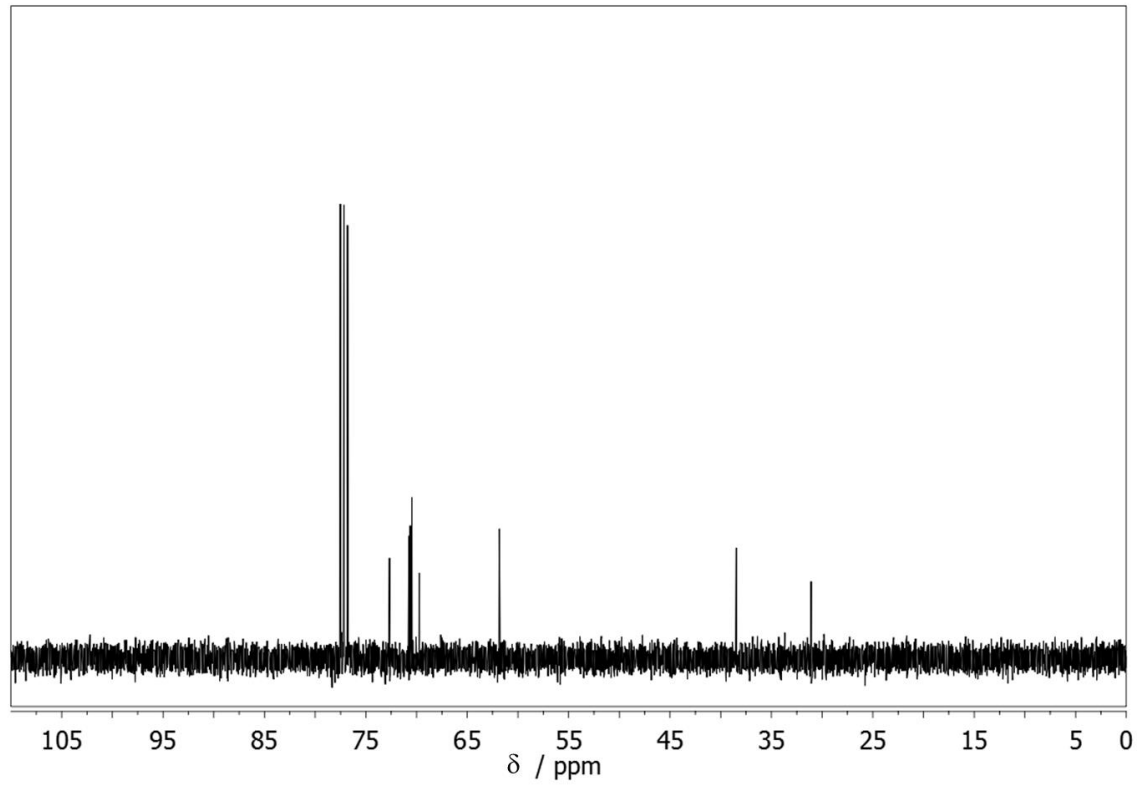

^{13}C-NMR (90 MHz, $CDCl_3$)

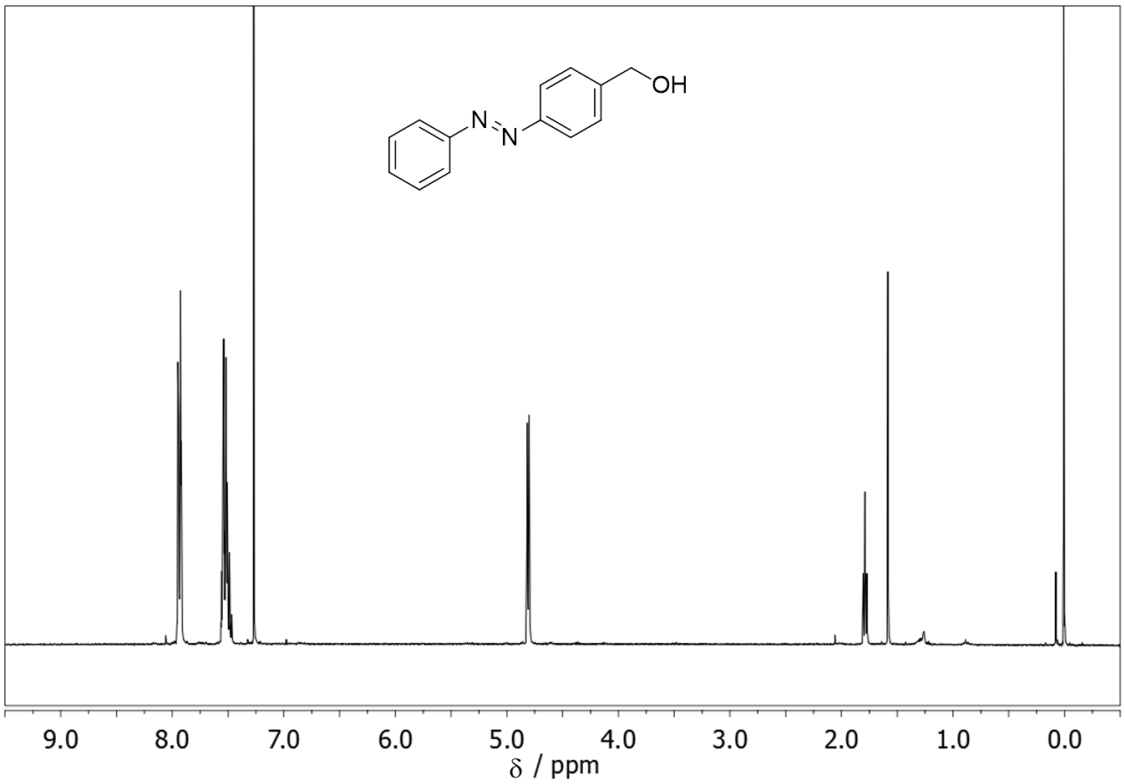

^{1}H-NMR (360 MHz, $CDCl_3$)

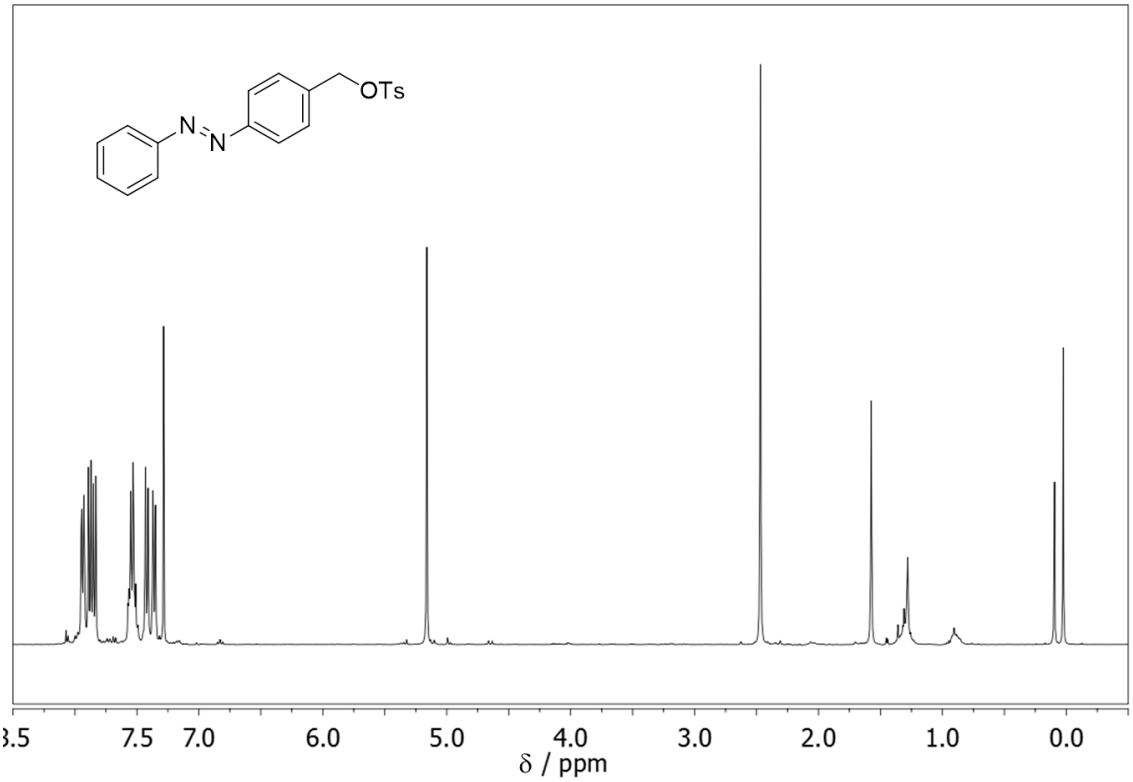

^{1}H-NMR (360 MHz, $CDCl_3$)

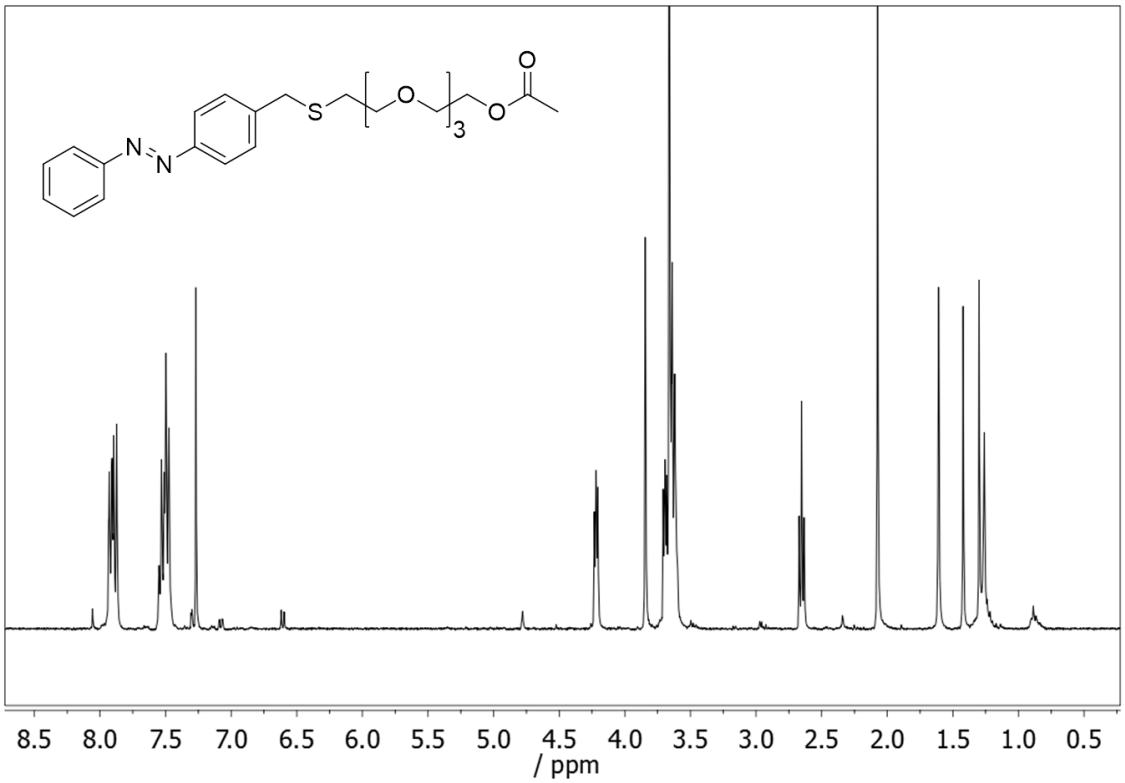

^{1}H-NMR (360 MHz, $CDCl_3$)

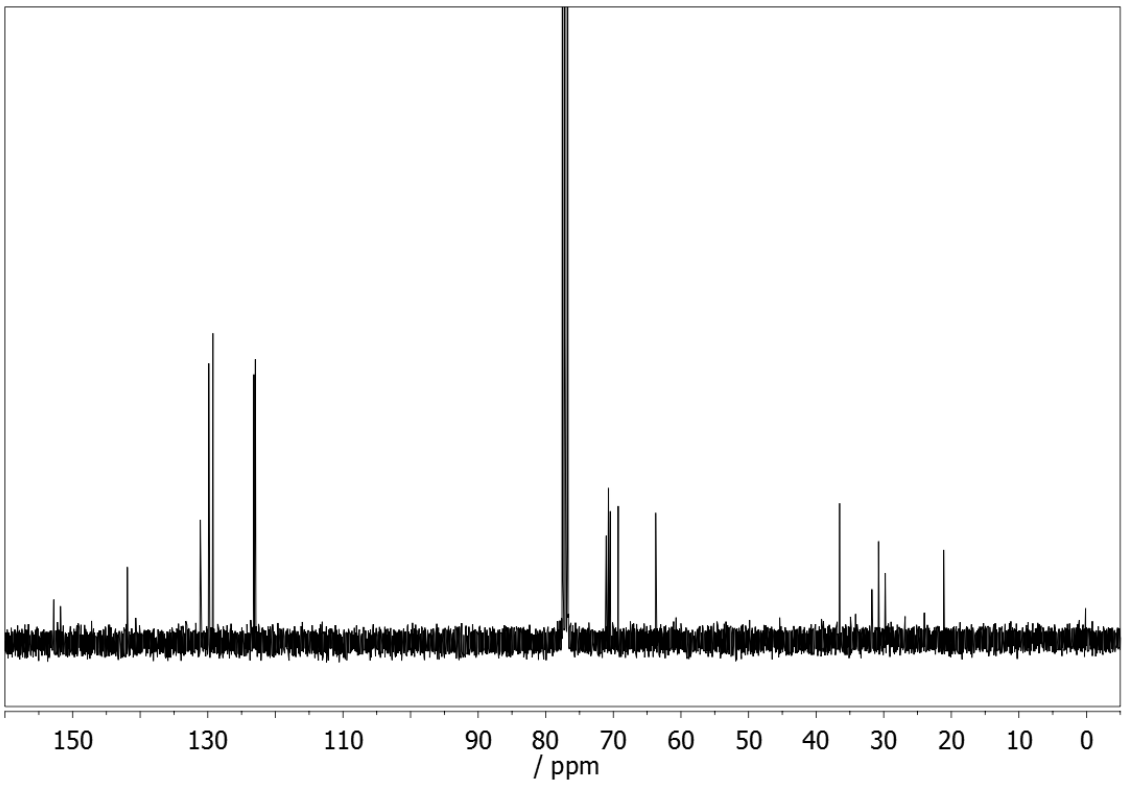

^{13}C-NMR (90 MHz, $CDCl_3$)

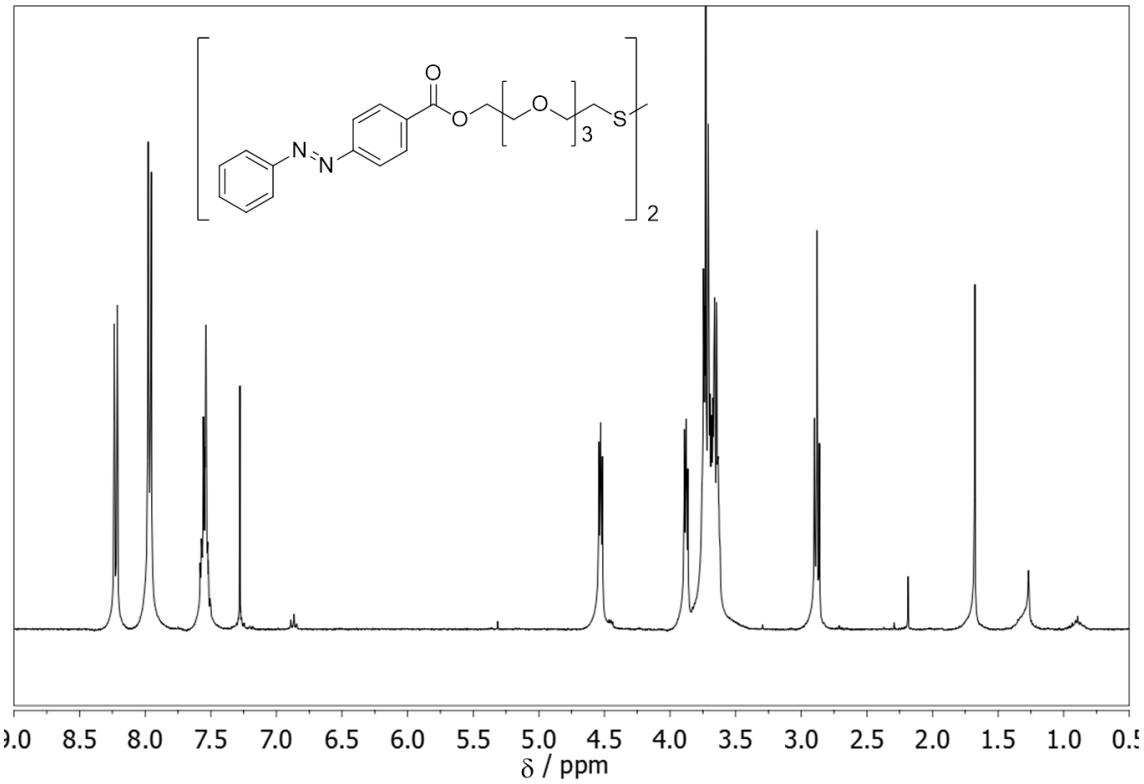

^{1}H-NMR (360 MHz, $CDCl_3$)

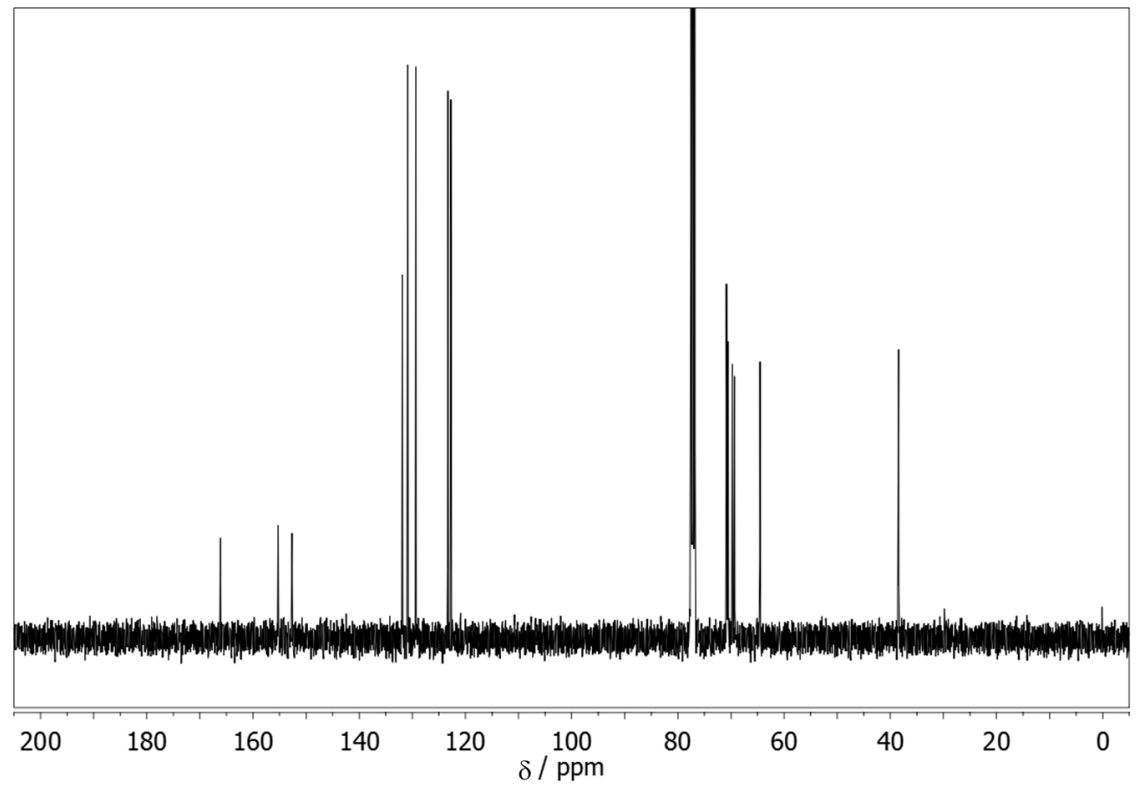

^{13}C-NMR (90 MHz, $CDCl_3$)

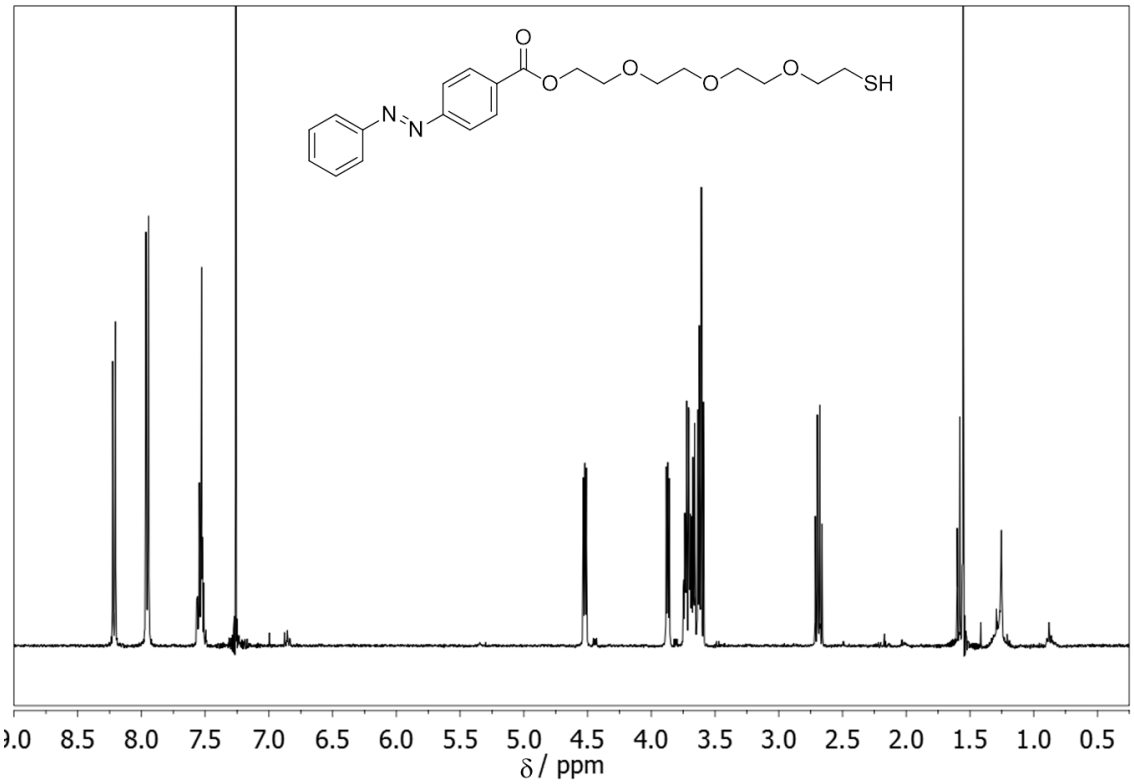

^{1}H-NMR (400 MHz, $CDCl_3$)

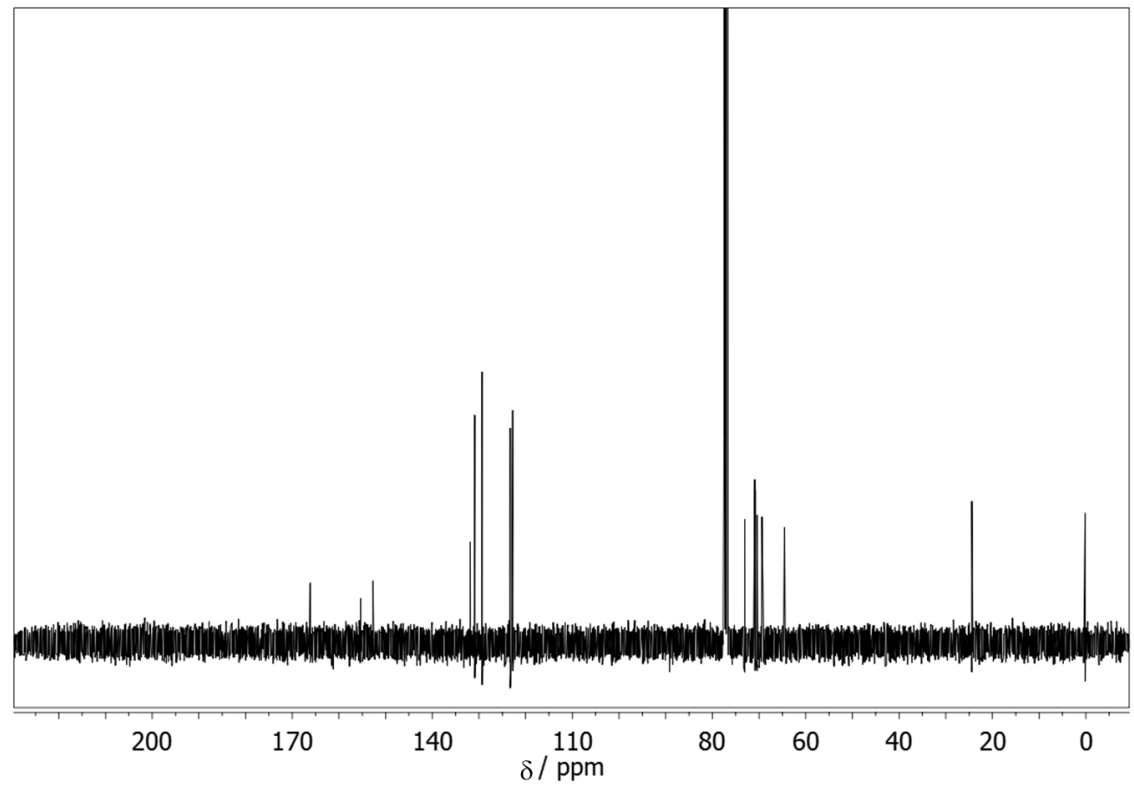

^{13}C-NMR (100.6 MHz, $CDCl_3$)